2014

Functionalized Surface-Cross-Linked Micelles for Catalysis and Light Harvesting

Geetika Chadha
Iowa State University

Functionalized surface-cross-linked micelles for catalysis and light harvesting

by

Geetika Chadha

A dissertation submitted to the graduate faculty

in partial fulfillment of the requirements for the degree of

DOCTOR OF PHILOSOPHY

Major: Organic Chemistry

Program of Study Committee:
Yan Zhao, Major Professor
Malika Jeffries-EL
Arthur Winter
Javier Vela
Ning Fang

Iowa State University

Ames, Iowa

2014

TABLE OF CONTENTS

ACKNOWLEDGEMENTS

I would like to express my deepest gratitude and sincere thanks to my major advisor, Dr. Yan Zhao. I truly appreciate his constant guidance and support through my Ph.D. journey. His words of wisdom have inspired me to think creatively and positively in both professional and personal fields. I will forever be indebted to his insightful comments, constant feedback, motivation, knowledge and expertise that he had successfully passed on to me during my graduate studies.

Secondly, I would like to extend my greatest thanks to all my graduate committee members, Dr. Malika Jeffries-EL, Dr. Arthur Winter, Dr. Javier Vela, and Dr. Ning Fang, for their time, exceptional support, and practical advice as I worked towards my Ph.D. degree. Their recommendations and feedback from time and again had helped to be where I am today. I owe a special thank you to Dr. Malika Jeffries-EL for being my mentor for Preparing Future Faculty (PFF) program and giving me invaluable advice. I am also grateful to Dr. Jesudoss Kingston for his endless mentoring, support and guidance during my course instructor position.

I would like to thank my family, relatives, and friends, especially my parents Renu Chadha and Gurpreet Chadha, for their unconditional support, prayers, and endless efforts to help me achieve my goal. They have always been there, standing by me during good and bad times and encouraging me in my educational efforts. I thank my brother, Karan Chadha, for his continuous love, trust, patience, and encouragement during all these years. Special thanks to Sivaram Pradhan, Naveen Malik, and Rajarshi Roychoudhury who helped me foster my intellectual growth and kept me going all these years. I thank them all for being my catalysts in helping me achieve my dreams and teaching me small things in life that I might overlook.

Lastly, I would like to thank all my present and past group members for their help and invaluable discussions, Department of Chemistry, Iowa State University, for giving me the platform to financially support myself and providing me with a healthy and encouraging environment for teaching and research.

CHAPTER 1

GENERAL INTRODUCTION

Dissertation Organization

This dissertation is organized into 6 chapters. The first chapter is a review focusing on the research and development of surface cross-linked micelles (SCMs) and their applications in different fields. Chapters 2 to 4 have already been published as peer-reviewed papers. Chapter 5 is a manuscript to be submitted. Chapter 6 is a general conclusion summarizing the significance and future growth of the research done in this dissertation.

The second chapter was published in the *Journal of Colloid and Interface Science* in 2013. Surface cross-linked micelle systems were studied and using fluorescent probes and chemical reactions; their surface properties were investigated. Cross-linking of a micelle showed profound impact on its properties, leading to higher surface basicity. The higher catalytic activity of the SCMs over their non-cross-linked counterparts (CTAB micelles) originated from the stronger surface basicity of the former.

The third chapter was published in the *Organic and Biomolecular Chemistry* in 2013. Histidine-functionalized SCMs were prepared and studied for their enhanced nucleophilicity and how they impacted ester hydrolysis in acidic medium. Crosslinking and polycationic nature of the SCMs has the ability to alter the pK_a value of the functional group attached to its surface. This effect was studied using fluorescence spectroscopy and phosphate ester hydrolysis. The functionalized SCMs displayed faster ester hydrolysis and excited state proton transfer (ESPT) of photo-acids than the parent SCMs.

The fourth chapter was published in the *Chemical Communications* in 2014. The SCMs were labeled with a catalytic group, 4-Dimethylaminopyridine (DMAP), internally and at the interface. This work demonstrated how control of the microenvironment around the catalyst affected the nature of nucleophilic catalysis of ester/phosphate ester hydrolysis. Internal functionalized SCMs displayed remarkable nucleophilic catalysis in acidic medium because the catalytic group had strong resistance to protonation. Also, the catalytic activity was enhanced for more hydrophobic substrates with the same catalytic group.

The fifth chapter is a manuscript to be submitted. SCMs containing chromophores are used as a platform for artificial light harvesting system. A crosslinkable surfactant bearing dansyl-like fluorophore was used to prepare dansyl-SCMs by a one-pot reaction at room temperature. Click cross-linking of the surfactants afforded a high-density of the antenna chromophores in the SCMs with minimal self-quenching and excimer formation. The hydrophobic and electrostatic interactions facilitated the energy transfer from the dansyls to the acceptor, Eosin Y (EY). The dissertation finishes in Chapter 6 with a general conclusion and an outline of the research for the future directions.

Literature Reviews

An interesting property of enzymes is their ability to modify acid/base properties of the active site to enhance the reactivity. It has been well documented in biological systems that unspecific hydrophobic interactions and specific electrostatic effects [1-4] are the principal ways to achieve such modifications. In supramolecular systems, water-soluble macrocyclic hosts like cyclodextrins, calixarenes, and cucurbiturils have been studied as enzyme mimics [5-8].

Micelles, also commonly classified as supramolecular nanoenzyme mimics, are small, spherical aggregates of surfactants with many applications in catalysis, drug delivery, cleaning, solubilization, sensing, molecular recognition, etc., [9-15]. "Functional micelles" are analogues of enzymatic catalysts with a non-polar interior and a polar exterior. These self-assembled structures are in dynamic equilibrium with the individual surfactants with a lifetime in the millisecond range. This constant rearrangement of surfactants is the reason behind reduced stability, rapid exchange of components, and fast disintegration upon dilution. Since locking them into stable structures may help address these challenges, intensive efforts have been made by researchers to capture micelles by covalent bonds. Surfmers have been useful in this regard as these surfactants contain polymerizable groups [16]. However, it is a challenge to control their degree of polymerization, which can lead to formation of oligomers instead of spherical, well-dispersed water-soluble nanostructures [17].

Working towards this end, our group reported a simple method to capture micelles by covalent fixation [18]. Unlike dynamic micellar systems that constantly exchange surfactants and their cargo, the surface cross-linked micelles (SCMs) are water-soluble organic nanoparticles with enhanced properties. They provide an excellent platform for multivalent interactions, facile post-modification, tunable surface potential, controlled release, surface and core functionalization, and encapsulation. [19-21].

In this dissertation, I present several applications of these surface cross-linked nanomaterials as potential catalysts and light-harvesting materials. The microenvironment of these covalently fixed micelles are studied and the impact of crosslinking on their surface properties is investigated. Different kinds of functionalized surfactants were synthesized and studied for their micelle formation and surface activity. Surfactants with polymerizable tail were

synthesized to facilitate covalent capture of catalytic groups in the core. Chromophore-containing surfactants were prepared and investigated for their energy transfer within and beyond a single SCM.

References:

(1) B. H. Oh, N. C. Ha, *J. Biol. Chem*., 2000, **52**, 411000.

(2) G. M. Whitesides, J. Rao, *J. Am. Chem. Soc*., 1997, **119**, 9336.

(3) B. Honig, A. Nicholls, *Science*, 1995, **268**, 1144.

(4) A. D. MacKerell, M. S. Sommer, M. Karplus, *J. Mol. Biol*., 1995, **247**, 774.

(5) V. M. Powers, J. A. Gerlt, J. W. Kozarch, *Biochemistry*, 1991, **30**, 9255.

(6) X. Zhang, G. Gramlich, X. Wang, W. M. Nau, *J. Am. Chem. Soc*., 2002, **124**, 254.

(7) J. Mohanty, A. C. Bhasikuttan, W. M. Nau, H. Pal, *J. Phys. Chem. B*, 2006, **110**, 5132.

(8) M. Shaikh, Y. M. Swamy, H. Pal, *J. Photochem. Photobiol. A*, 2013, **258**, 41.

(9) T. Dwars, E. Paetzold, G. Oehme, *Angew. Chem*., 2005, **117**, 7338.

(10) Y. Y. Peng, Q. P. Ding, Z. Li, P. G. Wang, J. P. Cheng, *Tetrahedron Lett*., 2003, **44**, 3871.

(11) J. Gong, M. W. Chen, Y. Zheng, S. P. Wang, Y. T. Wang, *J. Control Release*, 2012, **159**, 312.

(12) Y. S. Jo, A. J. van der Vlies, J. Gantz, T. N. Thacher, S. Antonijevic, S. Cavadini, D. Demurtas, N. Stergiopulos, J. A. Hubbell, *J. Am. Chem. Soc*., 2009, **131**, 14413.

(13) E. N. Savariar, S. Ghosh, D. C. Gonzalez, S. Thayumanavan, *J. Am. Chem. Soc*., 2008, **130**, 5416.

(14) L. Zhang, C. Zhao, J. Zhou, T. Kondo, *J. Mater. Chem. C*, 2013, **1**, 5756.

(15) J. S. Nowick, J. S. Chen, G. Noronha, *J. Am. Chem. Soc*., 1993, **115**, 7636.

(16) H. A. S. Schoonbrood, J. M. Asua, *Macromolecules*, 1997, **30**, 6034.

(17) H. Matahwa, J. B. McLeary, R. D. Sanderson, *J. Polym. Sci. Part A-Polym. Chem*., 2006, **44**, 427.

(18) S. Zhang, Y. Zhao, *Macromolecules*, 2010, **43**, 4020.

(19) (a) X. Li, Y. Zhao, *Langmuir*, **2012**, *28*, 4152; (b) S. Zhang, Y. Zhao, *J. Am. Chem. Soc.*, 2010, **132**, 10642; (c) G. Chadha, Y. Zhao, *Chem. Commun*., 2014, **50**, 2718.

(20) (a) G. Chadha, Y. Zhao, *J. Colloid Interface Sci*., 2013, **390**, 151; (b) G. Chadha and Y. Zhao, *Org. Biomol. Chem*., **2013**, *11*, 6849; (c) S. Zhang, Y. Zhao, *Chem. Commun*., 2012, **48**, 9998.

(21) (a) X. Li, Y. Zhao, *Bioconjugate Chem*., 2012, **23**, 1721; (b) H. Q. Peng, Y. Z. Chen, Y. Zhao, Q. Z. Yang, L. Z. Wu, C.H. Tung, L.-P. Zhang, Q. X. Tong, *Angew. Chem. Int. Ed*., 2012, **51**, 2088.

CHAPTER 2

PROPERTIES OF SURFACE-CROSS-LINKED MICELLES PROBED BY FLUORESCENCE SPECTROSCOPY AND THEIR CATALYSIS OF PHOSPHATE ESTER HYDROLYSIS

A paper published in *Journal of Colloid and Interface Science*, **2013**, *390*, 151-157.

Geetika Chadha and Yan Zhao

Abstract

Cross-linking of a tripropargylated ammonium surfactant by a diazide cross-linker in the presence of Cu(I) catalysts yielded surface-cross-linked micelles (SCMs) as water-soluble nanoparticles. Cross-linking had a profound impact on the properties of the micelles. The binding of 1-anilinonaphthalene-8-sulfonic acid (ANS) indicated that the SCMs contained two types of binding sites, favoring the polar and nonpolar excited states of the probe, respectively. The SCMs also shielded the excited states of ANS from solvent exposure better than the micelles of cetyltrimethylammonium bromide (CTAB). The SCMs inhibited the excited state proton transfer (ESPT) of a polyanionic probe, pyranine, more strongly than CTAB micelles. The ESPT of a more hydrophobic probe, 2-naphthol, was found to be influenced by the stronger surface basicity of the SCMs, as well as their better shielding of the probe from the aqueous phase than the CTAB micelles. The stronger surface basicity of the SCMs also enabled them to catalyze the hydrolysis of an activated phosphate ester at neutral pH better than CTAB micelles

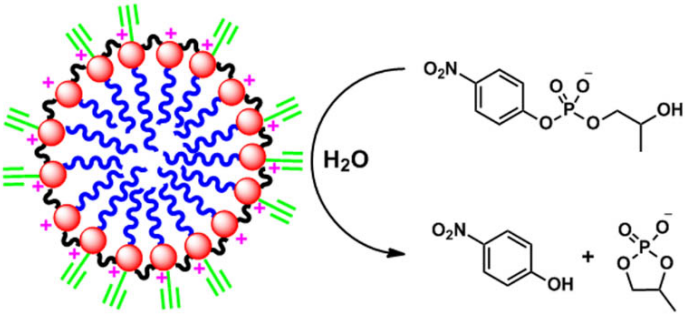

Introduction

Micelles are aggregates of surfactants formed normally in aqueous solution in a balance of hydrophobic interactions among the hydrophobic tails of the surfactants and electrostatic/steric repulsion among the headgroups [1,2]. The former provides the driving force to the aggregation and the latter creates boundaries for the self-assembly, preventing infinite growth of the aggregates. Micellization is the fundamental reason behind many applications of surfactants, including washing, solubilization, and catalysis.

Common surfactant micelles are dynamic assemblies with a lifetime of 10^{-3}–10^{-2} s [3]. Chemists have long been interested in capturing these noncovalent structures by covalent bonds [4,5]. If micelles can be locked into stable water-soluble nanoparticles and decorated with desired functional groups, many potential applications can be envisioned. Toward this end, chemists have prepared surfmers or surfactants with reactive functionalities that can undergo chemical ligation on the micelles. The most commonly used reactive group is a vinyl that can polymerize under thermal or photolytic initiation. The majority of surfmers in the literature have the vinyl on the hydrophobic tail or in the headgroup of the surfactant [6–8]. Sometimes, the polymerizable group is located on the counterion of ionic surfactants [9].

Although micellization was found to be highly important to the effective polymerization of surfmers, the materials obtained from such reactions frequently had a degree of

polymerization much higher than the aggregation number of the micelle [10]. Hence, the polymerization went beyond a single micelle and involved intermicellar reactions. Sometimes, oligomers were obtained that aggregated into particles significantly larger that the parent micelle [11]. These results are understandable. Because the exchange of surfactants between micelles generally is orders of magnitude faster than the rate of propagation in radical polymerization, topological polymerization within a single micelle is extremely difficult [10–12].

We recently reported a simple method to cross-link surfactant micelles by the click reaction (Scheme 1) [13]. The tripropargylated cationic surfactant (**1**) has a CMC of 0.14 mM. Because of the high density of terminal alkyne on the surface, the micelle of 1 under- goes facile 1,3-dipolar cycloaddition with azido cross-linkers such as **2** in the presence of Cu(I) catalysts. The large thermodynamic driving force of the cycloaddition, the high effective concentration of alkyne on the micelle surface, and the efficiency of the Cu(I) catalysts [14] all contributed to the successful capture of the micelles. The surface-cross-linked micelles (SCMs) obtained were characterized by a number of techniques including NMR spectroscopy, DLS, and TEM. When the 1,2-diol groups on the SCMs (see the structure of **2**) were cleaved by periodic acid, compounds 3 and 4 were identified by ESI–MS, with the former being the major product. The results were consistent with the 1:1 stoichiometry employed in the cross-linking. The residual alkyne left on the surface allowed facile surface modification, simply by adding any azido-functionalized ligands or polymers [13]. More recently, the SCM was used as a platform for artificial light harvesting. Interestingly, fluorescence quenching suggested that each SCM contained about 50 cross- linked surfactants [15], in agreement with our earlier DLS study that indicated 40–50 surfactant molecules per SCM.

In addition to its facile synthesis and post-modification, the SCMs have other interesting properties. When cleavable bonds were introduced in the azide cross-linkers, the SCMs could be broken apart with chemical triggers [16]. Because the cationically charged ammonium groups repel each other, the SCMs are under significant electrostatic stress, raising the ground state energy of the system and making the SCMs extremely sensitive to the cleaving agent. Guest molecules trapped within the SCMs were found to be ejected very rapidly (<1 min) with the addition of even a small amount of the cleaving agent. More recently, we found that these SCMs could serve as a reservoir of protected surfactants. The SCMs have low surface activity due to the hydrophilic exterior and completely buried hydrophobes. Cleavage of the reversible cross-linkages exposes the hydrophobic tails of the surfactants and releases surface-active materials that could be used for different purposes including the controlled leakage of liposomes [17].

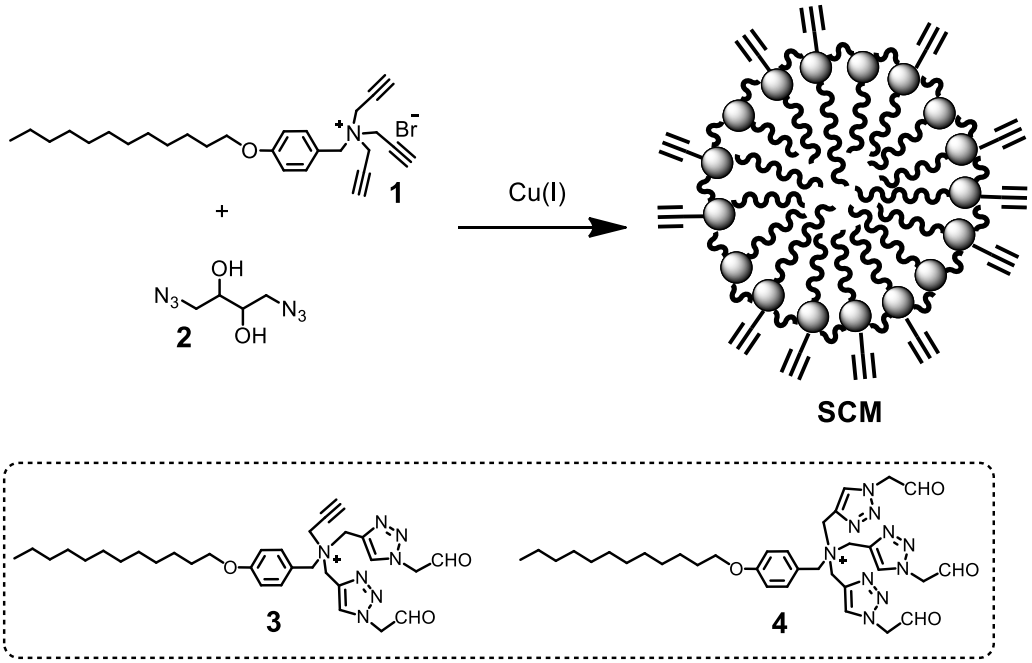

Scheme 1. Preparation of surface-crosslinked micelle (SCM).

Fluorescence spectroscopy can reveal a wealth of information about the local environment around the fluorophore [18]. In this paper, we report the investigation into the SCMs by fluorescence spectroscopy. Their local hydrophobicity, interactions with anionic guests, shielding of hydrophobic guests, and ability to influence excited state proton transfer (ESPT) were studied by a number of fluorescent probes. Interesting differences were observed between the SCMs and micelles formed by a control cationic surfactant, CTAB. The SCMs were found to have stronger surface basicity and able to hydrolyze activated phosphate esters better than their non-covalent counterpart, the CTAB micelles.

Experimental Section

General

All reagents and solvents were of ACS-certified grade or higher and used as received from commercial suppliers. Millipore water was used to prepare buffers. Routine ^{1}H and ^{13}C NMR spectra were recorded on a Varian VXR-400 or on a Varian MR-400 spectrometer. Fluorescence spectra were recorded on a Varian Cary Eclipse fluorescence spectrophotometer. UV–vis spectra were recorded on a Cary 100 Bio UV–visible spectrophotometer. The preparation and the characterization of the SCMs were reported previously [13].

Fluorescence Study

A typical procedure for the fluorescence experiment is as follows: Stock solutions of the SCM (the concentration of the cross-linked surfactant was 2.0 mM), ANS (80 μM), pyranine (80 μM), and 2-naphthol (80 μM) in Millipore water were prepared. An aliquot (1.20 mL) of the SCM solution was added to a cuvette containing 800 μL of HEPES buffer (25 mM, pH = 7),

followed by an aliquot (100 μL) of the stock solution of the appropriate dye. After the sample was vortexed briefly, the cuvette was placed in the spectrometer and equilibrated to 35.0 °C. The fluorescence spectrum was recorded, with the excitation wavelength for ANS, pyranine, and 2-naphthnol being 388, 390, and 315 nm, respectively. The same procedure was repeated for the CTAB samples. Triplicate data were generally collected for each sample.

Kinetic Measurement

HPNPP was prepared according to a literature procedure [19]. A stock solution (10 mM) of HPNPP in Millipore water was prepared. For the kinetic measurement, a typical procedure is as follows: Aliquots of the SCM solution were added to a series of cuvettes containing 800 μL of HEPES buffer (25 mM, pH = 7). The concentrations of cross-linked surfactant in the SCM in the samples were 0, 0.2, 0.4, 0.6, 0.8, 1.0, and 1.5 mM, respectively. The cuvettes were placed in the spectrometer and equilibrated to 35.0°C. After 5 min, aliquots (40 μL) of the HPNPP solution were added to the above cuvettes, and the absorbance of *p*-nitrophenolate at 400 nm was monitored over a period of 3 h. The same procedure was repeated for the CTAB samples. Triplicate data were generally collected for each sample.

Results and Discussion

Chart 1 shows the structures of the fluorescent and chemical probes used in this study. ANS (1-anilinonaphthalene-8-sulfonic acid, ammonium salt) is a fluorophore highly sensitive to environmental polarity [20]. It fluoresces weakly in water but strongly when bound to proteins or membranes. Its anionic character makes it particularly suitable for probing cationic micellar systems.

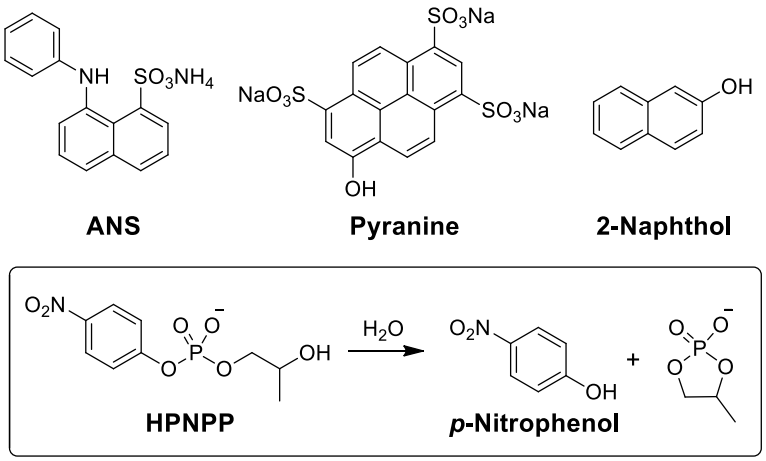

Chart 1. Fluorescent and Chemical Probes Used in the Study.

Pyranine and 2-naphthol are both photoacids. The pK_a values for the ground and excited state of pyranine are 7.2 and 0.5, respectively [21], and those for 2-naphthol are 9.3 and 2.8 [22,23]. Excitation thus makes both compounds more acidic, and the ratio between the protonated and deprotonated excited states can be used to probe a number of parameters including local pH, polarity, and the interactions between the probes and their surroundings [23,24]. In addition to their different pK* values (i.e., acidity constant of the excited state), the two probes are very different in polarity, allowing us to probe different locations of the micelles. Lastly, 2-hydroxylpropyl-4-nitrophenyl phosphate (HPNPP) is a model compound in RNA hydrolysis. Its hydrolysis releases *p*-nitrophenol that can be detected easily by UV–vis spectroscopy. Its anionic character also enables it to adsorb onto a cationic micelle easily, helping us understand the effects of the micelles on the chemical reaction.

Binding of ANS

Fig. 1a shows the fluorescence spectra of ANS in water, CTAB, and SCM, respectively. The concentration of the cross-linked surfactant in the SCM was kept the same as that of the CTAB, 1.2 mM, which is above the latter's CMC (0.9 mM). ANS was found to emit very weakly in water. In the presence of CTAB micelles, the emission became stronger with the maximum emission wavelength λ_{em} = 485 nm. The emission wavelength of ANS in solution depends on the polarity of the solvent, ranging from 523 nm in water to 465 nm in 1-octanol [25]. The observed emission wavelength in the CTAB solution was comparable to that in the ethylene glycol (λ_{em} = 484 nm). Thus, the ANS probe was in a fairly polar region of the micelle, most likely near the micellar surface [26].

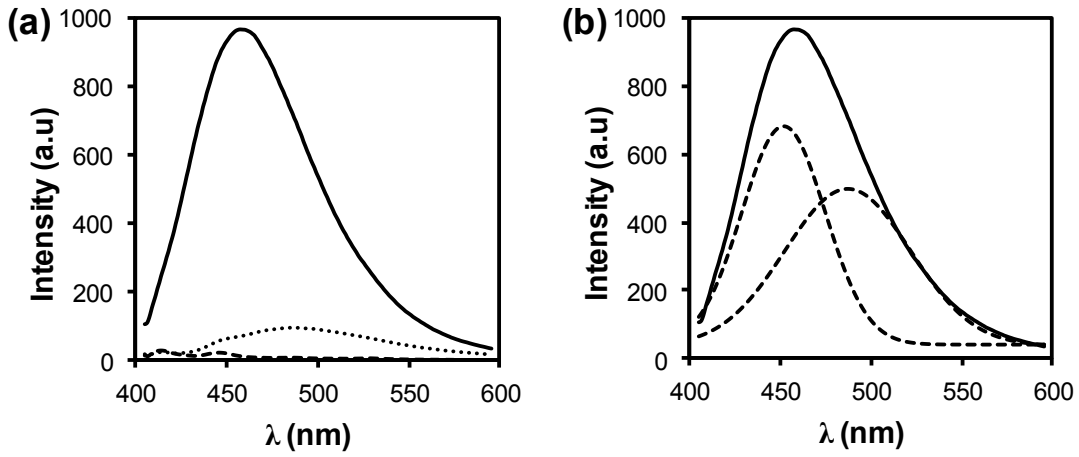

Fig. 1 (a) Emission spectra of ANS in HEPES buffer (dashed line), CTAB (dotted line), and SCM (solid line). pH = 7. [ANS] = 0.4 μM. [CTAB] = [crosslinked surfactant in SCM] = 1.2 mM. λ_{ex} = 388 nm. (b) Peak fitting of the emission spectra of ANS in SCM showing two peaks with λ_{em} = 452 and 487 nm, respectively. The dashed spectra were from peak fitting of the experimental spectrum.

Ion binding and reactivity on charged micelle surfaces have been described by pseudophase ion exchange and Poisson–Boltzmann models [27]. Regardless of the models used, because excitation and fluorescence are much faster than typical binding and chemical reactions, the fluorescence spectrum of a probe in a micellar solution is a superposition of the spectra of the dissolved and micelle- bound populations of the probe, even if the entry rate of the probe into the micelles is diffusion-controlled [28]. On the other hand, since over 95% of 2-naphthol, pyranine, and other similar sulfonated fluorescent probes in CTAB solutions were found to be bound by the micelles by fluorescence quenching [28], we assumed that the spectra obtained in our micellar solutions also came from the micelle-bound state. The assumption was reasonable given the negligible emission of ANS in the HEPES buffer (Fig. 1a).

As shown by Fig. 1b, the emission spectrum of ANS in SCM consisted of two peaks centered at 452 and 487 nm, respectively. Evidently, the SCM contained two types of binding sites. The microenvironment of one of them was similar to that found in the CTAB micelles, as the emission wavelengths (487 and 485 nm) were nearly identical. The other site seemed to be much less polar according to the highly blue-shifted emission wavelength (452 nm).

It might be surprising that the peak at 452 nm was even more blue-shifted than the emission in 1-octanol (λ_{em} = 465 nm). Given the amphiphilic nature of the ANS probe, it is unlikely for the molecule to penetrate deep inside the cross-linked micelle. Instead, the sulfonate group, due to its strong solvation by water, should be located on the surface of the micelle [26], where the polarity should be much higher than that of 1-octanol.

The environmental sensitivity of ANS derives from their two excited states—a nonpolar state that is less sensitive to the environment and a highly sensitive charge-transfer state [20]. It has been reported that, when these probes are in a highly viscous solvent such as glycerol [29] or

when bound to proteins [30,31], the non-polar state could dominate even when the environmental polarity was high. The result was attributed to the inhibition of the formation of the charge-transfer state, which involves a rotation of the phenyl group in the excited state [20]. It seems that the cross-linking has created binding sites in the SCM similar to those in proteins, which have high microviscosity and might have inhibited the rotation of the phenyl group of ANS.

Not only the polar and the nonpolar excited states of ANS appeared simultaneously when the probe was bound by the SCM, the emission of both states was also substantially higher than the (polar) excited state in CTAB (compare Fig. 1a and b). The weak emission of ANS derivatives in water is known to result from fast nonradiative relaxation caused by the solvent [20]. Clearly, the SCM provided better protection to the probe than the CTAB micelle, at least to the polar charge-transfer state. The nonpolar state could not be detected in the dynamic CTAB micelle at all.

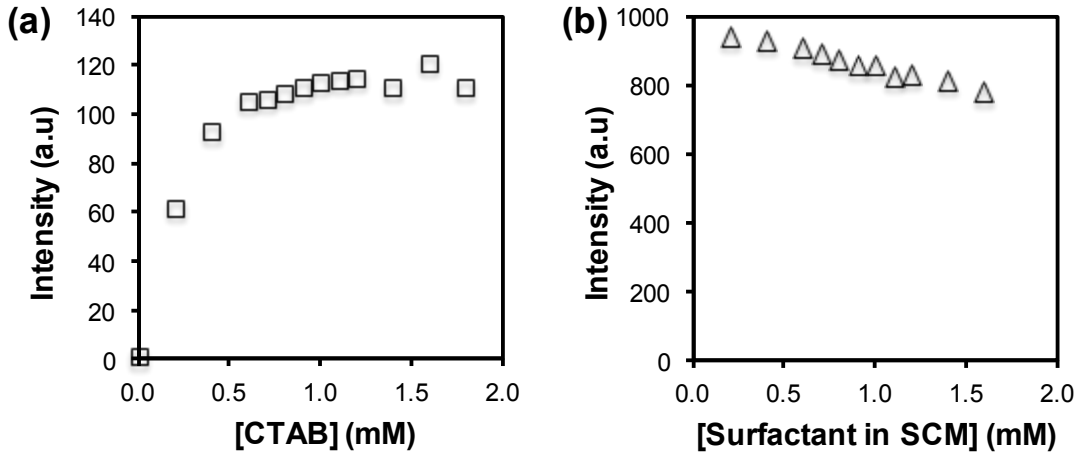

Fig. 2 (a) The emission intensity of ANS at 485 nm against the concentration of CTAB in water. (b) The emission intensity of ANS at 460 nm against the concentration of the cross-linked surfactant in SCM in water. [ANS] = 0.4 μM. λ_{ex} = 388 nm.

Another difference in the CTAB micelle and the SCM was in their concentration-dependency on the surfactant. Fig. 2 plots the maximum emission intensity of ANS against increasing concentrations of the surfactant (free or cross-linked). Not surprisingly, the ANS emission in the CTAB solution was highly sensitive to the surfactant concentration and increased until it reached the CMC (0.9 mM). The data also suggested pre-micellar association between the surfactant and the probe, possibly due to the opposite charges of the two. In contrast, the emission was fairly constant over the same range of concentration for the SCM [32]. The crosslinking, as expected, fixed the micelles into nanoparticles stable at all concentrations, making the ANS emission quite concentration independent for the SCM [13]. Also note that the emission intensity of ANS in SCM was much stronger than that in the CTAB solution, as a result of the better protection provided by the former.

Inhibition of ESPT

Pyranine is a photoacid whose excited state (pK^* = 0.5) is much more acidic than the ground state (pK_a = 7.2) [21]. As shown by Fig. 3a, at pH = 6–8, the dominant emission appeared at ca. 510 nm, which corresponds to that of the deprotonated excited state. The acidic form (λ_{em} ≈ 445 nm) was very weak, in agreement with what was reported in the literature [21]. This was due to the very fast deprotonation step of the excited photoacid with a rate constant of ca. 10^{10} s^{-1} in pure water. In the presence of CTAB micelles, the emission from the protonated form was greatly enhanced (Fig. 3b). Thus, interactions with the CTAB micelle inhibited the proton transfer in the excited state. Consistent with a literature report [33], some spectroscopic shifts occurred with the acidic form emitting at 430 nm and the basic form at ~530 nm. According to

the laser-initiated pH-jump experiments, the deprotonation of the excited pyranine was slowed down by over an order of magnitude on the CTAB micelles [33].

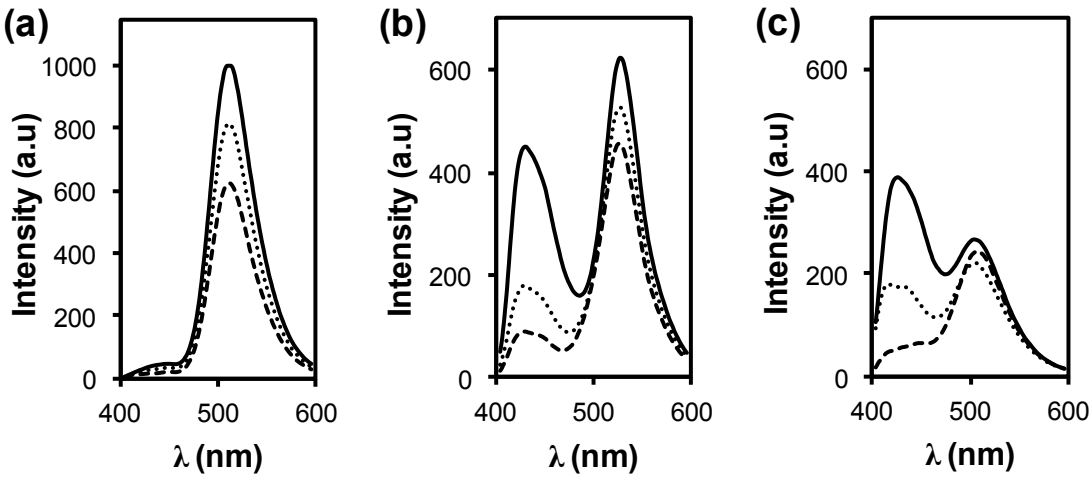

Fig. 3 Emission spectra of pyranine in (a) buffer, (b) CTAB solution, and (c) SCM solution at pH = 6 (solid line), 7 (dotted line), and 8 (dashed line). [pyranine] = 0.4 μM. [CTAB] = [crosslinked surfactant in SCM] = 1.2 mM. λ_{ex} = 390 nm.

The SCM had a noticeably larger inhibiting effect on the photolytic deprotonation, evident from the even stronger emission of the protonated probe (Fig. 3c). The effect was particularly noticeable at pH = 6. The ratio between the protonated form and the deprotonated form, as measured by the intensity ratio at 430 and 520 nm, went from 0.72 in the CTAB micelles to 2.0 in the SCMs. Since the interactions between the anionic probe and the cationic CTAB micelle were responsible for the inhibited deprotonation in the excited state [33], the interactions between pyranine and the SCM must be significantly stronger. The results are quite reasonable—as the cationic surfactants get cross-linked into a stable polycationic nanoparticle, the electrostatic interactions with a polyanionic guest are expected to increase.

Given the large size of pyranine and its polyanionic character, it is unlikely for the probe to penetrate into the micellar core (whether in the case of cross-linked or the regular micelle). Behavior of the photoacid most likely reflects the property of the micelle/ water interface, where the majority of the probe should be located. 2-Naphthol is quite different, on the other hand. Being neutral and possessing a fairly hydrophobic naphthyl ring, most of the probe should be located in a more hydrophobic region of the micelle when solubilized by the micelle.

Fig. 4a shows the normalized fluorescence spectra of 2-naphthol in buffer at pH = 6, 7, and 8. The pK_a values for the ground and excited states of 2-naphthol are 9.3 and 2.8, respectively [22,23]. If the rate of deprotonation is faster than fluorescence, the fluorescence spectrum will only show the deprotonated species at these pH values. In reality, the rate of the excited state deprotonation for the probe, its fluorescence, and the nonradiative decay are known to be competitive, making the emission of 2-naphthol highly sensitive to its environment [34]. As can be seen from the fluorescence spectra, 2-naphthol gave two emission peaks at 355 and 410 nm in aqueous buffer. The former corresponds to the protonated excited state and the latter deprotonated. The spectra were normalized to the emission intensity of the protonated form, allowing us to compare the ESPT in different situations more easily. With an increase of the solution pH, the deprotonated form showed a gradual increase from 0.66 to 0.72 to 0.78 (Fig. 4a).

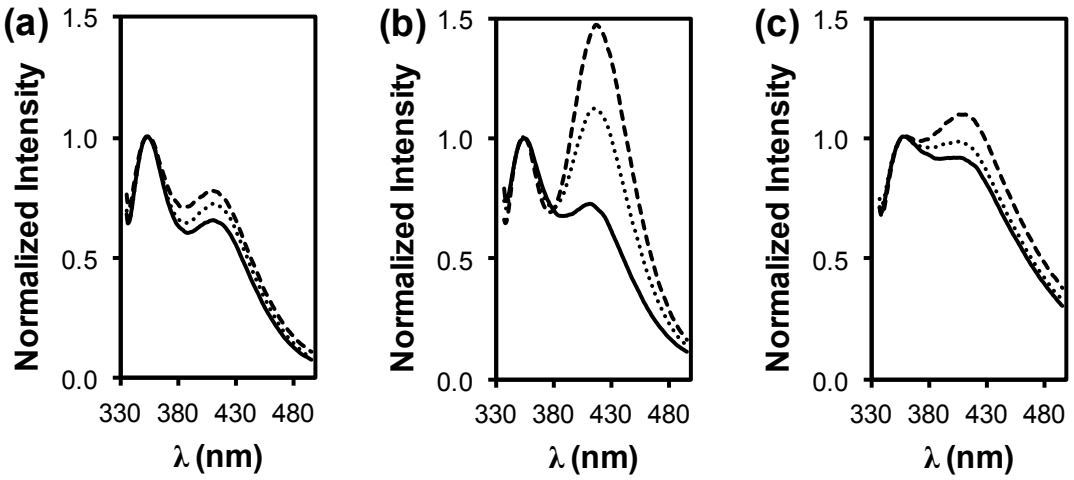

Fig. 4 Emission spectra of 2-napthol in (a) buffer, (b) CTAB solution, and (c) SCM solution at pH = 6 (solid line), 7 (dotted line), and 8 (dashed line). [2-napthol] = 0.4 μM. [CTAB] = [cross-linked surfactant in SCM] = 1.2 mM. λ_{ex} = 315 nm.

The CTAB micelles had a large impact on the ESPT of 2-naphthol. The normalized intensity of the deprotonated probe was 0.73, 1.12, and 1.48 at pH = 6, 7, and 8, respectively (Fig. 4b). Clearly, at every solution pH tested, the CTAB micelles assisted the deprotonation of the excited probe. The effect of micelles on the ESPT of 2-naphthol has been reported (albeit at different pH values) [35,36]. The hydrophobic probe, although solubilized easily by a micelle, tends to stay near the surface of the micelle. Because both the deprotonated species and the proton released during deprotonation are better solvated by water instead of hydrocarbon, a hydrophobic environment inhibits the ESPT of the probe [37]. In neutral and anionic micelles, significant retardation of the deprotonation was observed. The effect was counterbalanced by positively charged micelles due to their electrical potential [38]. Our fluorescence data supported this conclusion, as the presence of CTAB micelles generally promoted the deprotonated species (compare Fig. 4a and b).

Another difference between the fluorescence spectra in aqueous buffer and in the CTAB micelle is the magnitude of the pH effect on the ESPT. When the solution pH was increased from 6 to 8, the relative intensity of the deprotonated probe increased by <20% in aqueous solution but more than doubled in CTAB micelle. Thus, the increasing hydroxide concentration in the bulk had a much larger effect on the ESPT of 2-naphthol when the probe was solubilized by the cationic micelle. A very likely reason for the stronger pH effect in the CTAB micelle comes from its cationic character. Essentially, the positively charged micelle is able to concentrate hydroxide ions near its surface, increasing the local pH on the surface of the micelle. In fact, the surface potential of the cationic micelle is estimated to afford a local pH of 9.5 when the bulk pH is 7 [39].

Given the effect of the cationic micelle on the ESPT of 2-naphthol, it is interesting to see that the probe behaved very differently when solubilized by the cationic SCM (Fig. 4c). The relative intensity of the deprotonated probe was 0.92, 0.99, and 1.10 at pH = 6, 7, and 8, respectively. These numbers were larger than the corresponding values in aqueous buffer (0.66, 0.72, and 0.78). In comparison with water, therefore, the positively charged SCMs did promote the photo-deprotonation of 2-naphthol.

When the relative intensities of the deprotonated 2-naphthol in CTAB micelles (0.73, 1.12, and 1.48) and SCMs (0.92, 0.99, and 1.10) are compared, no consistent trend was observed. At pH = 6, the SCM seemed to be better than the CTAB micelle at promoting the ESPT, but the effect was reversed at pH = 7 and 8. The magnitude of the pH effect, on the other hand, was noticeably smaller in the cross-linked micelles. The pH change from 6 to 8, for example, increased the emission intensity of the naphthoxide solubilized by the SCM by 20% but more than doubled the intensity of the naphthoxide solubilized by CTAB.

A possible reason for the overall lower intensity of the SCM solubilized naphthoxide is its better protection of the probe by the cross-linked micelle—this was already observed in the ANS fluorescence. If the anionic ANS is better shielded by SCM from water exposure (*vide supra*), the neutral 2-naphthol probe should be located in an even more hydrophobic region of the nanoparticle and better shielded from water and the hydroxide ions in it.

According to the hydrolysis of HPNPP (*vide infra*), the SCM has a stronger surface basicity than the CTAB micelle, that is, higher location concentration of hydroxide ions. Most likely, two opposing effects were operating on the SCM simultaneously during the photo-deprotonation of the probe. At pH = 6, the concentration of hydroxide ions in the solution was low. The stronger ability of the SCM to concentrate hydroxide ions to the surface is the dominant effect, promoting the ESPT of 2-naphthol as a result. With an increase of the solution pH, more hydroxide is available, and the difference in surface basicity between the SCM and the CTAB micelle becomes less important. Because the probe is more exposed to the solvent in the dynamic CTAB micelle, the increasing hydroxide concentration has a larger effect on the ESPT. When the probe is solubilized by the SCM, although an even higher concentration of hydroxide ions is present on the surface of the cross-linked micelle, the hydroxide has difficulty accessing the probe. Also, if a larger population of the probe is located in a hydrophobic microenvironment, deprotonation will be more difficult, as the deprotonated species (phenoxide and proton) need to be solvated by water.

It should be mentioned that the slowing down of ESPT by ‘‘hydrophobic shielding’’ of the probe has been reported before, although not in covalent systems. Kuzmin and coworkers compared the photo-deprotonation of 2-naphthol and 2-naphthol derivatives with long alkyl chains. The ESPT of the more hydrophobic probes was found to slow down by 5–8-fold in

CTAB micelles. The differences were attributed to the translocation of the hydrophobic naphthols into the more nonpolar region of the micelle, where deprotonation is more difficult [35].

Catalysis of the Hydrolysis of HPNPP

As mentioned earlier, the surface potential of a cationic micelle makes its surface more basic than the bulk solution. The surface pH of the CTAB micelle is 9.5 in a neutral aqueous solution [39]. One way to investigate the local pH of a micelle surface is through a pH-sensitive probe [40–42]. As shown in the studies above, however, the binding properties of the SCM differ significantly from those of conventional micelles. Since environmental hydrophobicity, microviscosity, and surface potential can all influence the acid–base equilibrium of an indicator, we decided to examine the surface basicity of the SCM by a chemical reaction.

HPNPP is an activated phosphate ester. Its anionic character makes it particularly suitable to probe the properties of a cationic micelle. It hydrolysis releases *p*-nitrophenol, which can be easily monitored by UV–Vis spectroscopy. HPNPP is often studied as a model compound for RNA hydrolysis. Although the hydrolysis of this and other activated phosphate esters has been studied in micelles, metal ions were generally responsible for the rate acceleration [43–45]. Fig. 5a and b compares the UV–Vis spectra of HPNPP in the presence of the SCMs and CTAB micelles over a period of 3 h. A distinctive peak appeared near 400 nm corresponding to *p*-nitrophenolate for the SCM sample, but that for the CTAB solution was much weaker. The absorbance at 400 nm can be fitted into first-order kinetics to give the rate constants for the hydrolysis of HPNPP (Table 1).

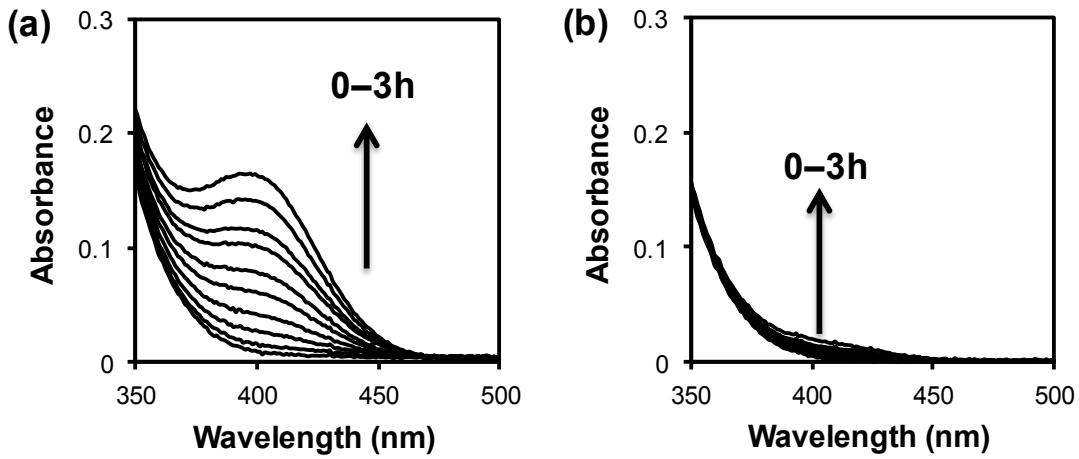

Fig. 6 UV-Vis spectra of an aqueous solution of HPNPP in HEPES buffer over a period of 3 h in the presence of (a) SCM and (b) CTAB at 35 °C. [HPNPP] = 0.2 mM. [CTAB] = [cross-linked surfactant in SCM] = 1.0 mM.

According to the data in Table 1, both the SCMs and the CTAB micelles were able to catalyze the hydrolysis of the activated phosphate ester. The background hydrolysis of HPNPP at pH = 7 was too slow to be measured accurately (entry 17). At [surfactant] = 1.0 mM, the SCMs and the CTAB micelles accelerated the hydrolysis by 3300 and 230 times, respectively, compared to that in the same aqueous buffer (compare entries 9 and 10 with entry 17). One likely reason for the accelerated hydrolysis was the above-mentioned higher surface pH of the positively charged micelles, whether cross-linked or not [27,46,47]. Another reason could be the higher negative charge of the transition state for the hydrolysis in comparison with that of the ground state, making the former stabilized relatively to the latter by a polycationic host.

Table 1. Rate constants for the hydrolysis of HPNPP in aqueous buffer catalyzed by the SCMs and CTAB micelles.

Entry	Micelle	[Surfactant] (mM)	Solution pH	$k \times 10^5$ (min^{-1})	k_{SCM}/k_{CTAB}
1	SCM	0.2	7.0	32	1600
2	CTAB	0.2	7.0	~0.02[a]	---
3	SCM	0.4	7.0	62	77
4	CTAB	0.4	7.0	0.81	---
5	SCM	0.6	7.0	81	35
6	CTAB	0.6	7.0	2.3	---
7	SCM	0.8	7.0	81	18
8	CTAB	0.8	7.0	2.3	---
9	SCM	1.0	7.0	93	14
10	CTAB	1.0	7.0	5.1	---
11	SCM	1.5	7.0	100	11
12	CTAB	1.5	7.0	7.0	---
13	SCM	1.0	7.5	190	9
14	CTAB	1.0	7.5	22	---
15	SCM	1.0	8.0	290	5
16	CTAB	1.0	8.0	54	---
17	none	0	7.0	~0.03[a]	---

[a] The reaction rate was too slow to be measured accurately.

According to the pseudophase ion exchange model, the observed rate of a chemical reaction is determined by the reaction rates of the substrate in solution and in the micelle-bound state, as well as the binding equilibrium between the substrate and the micelle pseudophase [27].

In our case, the reactivity in the aqueous pseudophase is negligible at pH = 7 (Table 1, entry 17), and thus, the observed reactivity must have come from the micelle-bound substrate.

Table 1 also shows that the SCMs were consistently more capable of catalyzing the HPNPP hydrolysis than the noncovalent CTAB micelles. The results support the stronger surface basicity of the former, possibility due to the covalent nature of the SCMs. The surface basicity of the cationic micelles derives from the electrical potential of the micelles, whether cross-linked or not. As mentioned in the beginning of the paper, the driving force for micellization is the hydrophobic interactions among the tails of the surfactants. The electrostatic repulsion between the headgroups of the surfactants represents the opposing force. Put in a different way, the electrostatic repulsion by itself goes against the formation of the polycationic structure, whose electrical potential is responsible for its higher surface basicity. By connecting the cationic surfactants with covalent bonds, the cross-linking in a sense ‘‘over-comes’’ the electrostatic repulsion that opposes the formation of the polycationic structure. Thus, by weakening the opposing force, the cross-linking could enhance the surface basicity of the SCM and facilitate the hydrolysis of the SCM-bound HPNPP. Another feature of the SCM is the presence of numerous triazole and hydroxyl groups. Although it is possible that these groups could also be helpful to the hydrolysis, the first pK_a of 1H-1,2,3-triazole is only 1.17 [48]. The weak basicity (and thus nucleophilicity) of triazole would make it difficult for it to participate in the catalysis.

Table 1 also shows that the largest k_{SCM}/k_{CTAB} (=1600) was observed at pH = 7 when the concentration of the surfactant was 0.2 mM. The k_{SCM}/k_{CTAB} was found to decrease with increasing surfactant concentration. These results are consistent with the lack of CMC for the SCM. The CMC of CTAB is 0.9 mM. Below this concentration, the surfactant has limited ability to promote HPNPP hydrolysis. In fact, at 0.2 mM of CTAB, the rate constant for the hydrolysis

was nearly identical to that of the background reaction (entries 2 and 17). The SCM, however, maintains the polycationic structure at all concentrations, thus being able to accelerate the hydrolysis at all concentrations.

The final observation from Table 1 is related to the pH effect. An increase of pH from 7 to 7.5 to 8.0 was found to increase the rate of HPNPP hydrolysis for both the SCMs and the CTAB micelles. The k_{SCM}/k_{CTAB} ratio decreased steadily from 14 to 9 to 5 at the three pHs, respectively. The result is not surprising. The increasing hydroxide concentration has a general positive effect on the hydrolysis. As the background reaction becomes faster, the catalysis of the SCMs and the CTAB micelles becomes less important.

Conclusions

Cross-linking of a micelle strongly impacts its properties [4–12]. Not only the surfactants no longer undergo intermicellar exchange, the cross-linked micelles, as shown by this work, also differ from the non-covalent assemblies in profound ways. We have already demonstrated several applications for the SCMs including stimuli-sensitive delivery of hydrophobic agents [16], controlled release of surfactants [17], as a scaffold for artificial light-harvesting system [15], and in aqueous biphasic catalysis [49]. The current study revealed additional features of these novel water-soluble nanoparticles. They possess two types of binding sites for the non-polar and the polar excited states of the polarity-sensitive ANS probe, respectively. Both binding sites shielded the probe better from solvent exposure than the dynamic CTAB micelles. The SCMs could inhibit the ESPT of pyranine, possibly due to strong interactions between the probe and the oppositely charged SCM. The less polar photoacid (2-napthol) tends to stay in the more hydrophobic region of a micelle than pyranine. Notably, the higher surface basicity of the SCMs

and their stabilization of an anionic transition state make them capable catalysts in the hydrolysis of an activated phosphate ester (HPNPP). Given their easy preparation [13] and numerous features, the SCMs should become a versatile platform for chemical and biological applications.

Acknowledgment

We thank US Department of Energy-Office of Basic Energy Sciences (Grant DE-SC0002142) for supporting the research.

Notes and References

(1) M.J. Rosen, Surfactants and Interfacial Phenomena, second ed., Wiley, New York, 1989.

(2) D. Myers, Surfactant Science and Technology, second ed., VCH, New York, 1992.

(3) J.H. Clint, Surfactant Aggregation, Chapman and Hall, New York, 1992.

(4) C.E. Larrabee, E.D. Sprague, *J. Polym. Sci. Polym. Let. Ed*., 1979, **17**, 749.

(5) C.M. Paleos, C.I. Stassinopoulou, A. Malliaris, *J. Phys. Chem*., 1983, **87**, 251.

(6) J.H. Fendler, P. Tundo, *Acc. Chem. Res*., 1984, **17**, 3.

(7) K. Tajima, T. Aida, *Chem. Commun*., 2000, 2399.

(8) M. Summers, J. Eastoe, *Adv. Colloid Interface Sci*., 2003, **100**, 137.

(9) S.R. Kline, *Langmuir*, 1999, **15**, 2726.

(10) S. Hamid, D. Sherrington, *J. Chem. Soc. Chem. Commun*., 1986, 936.

(11) S.M. Hamid, D.C. Sherrington, *Polymer*, 1987, **28**, 332.

(12) D. Cochin, R. Zana, F. Candau, *Macromolecules*, 1993, **26**, 5765.

(13) S. Zhang, Y. Zhao, *Macromolecules*, 2010, **43**, 4020.

(14) V.V. Rostovtsev, L.G. Green, V.V. Fokin, K.B. Sharpless, *Angew. Chem., Int. Ed*., 2002,

41, 2596.

(15) H.-Q. Peng, Y.-Z. Chen, Y. Zhao, Q.-Z. Yang, L.-Z. Wu, C.-H. Tung, L.-P. Zhang, Q.-X. Tong, *Angew. Chem., Int. Ed*., 2012, **51**, 2088.

(16) S. Zhang, Y. Zhao, *J. Am. Chem. Soc*., 2010, **132**, 10642.

(17) X. Li, Y. Zhao, *Langmuir*, 2012, **28**, 4152.

(18) J.R. Lakowicz, Principles of Fluorescence Spectroscopy, second ed., Kluwer Academic/Plenum, New York, 1999.

(19) J.S.W. Tsang, A.A. Neverov, R.S. Brown, *J. Am. Chem. Soc*., 2003, **125**, 1559.

(20) E.M. Kosower, *Acc. Chem. Res*., 1982, **15**, 259.

(21) E. Bardez, B.T. Goguillon, E. Keh, B. Valeur, *J. Phys. Chem*., 1984, **88**, 1909.

(22) J.F. Ireland, P.A.H. Wyatt, *Adv. Phys. Org. Chem*., 1976, **12**, 131.

(23) L.G. Arnaut, S.J. Formosinho, *J. Photochem. Photobiol., A*, 1993, **75**, 1.

(24) L.M. Tolbert, K.M. Solntsev, *Acc. Chem. Res*., 2002, **35**, 19.

(25) J. Slavík, *Biochim. Biophys. Acta*, 1982, **694**, 1.

(26) B. Rubalcava, D. Martinez de Munoz, C. Gitler, *Biochemistry*, 1969, **8**, 2742.

(27) C.A. Bunton, F. Nome, F.H. Quina, L.S. Romsted, *Acc. Chem. Res*., 1991, **24**, 357.

(28) S. Abou-Al Einin, A.K. Zaitsev, N.K. Zaitsev, M.G. Kuzmin, *J. Photochem. Photobiol., A*, 1988, **41**, 365.

(29) E.M. Kosower, H. Dodiuk, *J. Am. Chem. Soc*., 1974, **96**, 6195.

(30) L.D. Weber, A. Tulinsky, J.D. Johnson, M.A. El-Bayoumi, *Biochemistry*, 1979, **18**, 1297.

(31) H. Dodiuk, H. Kanety, E.M. Kosower, *J. Phys. Chem*., 1979, **83**, 515.

(32) The gradual decrease of the intensity with increasing SCM concentration mostly resulted from the weakening of the emission from the nonpolar excited state of ANS, as revealed

from peak fitting. This change was most likely due to a slightly lower binding affinity of the SCM for the nonpolar state than for the polar state. As the concentration of the SCM increases, more binding sites became available. As more of the ANS probes occupied the polar binding sites, the overall emission intensity decreased gradually.

(33) M.J. Politi, J.H. Fendler, *J. Am. Chem. Soc*., 1984, **106**, 265.

(34) M. Lawrence, C.J. Marzzacco, C. Morton, C. Schwab, A.M. Halpern, *J. Phys. Chem*., 1991, **95**, 10294.

(35) K.M. Solntsev, Y.V. Ilichev, A.B. Demyashkevich, M.G. Kuzmin, *J. Photochem. Photobiol., A*, 1994, **78**, 39.

(36) Y.V. Ilichev, A.B. Demyashkevich, M.G. Kuzmin, *J. Phys. Chem*., 1991, **95**, 3438.

(37) K. Bhattacharyya, *Acc. Chem. Res*., 2002, **36**, 95.

(38) S.A. Einin, A.K. Zaitsev, N.K. Zaitsev, M.G. Kuzmin, *J. Photochem. Photobiol. A*, 1988, **41**, 365.

(39) D. Roy, R. Karmakar, S.K. Mondal, K. Sahu, K. Bhattacharyya, *Chem. Phys. Lett*., 2004, **399**, 147.

(40) P. Mukerjee, K. Banerjee, *J. Phys. Chem.,* 1964, **68**, 3567.

(41) M.S. Fernandez, P. Fromherz, *J. Phys. Chem*., 1977, **81**, 1755.

(42) S. Lukac, *J. Phys. Chem*., 1983, **87**, 5045.

(43) E. Kimura, H. Hashimoto, T. Koike, *J. Am. Chem. Soc*., 1996, **118**, 10963.

(44) R.A. Moss, K.G. Ragunathan, *Langmuir*, 1999, **15**, 107.

(45) R.A. Moss, W.G. Jiang, *Langmuir*, 2000, **16**, 49.

(46) F.M. Menger, C.E. Portnoy, *J. Am. Chem. Soc*., 1967, **89**, 4698.

(47) F.M. Menger, L.G. Whitesell, *J. Am. Chem. Soc*., 1985, **107**, 707.

(48) J. Catalan, J. Elguero, *Adv. Heterocycl. Chem*., 1987, **41**, 187.

(49) S. Zhang, Y. Zhao, *Chem. Commun*., 2012, **48**, 9998.

CHAPTER 3

HISTIDINE-FUNCTIONALIZED WATER-SOLUBLE NANOPARTICLES FOR BIOMIMETIC NUCLEOPHILIC/GENERAL-BASE CATALYSIS UNDER ACIDIC CONDITIONS

A paper published in *Organic and Biomolecular Chemistry*, **2013**, *11*, 6849-6855.

Geetika Chadha and Yan Zhao

Abstract

Cross-linking the micelles of 4-dodecyloxybenzyltripropargylammonium bromide by 1,4-diazidobutane-2,3-diol in the presence of azide-functionalized imidazole derivatives yielded surface-cross-linked micelles (SCMs) with imidazole groups on the surface. The resulting water-soluble nanoparticles were found, by fluorescence spectroscopy, to contain hydrophobic binding sites. The imidazole groups promoted the photo-deprotonation of 2-naphthol at pH 6 and catalyzed the hydrolysis of *p*-nitrophenylacetate (PNPA) in aqueous solution at pH > 4. Although the overall hydrolysis rate slowed down with decreasing solution pH, the catalytic effect of the imidazole became stronger because the reactions catalyzed by unfunctionalized SCMs slowed down much more. The unusual ability of the imidazole–SCMs to catalyze the hydrolysis of PNPA under acidic conditions was attributed to the local hydrophobicity and the positive nature of the SCMs.

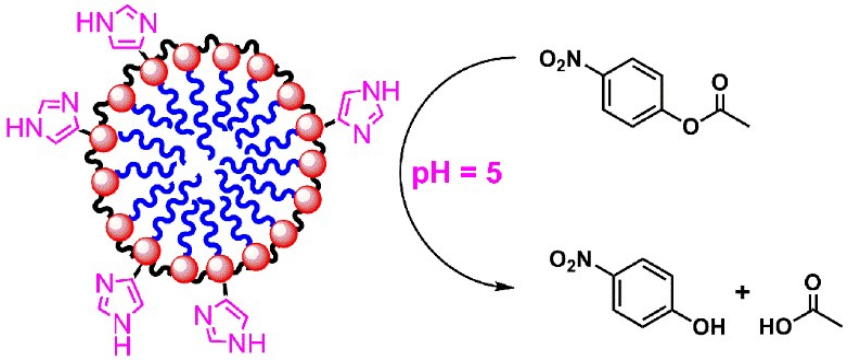

Introduction

Enzymes frequently perform chemical reactions under mild conditions that are difficult from a purely synthetic point of view—e.g., amide hydrolysis at physiological pH. The various functional groups in the enzyme active site are undoubtedly vital to the catalysis. On the other hand, because the active site differs greatly from the bulk aqueous solution where most enzymes reside, an enormous "environmental effect" also exists that relates to how differently these catalytic groups behave in the unique environment of the active site. For example, acids and bases are among the most common catalytic species in organic chemistry but strong acids and bases are not available in typical biological reactions. Many enzymes, not surprisingly, have developed remarkable capabilities to alter the pK_a of the functional groups used in catalysis. In acetoacetate decarboxylase, the amino side chain of a lysine in the active site has its pK_a shifted from 10.6 to 5.6, due to the electrostatic interactions of a proximal ammonium group (which repels an incoming proton) [1]. Similar pK_a shifts also occur in thiomethyl papain [2], subtilisin [3], and ribonuclease [4] for histidine.

Chemists have long been interested in creating synthetic systems mimicking key functions of enzymes, including their abilities to modify the acid/base properties of encapsulated

functional groups. Werner Nau et al. demonstrated the pK_a shift of cyclohexylmethyl amine by ion–dipole interactions with a cucurbit[6]uril host [5]. The same group later showed that sulfonated calixarenes could shift the pK_a of azoalkane guests and the pK_a shifts increased the binding affinity of the guests in acidic solution [6]. Raymond and co-workers assembled metal–organic nanocapsules with a hydrophobic interior and used them to perform acid-catalyzed hydrolysis of orthoformates and acetals in basic solution [7]. The seemingly impossible reactions were proposed to occur via the stabilization of the positively charged transition states by the highly negatively charged nanocapsules.

Our group recently reported a simple method for covalently capturing micelles of 4-dodecyloxybenzyltripropargyl-ammonium bromide (**1**) *via* the copper-catalyzed azide–alkyne cycloaddition (CuAAC) [8]. The click reaction employed in both the cross-linking and post-functionalization of the micelles ensured unparalleled functional-group-compatibility [9] and made the entire synthesis straightforward. Preparation of the final functionalized surface-cross-linked micelles (SCMs) is accomplished typically in a one-pot reaction at room temperature in water. The SCMs are versatile water-soluble nanoparticles with a number of interesting properties, including multivalency [8], facile surface-functionalization [8,10], encapsulation of hydrophobic guests [11], tunable surface potential [12], membrane permeability [13], and controlled release under chemical stimulation [11a,14]. More recently, the SCMs were found to have enhanced surface basicity as a result of their polycationic nature [15].

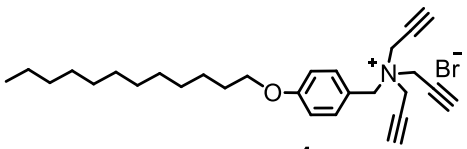

1

In this work, we decorated the SCMs with histidine derivatives [16]. The resulting materials resemble hydrolytic enzymes containing hydrophobic binding sites and catalytic functionalities. In both basic and acidic solution, these SCMs catalyzed the hydrolysis of an activated ester, presumably by the nucleophilic/general-base catalysis of the imidazole groups. Most importantly, the catalytic effect of the imidazole on the SCM surface was more pronounced in more acidic solutions, contrary to conventional expectations, which predicts that the imidazole groups would be protonated at lower pH and lose their catalytic activity.

Results and Discussion

Material Design and Synthesis

Our main objective in this study was to use the SCM as a platform to control the acid/base properties of functional groups for enzyme-mimetic catalysis. There are two general strategies to shift the pK_a of a functional group—hydrophobic interactions [17] and ionic interactions [18]. The former exploits the change in solvation when a chemical functionality undergoes protonation or deprotonation: because an ionic group is better solvated by polar solvents, it is more difficult to protonate an amine or deprotonate a carboxylic acid if the resulting ammonium ion or carboxylate is insufficiently solvated in a microenvironment. As mentioned earlier, the pK_a shift could also occur with specific ionic interactions: vicinal positive charges tend to make protonation more difficult and deprotonation easier.

The SCM should allow us to implement the above two strategies readily. Although water-soluble, the parent, unmodified SCM is dominated by hydrophobic functionalities [19]. Since the SCM of **1** carries numerous positive charges on the surface, protonation of amines attached to the SCM should be hindered electrostatically. Imidazole is on the side chain of L-histidine and is

commonly involved in hydrolytic enzymes. Its pK_a is close to seven, making both protonation of imidazole and deprotonation of imidazolium facile under physiological pH, at least in aqueous solution. The unprotonated imidazole is a good nucleophile and particularly useful in acyl-transfer reactions. If its protonation can be successfully altered by the SCM, we should expect an unusual catalytic behavior for the attached imidazole groups.

To construct imidazole–SCMs, we first prepared azide-functionalized L-histidine derivative **2**. The azide was installed to ensure covalent incorporation of the histidine functionality (Scheme 1). The C16 chain was included as a hydrophobic anchor. Because the azide is covalently attached to the SCM and the C16 chain needs to stay in the hydrophobic core of the SCM, the imidazole group should be close to the surface of the SCM instead of staying in the aqueous phase. Both a close distance to the positively charged micelle surface and strong environmental hydrophobicity, as mentioned above, should make the protonation of the imidazole difficult.

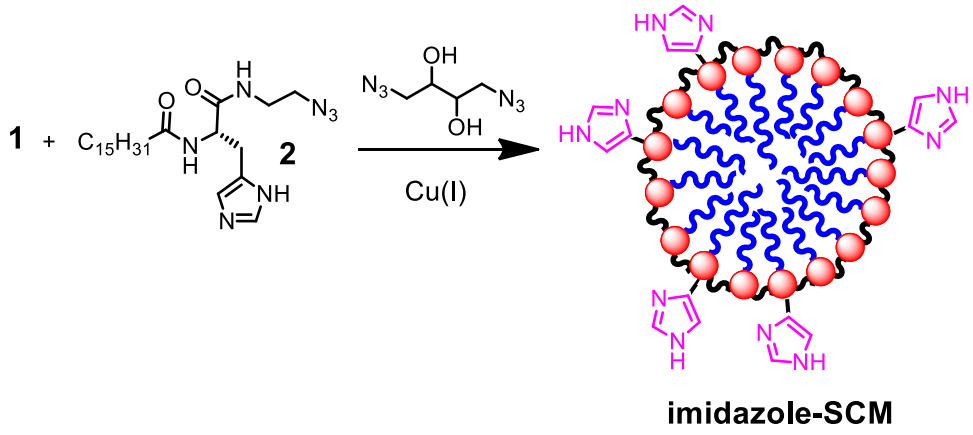

Scheme 1. Preparation of imidazole-functionalized SCM (imidazole-SCM).

The CMC of surfactant **1** is 0.14 mM in water [8,11a]. The imidazole–SCMs were prepared at [**1**] = 7.4 mM and [**2**] = 3.7 mM. The amount of 1,4-diazidobutane-2,3-diol was such that the overall ratio of alkyne/azide was ~1 : 1 to maximize the cross-linking density. The SCMs were typically characterized by ^{1}H NMR spectroscopy, dynamic light scattering, and FT-IR spectroscopy (see Experimental Section for details). The cross-linking chemistry and covalent structure of the SCMs have been previously characterized by mass spectrometry (after cleaving reversible cross-linkages on the SCMs) and TEM [8].

Characterization using Fluorescence Probes

Because the emission of many fluorophores is highly sensitive to their surroundings, they can be used to probe the hydrophobicity, acidity/basicity, and other environmental properties in their vicinity [20]. Since we are particularly interested in two aspects of the imidazole-functionalized SCMs (i.e., basicity and local hydrophobicity), we chose to study the SCMs using two fluorescent probes—2-naphthol and ANS (1-anilino-naphthalene-8-sulfonic acid, ammonium salt). The former is a photoacid with pK_a of 9.3 and 2.8 for the ground and the excited state, respectively [21]. Its excited-state proton transfer (ESPT) is known to be affected by a number of parameters, including local pH, polarity, and the interactions between the probes and their surroundings [21b,22]. ANS, on the other hand, is highly sensitive to environmental polarity, emitting weakly in water but strongly in a hydrophobic environment [23].

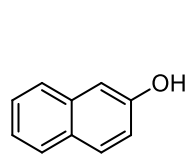

2-Naphthol

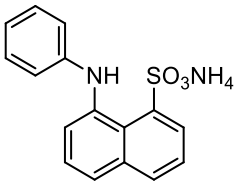

ANS

Fig. 1(a–c) shows the emission spectra of 2-naphthol in the presence of imidazole–SCMs, SCMs, and micelles of cetyl-trimethylammonium bromide (CTAB) in HEPES buffer at different pHs. The CTAB micelles were mostly used as a control to illustrate the effect of covalent fixation of the micelles. 2-Naphthol generally gives two emissive peaks at 355 and 420 nm, corresponding to the protonated and the deprotonated probe, respectively [21]. If ESPT is slow during the lifetime of the excited state, the acidic form at 355 nm will dominate. The faster the photo-deprotonation, the stronger the peak at 420 nm will be.

The emission of 2-naphthol in the different samples supports the local hydrophobicity and basicity of the imidazole– SCMs. Unlike 2-naphthol solubilized by the CTAB micelles (Fig. 1c) that was strongly affected by the solution pH, the probe bound to the SCMs (Fig. 1b) and particularly to imidazole–SCMs (Fig. 1a) displayed small to negligible changes at pH 6–8 [24]. We believe that the insensitivity of the latter two to pH reflects the better "shielding effect" of the cross-linked micelles [15]. A micelle is an assembly of surfactants that constantly exchanges surfactants with other micelles. A probe solubilized by a micelle, whether at the water–surfactant interface or in the interior of the micelle, is inevitably exposed to the aqueous solution during the dynamic assembling and exchanging processes. SCMs, on the other hand, are totally stable, covalent structures. When a probe is bound to an SCM, as long as it is located in a relatively hydrophobic environment after binding, its emission should reflect the property of the local binding site instead of that of the aqueous phase. Given the hydrophobicity of the probe, it is most likely located in a fairly hydrophobic region of the nanoparticle [15,25]. To the degree that the lack of pH-response in the 2-naphthol emission can be used as a measure for the shielding of

the probe from the aqueous solution, the shielding effect followed the order of imidazole–SCMs > SCMs > CTAB micelles.

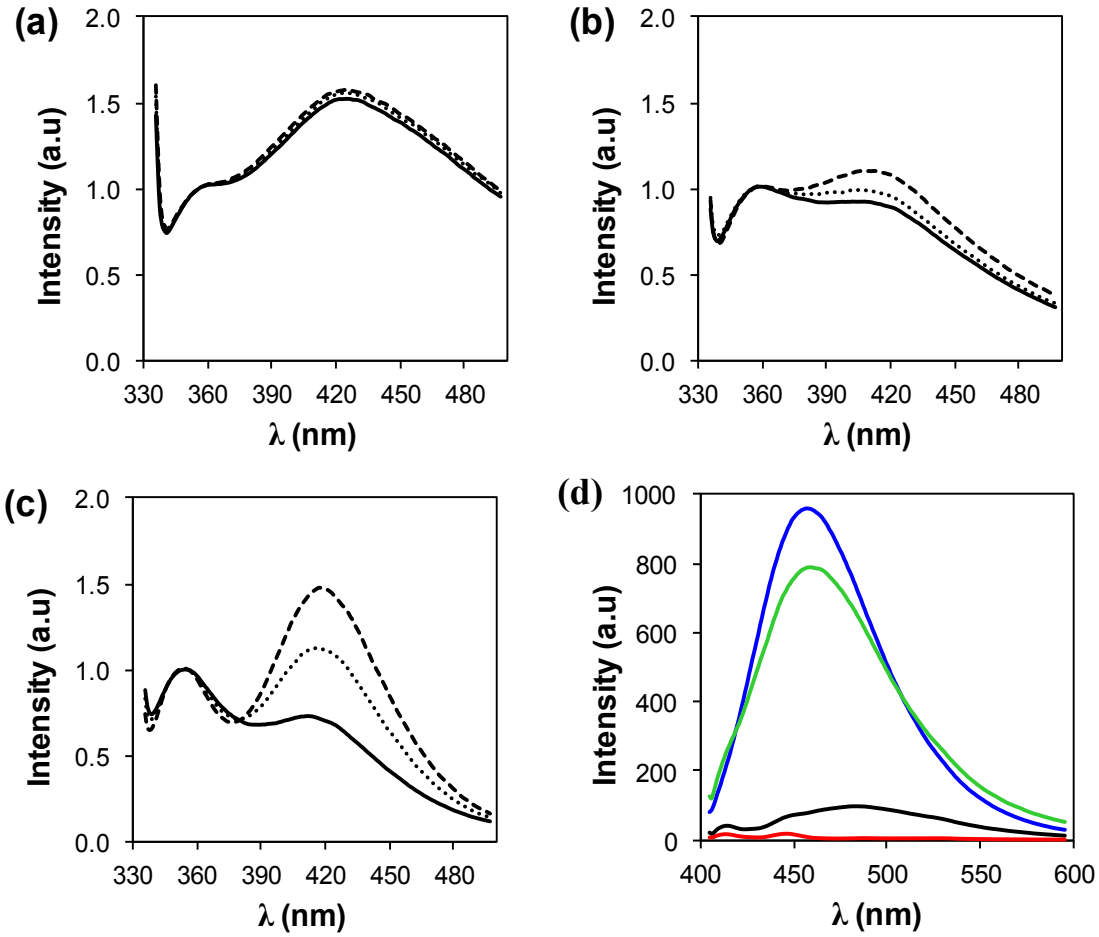

Fig. 1 Emission spectra of 2-napthol in aqueous solutions of (a) imidazole-SCM, (b) SCM, and (c) CTAB at pH = 6 (solid line), 7 (dotted line), and 8 (dashed line). [2-napthol] = 0.4 μM. [CTAB] = [cross-linked surfactant in the SCMs] = 1.2 mM. λ_{ex} = 315 nm. (d) Emission spectra of ANS in aqueous solutions of HEPES buffer (red line), CTAB (black line), SCMs (blue line), and imidazole-SCMs (green line) at pH = 7. [ANS] = 0.4 μM. [CTAB] = [cross-linked surfactant in SCM] = [cross-linked surfactant in imidazole-SCMs] = 1.2 mM. λ_{ex} = 388 nm.

Another observation in the fluorescence experiments was the strong ability of the imidazole–SCMs to promote photo-deprotonation of 2-naphthol. The deprotonated excited state (at 420 nm) dominated in all three pHs, even at pH 6 (Fig. 1a). As discussed above, the probe was expected to reside in a hydrophobic region of the cross-linked micelles [15,25]. Because the deprotonated species, i.e., the corresponding phenoxide and proton, are better solvated by water, photo-deprotonation in a hydrophobic environment is difficult [25]. This point makes the dominance of the phenoxide emission in Fig. 1a even more significant, as the probe is known to be located in a region not easily accessed by hydroxide ions and difficult for the deprotonation to occur. The result also implies that the observed fast ESPT in the imidazole–SCMs should result mainly from the attached imidazoles instead of bases located in the aqueous solution [26]. When Fig. 1a and 1c are compared, the effect of the imidazoles at pH 6 on the SCMs was comparable to that of the hydroxide ions in the CTAB case at pH 8, as far as the ESPT of 2-naphthol was concerned.

The local hydrophobicity of the SCMs was confirmed additionally by the polarity-sensitive ANS (Fig. 1d). The emission of this probe in HEPES buffer was extremely weak—a result of the fast nonradiative relaxation caused by the solvent [23]. Once bound to a CTAB micelle, ANS emitted more strongly, as expected from the higher environmental hydrophobicity. (It is known from fluorescence quenching that >95% 2-naphthol was bound by the micelles in CTAB micellar solution [27].) The emission wavelength of ANS has a strong dependence on the solvent polarity [28]. The emission wavelength (λ_{em} = 485 nm) of ANS bound to CTAB micelles was similar to that in ethylene glycol (λ_{em} = 484 nm), suggesting that the probe was located in a relatively polar environment of the micelle, possibly near the surface [29]. Note that the same concentration of ANS emitted much more strongly in the presence of SCMs and imidazole–

SCMs and the emission shifted to the blue in comparison to that in the CTAB solution (Fig. 1d). Clearly, the probe was in a more hydrophobic environment when bound to the covalently fixed micelles. Related to some earlier discussions, if the ionic ANS was located in a hydrophobic environment when bound to SCM, it is not surprising that the neutral probe, 2-naphthol, could do at least the same.

Catalysis of the Hydrolysis of PNPA

The fluorescence study gave us confidence that the hydrophobicity and positive charges of the SCMs indeed strongly influenced the acid/base properties of the attached imidazoles. We then decided to investigate the hydrolysis of PNPA catalyzed by the functionalized SCMs. Fig. 2 shows the UV-Vis spectra of PNPA in the presence of imidazole–SCMs and SCMs at pH 6 over a period of 1 h. The background rate of hydrolysis for PNPA at this pH was negligible (data not shown). In the presence of SCMs, a distinctive peak appeared near 400 nm corresponding to *p*-nitrophenolate, with the imidazole–SCMs being clearly more potent catalysts than the unfunctionalized SCMs.

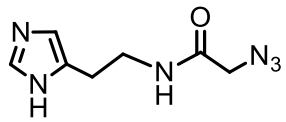

3

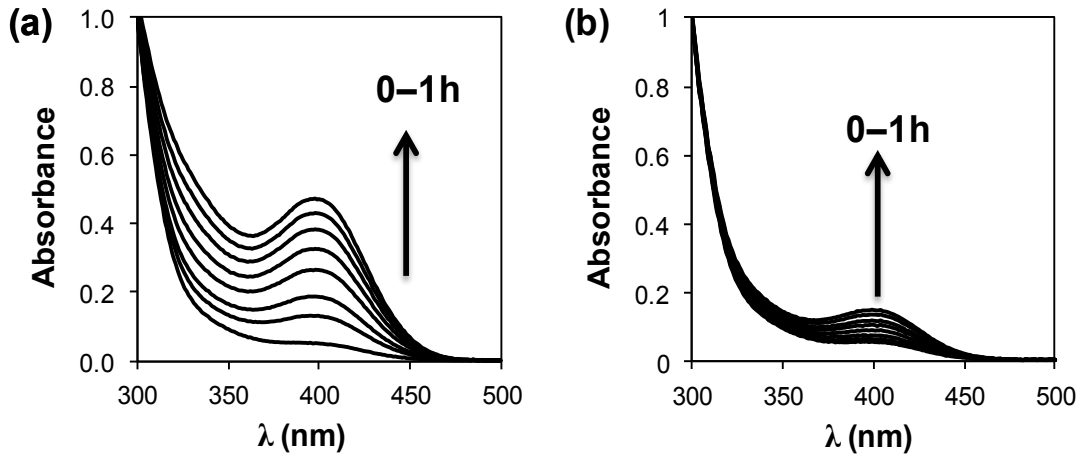

Fig. 2 UV-Vis spectra of an aqueous solution of PNPA in HEPES buffer over a period of 1 h in the presence of (a) imidazole-SCMs and (b) SCMs at pH 6 at 35 °C. [PNPA] = 0.2 mM. [cross-linked surfactant in imidazole-SCMs] = [cross-linked surfactant in SCMs] = 0.4 mM.

The absorbance at 400 nm could be fitted to first-order kinetics to give the rate constants of the hydrolysis. Table 1 summarizes all the kinetic data obtained in this study. For comparison purposes, we also prepared imidazole*–SCMs from compound **3** and cross-linkable surfactant **1**, following identical procedures as those for the synthesis of imidazole–SCMs. Our expectation was that, without the C16 chain (attached to **3**), it should be easier for the imidazole groups on the surface of the resulting SCMs to move into the aqueous phase. If local hydrophobicity is important to the catalysis of the imidazole groups, imidazole and imidazole*–SCMs should behave differently. In addition, we varied the density of the catalytic groups on the micelle surface of imidazole*–SCMs, with the relative percentage of the imidazole to surfactant **1** increased from 25% to 50% to 75%. We used compound **3** for this purpose because its better water-solubility enabled us to achieve high surface coverage. The kinetic experiments were repeated three times and the errors in the data were generally <5%.

According to Table 1, the rate constants increased generally with the solution pH, whether for the imidazole-functionalized SCMs, SCMs, CTAB micelles, or other controls (imidazole or a physical mixture of imidazole and SCMs). This trend should just reflect the higher concentration of the nucleophile (hydroxide) at higher pH. When multiple imidazole groups are in close proximity, the imidazole groups sometimes display cooperative catalysis [30] (i.e., general acid/general base or nucleophilic catalysis). Such catalysis, however, normally displays a maximum near the pK_a of imidazole, unlike the monotonous decrease of hydrolysis rate with decreasing pH (see more discussions toward the end of the paper) [30b].

Another consistent trend, observed at all pHs, was the rate of hydrolysis in the order of imidazole–SCM > imidazole*–SCM > (imidazole + SCM) > SCM > CTAB [31]. The higher catalytic activity of the unfunctionalized SCMs over CTAB micelles originated from the stronger surface basicity of the former, as revealed in another study [15]. The imidazole groups were clearly helpful, since both imidazole-functionalized SCMs gave faster hydrolysis than the parent SCMs. Related to a point made earlier, the hydrolytic rate constants for PNPA in the CTAB solution at pH 8 (entry 30) and in the imidazole–SCM solution at pH 6 (entry 13) were comparable, similar to what occurred in the ESPT of 2-naphthol with the two systems.

Table 1. Rate constants for the hydrolysis of PNPA in aqueous buffer catalyzed by the SCMs and CTAB micelles at 35 °C.[a]

Entry	Micelle	Solution pH	$k \times 10^5$ (min^{-1})	k/k_{SCM}
1	imidazole-SCM	4	20	40[c]
2	imidazole*-SCM	4	10	20[c]
3	SCM	4	0.5[b]	1.0
4	CTAB	4	---	---
5	imidazole-SCM	5	300	15
6	imidazole*-SCM	5	270	13.5
7	SCM	5	20	1.0
8	CTAB	5	~2[b]	---
9	imidazole-SCM	6	740	3.2
10	imidazole*-SCM	6	580	2.5
11	SCM	6	230	1.0
12	CTAB	6	10	---
13	imidazole-SCM	7	1870	2.4
14	imidazole*-SCM	7	1270	1.6
15	SCM	7	770	1.0
16	CTAB	7	180	---
17	imidazole-SCM	8	5750	3.0
18	imidazole*-SCM	8	4080	2.1
19	SCM	8	1930	1.0
20	CTAB	8	820	---
21	imidazole*-SCM	7	2360[d]	---
22	imidazole*-SCM	7	2840[e]	---

[a] Imidazole-SCMs were prepared from compounds **1** and **2**; imidazole*-SCMs were prepared from compounds **1** and **3**. The concentration of the cross-linked surfactant was 0.4 for all the SCMs. The concentration of CTAB was 1.2 mM. The relative percentage of the imidazole to **1**

was 25% unless otherwise noted. [b] The reaction rate was too slow to be measured accurately. [c] These ratios were not accurate because the PNPA hydrolysis rate catalyzed by the SCMs was too slow to be measured accurately. [d] The relative percentage of the imidazole to **1** on the SCM surface was 50%. [e] The relative percentage of the imidazole to **1** on the SCM surface was 75%.

Table 1 also gives the relative rates of imidazole–SCMs over those of SCMs (i.e., k/k_{SCM}). Because the functionalized SCMs and the parent SCMs had similar structures other than the presence of histidine groups, we could treat k/k_{SCM} as an indicator of the catalytic effect of imidazole groups on the SCMs. When k/k_{SCM} was plotted against the solution pH, an interesting and unusual trend was revealed (Fig. 3a). The ratio was fairly constant at pH 6–8 but increased dramatically at pH 4 and 5. This, to us, was the most exciting result in this study. The imidazole group of histidine has a pK_a of 6.8. At least in water, its catalysis should be more pronounced at pHs where there is a substantial population of the un-protonated form (i.e., pH = 7 or 8, see Table 1, entries 23 and 29). The fact that k/k_{SCM} was larger at pH = 4 and 5 suggests that a substantial population of the imidazole groups was un-protonated on SCMs under these acidic conditions, in agreement with the fluorescence study.

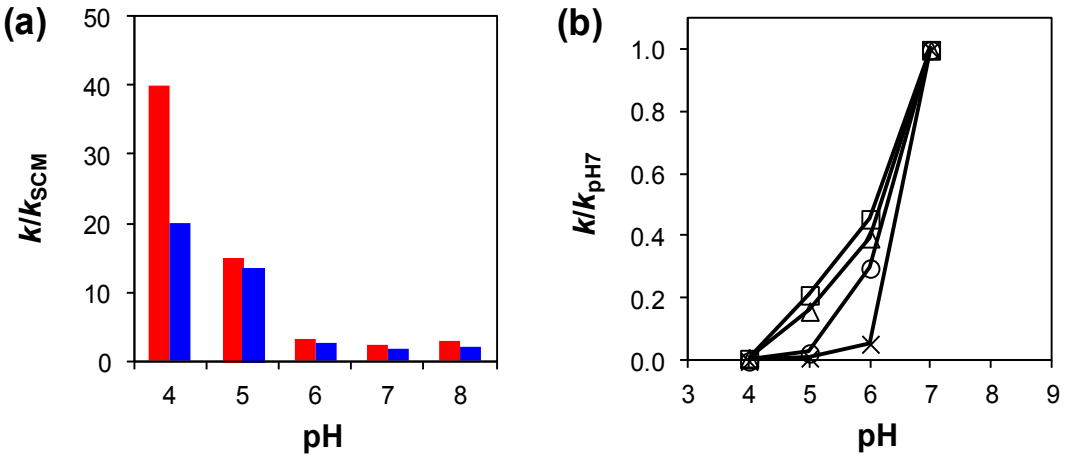

Fig. 3 (a) Relative rate constants of PNPA hydrolysis catalyzed by imidazole-SCMs (red bars) and imidazole*-SCMs (blue bars) over those catalyzed by SCMs. (b) Rate of hydrolysis normalized to that at pH 7 for imidazole-SCMs (△), imidazole*-SCMs (□), SCMs (○), and CTAB micelles (×).

It should be also pointed out that the imidazole–SCMs consistently outperformed imidazole*–SCMs in catalyzing PNPA hydrolysis at all pHs (Fig. 3a). The result suggests that our initial hypothesis was correct. In other words, the C16 chain did serve as a hydrophobic anchor for the imidazole groups. When located in a more hydrophobic local environment, possibly closer to the positively charged micellar surface, the imidazole groups were more resistant toward protonation and thus more effective in the catalysis. What was interesting was that the largest "hydrophobic anchoring effect" (i.e., the largest difference between imidazole/SCMs and imidazole*–SCMs) was observed at pH 4 (Table 1, entries 1 and 2, also Fig. 3a). This observation is consistent with the earlier explanation that the unusual catalysis of the imidazole–SCMs originated from hindered protonation of the imidazole groups by the local hydrophobicity and positive charges.

At all pHs, both imidazole–SCMs and imidazole*–SCMs gave faster hydrolysis than the physical mixture of imidazole and SCMs (i.e., imidazole + SCM). Thus, covalent attachment was better than mere mixtures. In the meantime, our data clearly show that non-covalently bound imidazole could work together with SCMs, as the physical mixture worked better than either imidazole or SCMs. At lower pHs (pH = 5 and 6), there was some synergism between the two, since the rate constant for the mixture was larger than the combined rate constants for imidazole

and SCMs (entries 9–11 and 15–17). Presumably, SCMs could bind both imidazole and PNPA, facilitating their reaction as a result.

As mentioned above, hydrolysis slowed down generally as the solution became more acidic. It is the slower decrease of the reaction rate in the imidazole–SCMs that is significant. The trend can be seen more clearly in Fig. 3b, in which each rate constant for a catalyst was normalized to that of the same catalyst at pH 7. According to the normalized rates, in the case of CTAB micelles (×), a change of solution pH from 7 to 6 caused a precipitous drop in the hydrolysis rate—a result attributed to a decrease of hydroxide concentration on the micellar surface. The same was observed for imidazole in solution (see Table 1 for details, data not shown in Fig. 3b for clarity). For the SCMs (O), the precipitous drop was "delayed" to pH 5. The result was in agreement with our previous finding of the higher surface basicity of SCMs [15]. As shown by Fig. 3b, the precipitous drop was delayed even more in the imidazole-functionalized SCMs, to pH 4 [32]. These results demonstrate that a systematic fine tuning of surface basicity could be easily achieved on the SCM platform by taking advantage of its surface potential, covalent structure, and facile functionalization.

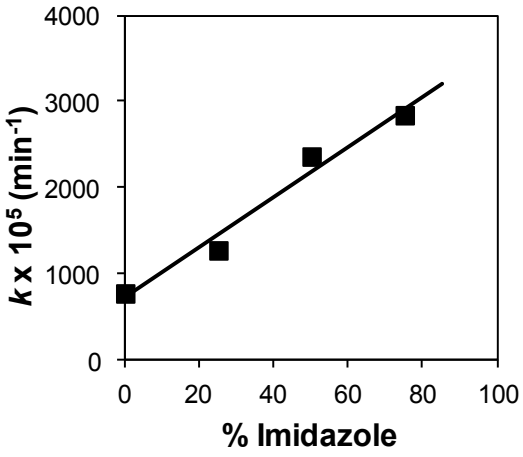

Fig. 4 Rate constant of the PNPA hydrolysis catalyzed by imidazole*-SCMs as a function of the percentage of imidazole with respect to surfactant **1**. pH = 7.

A distinct advantage of the SCM is its easy multifunctionalization [8,10]. Because imidazole groups sometimes display cooperative catalysis in multifunctionalized systems [30], we measured the rate of PNPA hydrolysis as a function of imidazole coverage on the SCM surface (Fig. 4). The imidazole*–SCMs were simply prepared by varying the ratio of [**3**]/[**1**] in the synthesis and the materials were purified in a similar manner. Since the concentration of the cross-linked surfactant was kept the same (0.4 mM), the concentration of the imidazole groups increased monotonously in the resulting SCMs. The linear relationship between the rate of PNPA hydrolysis and the percentage of imidazole on the SCM surface in Fig. 4 indicates that the catalytic groups worked individually. It appears that the imidazoles were too far away on these SCMs to perform cooperative catalysis.

Conclusions

This work demonstrates that the SCM could be used as a platform not only for installing catalytic groups but also to modulate the chemical reactivity of these groups. For the imidazole-functionalized cross-linked micelles, the local hydrophobicity and the positive nature of the SCM altered the reactivity of the functionality significantly. The catalytic effect of the attached imidazoles, for example, was maintained and became even stronger at lower pHs. This result underscores the importance of the environmental effect in catalysis. Chemists traditionally seek active catalysts by manipulating the catalytic center (e.g., a transition metal with its first-sphere ligands or organic catalytic groups). Environmental effects are now being recognized as another

vital factor [33]. Exemplified most elegantly in enzymatic catalysis, the unique microenvironment of the catalytic groups can have a profound impact on their behavior and is a large contributor to the observed selectivity and/or activity. Enzymes frequently perform seemingly impossible reactions under mild conditions. As chemists better understand the environmental control of catalysis, we should be able to use these biomimetic strategies to achieve transformations that are otherwise difficult.

Experimental Section

General

All reagents and solvents were of ACS-certified grade or higher and used as received from commercial suppliers. Millipore water was used to prepare buffers and nanoparticles. ^{1}H and ^{13}C NMR spectra were recorded on a VARIAN MR-400 or on a BRUKER AV III-600 spectrometer. Dynamic light scattering (DLS) was performed on a PD2000DLSPLUS dynamic light scattering detector. Mass spectrometry was performed on AGILENT 6540 QTOF mass spectrometer. Fourier-Transform Infrared (FT-IR) Spectra were recorded on a BRUKER IFS 66V spectrometer. UV-Vis spectra were recorded on a Cary 100 Bio UV-Visible spectrophotometer and fluorescence spectra were recorded on a Varian Cary Eclipse Fluorescence spectrophotometer.

Material Synthesis

The preparation and the characterization of the SCMs were reported previously [8]. A typical procedure for the preparation of the imidazole–SCMs is as follows. Compound **2** (0.0068 mmol), 1,4-diazidobutane-2,3-diol (4.7 mg, 0.027 mmol), $CuCl_2$ (10 μL of a 9 mg mL^{-1} aqueous

solution, 0.5 μmol), and sodium ascorbate (100 μL of a 13 mg mL^{-1} aqueous solution, 5 μmol) were added to a micellar solution of **1** (10 mg, 0.02 mmol) in Millipore water (2.5 mL). The reaction mixture was stirred slowly at room temperature for 24 h after which the mixture was dialyzed for 3 days against deionized water using 500 Da molecular weight cut-off tubing. The characterization of the functionalized-SCMs is reported below.

Fluorescence Study

A typical procedure for the fluorescence experiment is as follows. Stock solutions of the SCM (with a concentration of the cross-linked surfactant of 2.0 mM), ANS (80 μM), and 2-naphthol (80 μM) in Millipore water were prepared. An aliquot (1.20 mL) of the SCM solution was added to a cuvette containing 800 μL of HEPES buffer (25 mM, pH = 7), followed by an aliquot (100 μL) of the stock solution of the appropriate dye. After the sample was vortexed briefly, the cuvette was placed in the spectrometer and equilibrated to 35.0 °C. The fluorescence spectrum was recorded with excitation wavelengths for ANS and 2-naphthol of 388 and 315 nm, respectively. The same procedure was repeated for the SCM and CTAB samples. Triplicate data were generally collected for each sample.

Kinetic Measurement

p-Nitrophenyl acetate (PNPA, 50 mg) was dissolved in 10 mL of methanol. The methanol stock solution (10 mM) was stored in a refrigerator and used within a week. For the kinetic experiments, aliquots of the SCM solution were added to a series of cuvettes containing 800 μL of HEPES buffer (25 mM, pH = 4, 5, 6, 7, 8). The concentration of the (cross-linked) surfactant in the SCM solution was 1.2 mM. The cuvettes were placed in the UV-Vis

spectrometer and equilibrated to 35.0 °C. After 5 min, aliquots (40 μL) of the PNPA aqueous solution, prepared freshly each day by mixing 3.7 mL of the methanol PNPA stock solution with 6.3 mL of deionized water, were added to the cuvettes. The hydrolysis was monitored by the absorbance of *p*-nitrophenolate at 400 nm over a period of 66 min. The experiments were generally repeated three times for each sample.

Syntheses

Scheme 2. Synthesis of compound **2**

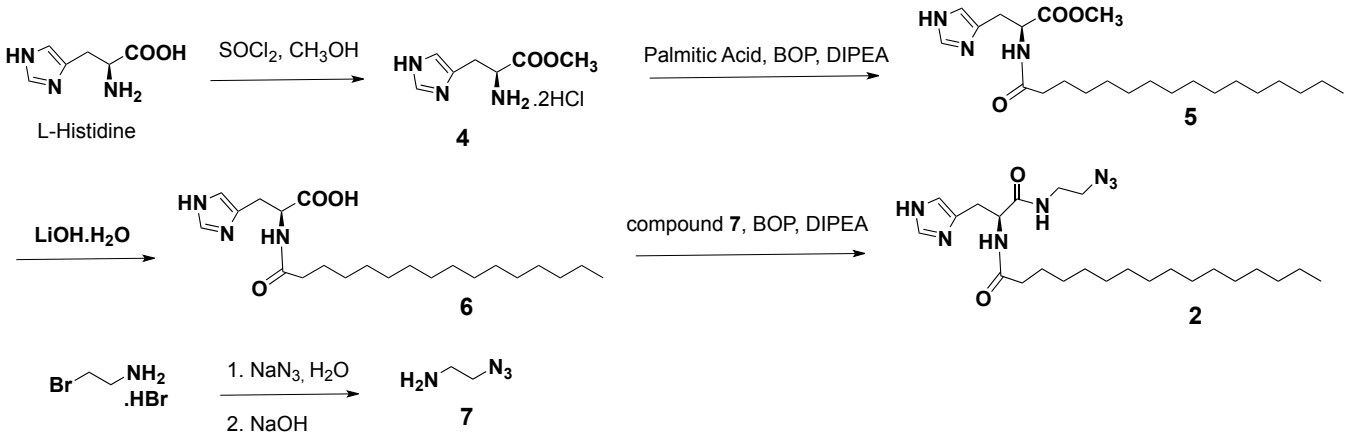

Scheme 3. Synthesis of compound **3**

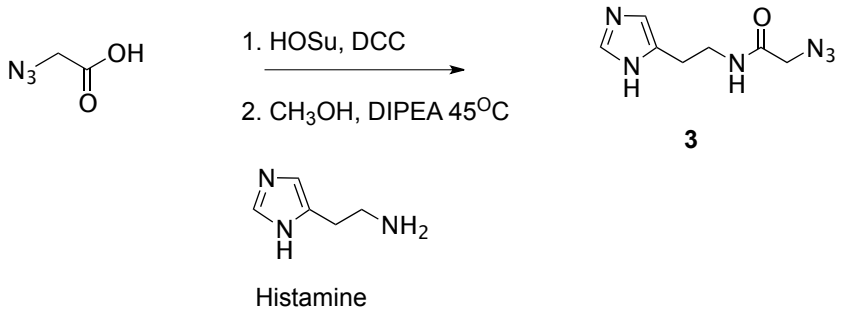

Compound 4 [34]**.** Thionyl chloride (11.5 g, 97.1 mmol) was added dropwise to a solution of L-histidine (1.51 g, 9.71 mmol) in anhydrous MeOH (40 mL) at 0 ºC under nitrogen atmosphere. The reaction mixture was heated to refluxed for 16 h and then allowed to cool to room temperature. The organic solvent was removed by rotary evaporation to yield a pale yellow solid (2.23 g, 95%). ^{1}H NMR (400 MHz, CD_3OD, δ): 8.93 (s, 1H), 7.53 (s, 1H), 4.45 (t, J = 6.8 Hz, 1H), 3.85 (s, 3H), 3.42 (qd, J = 15.7, 6.9 Hz, 2H).

Compound 5. *N,N*-Diisopropylethylamine (DIPEA, 2.80 mL, 16.4 mmol) was added dropwise to a solution of compound **4** (1.00 g, 4.13 mmol), palmitic acid (1.06 g, 4.13 mmol), and BOP (3.65 g, 8.26 mmol) in anhydrous DMF (5 mL) at 0 ºC. The reaction mixture was warmed to room temperature and reacted at 100 ºC in microwave oven (power = 150 watt) for 40 min. After allowing to it cool to room temperature, the reaction mixture was poured into 1M HCl (~20 mL) over a period of 5 min. A light brown precipitate was obtained upon neutralization of the reaction mixture via drop-wise addition of saturated aqueous $NaHCO_3$. The precipitate was collected by vacuum filtration and re-dissolved in $CHCl_3$ (20 mL), washed with brine (2 × 20 mL), dried with sodium sulfate, and concentrated under reduced pressure. The crude mixture was further purified by silica gel column chromatography using 1: 10 methanol/CH_2Cl_2 as eluent to afford the pure product as a white solid (1.11 g, 63 %). ^{1}H NMR (400 MHz, CD_3OD, δ): 7.56 (s, 1H), 6.84 (s, 1H), 4.67 – 4.63 (q, 1H), 3.68 (s, 3H), 3.11 – 2.92 (m, 2H), 2.17 (t, J = 7.2 Hz, 2H), 1.57 – 1.49 (m, 2H), 1.27 (m, 24H), 0.88 (t, J = 6.7 Hz, 3H). ^{13}C NMR (100 MHz, CD_3OD, δ) 176.23, 173.50, 136.30, 53.94, 52.68, 36.71, 33.09, 30.82, 30.81, 30.78, 30.75, 30.64, 30.49, 30.46, 30.15, 30.08, 26.87, 23.75, 14.46. ESI-HRMS (*m/z*): $[M + H]^+$, calcd for $C_{23}H_{42}N_3O_3^+$, 408.3221; found 408.3218.

Compound 6. Compound **5** (100 mg, 0.25 mmol) obtained in the above procedure was dissolved in MeOH (3 mL). A solution of 2 M LiOH (1.00 mL, 1.85 mmol) was added. The reaction was monitored by TLC and was complete in 6–10 h. The organic solvent was removed by rotary evaporation. The resulting solution was neutralized by drop-wise addition of 2M HCl solution (~3 mL). The reaction mixture was concentrated under reduced pressure and the pure product was obtained as a pale white solid (0.087 g, 90%). ^{1}H NMR (400 MHz, CD_3OD, δ): 8.70 (s, 1H), 7.28 (s, 1H), 4.64 – 4.61 (q, 1H), 3.11 (m, 1H), 2.22 – 2.15 (m, 2H), 1.51 (t, J = 7.1 Hz, 2H), 1.24 (m, 24H), 0.85 (t, J = 6.8 Hz, 3H). ^{13}C NMR (100 MHz, CD_3OD, δ): 176.10, 172.40, 134.58, 132.04, 118.09, 54.18, 36.97, 32.97, 30.69, 30.67, 30.65, 30.56, 30.54, 30.39, 30.36, 30.21, 28.75, 26.80, 23.65, 14.44.

Compound 7 [35]**.** Sodium azide (1.58 g, 24.4 mmol) was added to solution of 2-bromoethanamine hydrobromide (2.00 g, 9.76 mmol) in H_2O (12 mL) and the resulting solution was stirred for 10 h at 75 ºC. After cooling to room temperature, sodium hydroxide (1.90 g, 45.0 mmol) was added and stirred for another 5 minutes. The solution was then extracted with ether (5 × 15 mL). The collected organic layer was washed with brine (2 × 20 mL), dried with sodium sulfate and concentrated by rotary evaporation to give a colorless liquid (0.58 mg, 69%). ^{1}H NMR (400 MHz, $CDCl_3$, δ): 3.37 (t, J = 5.7 Hz, 2H), 2.88 (q, J = 5.7 Hz, 2H), 1.45 (bs, 2H).

Compound 2. *N,N*-Diisopropylethylamine (DIPEA, 0.46 mL, 2.65 mmol) was added drop-wise to a solution of compound **6** (0.21 g, 0.53 mmol), 2-azidoethanamine (0.05 g, 0.53 mmol), BOP (0.47 g, 1.06 mmol), and HOBt (0.14 g, 1.06 mmol) in anhydrous DMF (2 mL) at 0 ºC. The reaction mixture was warmed to room temperature and reacted at 100 ºC in microwave oven (power = 150 watt) for 40 min. After allowing it to come to room temperature, the reaction

mixture was slowly poured into 1M HCl (~20 mL). A sticky light brown precipitate was obtained upon neutralization of the reaction mixture via drop-wise addition of saturated aqueous $NaHCO_3$. The precipitate was collected by vacuum filtration and then re-dissolved in $CHCl_3$ (20 mL), washed with brine (2 × 20 mL), dried with sodium sulfate and concentrated under reduced pressure. The crude mixture was further purified by silica gel column chromatography using 1: 8 methanol/CH_2Cl_2 as eluent to afford a white solid product (1.61 g, 66 %). ^{1}H NMR (600 MHz, CD_3OD, δ): 7.76 (s, 1H), 6.91 (s, 1H), 4.60 – 4.57 (q, 1H), 3.29 (m, 4H), 3.09 (dd, *J* = 15.2, 5.9 Hz, 1H), 2.93 – 2.88 (m, 1H), 2.17 (t, *J* = 7.9 Hz, 2H), 1.54 – 1.49 (m, 2H), 1.26 (m, 24H), 0.88 (t, *J* = 7 Hz, 3H). ^{13}C NMR (150 MHz, CD_3OD, δ) 176.27, 173.24, 135.65, 133.11, 118.21, 54.14, 51.37, 39.91, 36.82, 33.06, 30.78, 30.74, 30.60, 30.45, 30.23, 29.37, 26.77, 23.72, 14.42. ESI-HRMS (*m/z*): $[M + H]^+$ calcd for $C_{24}H_{44}N_7O_2^+$, 462.3551; found 462.3549.

Compound 3. *N,N′*-Dicyclohexylcarbodiimide (DCC, 2.51 g, 12.4 mmol) was added to a solution of 2-azidoacetic acid [36] (1.21 g, 12.4 mmol) and *N*-hydroxysuccinimide (1.41 g, 12.4 mmol) in acetonitrile (8 mL) at 0 ^{O}C. The reaction was stirred overnight at room temperature, under nitrogen. The precipitate formed was removed by suction filtration. The filtrate was concentrated by rotary evaporation solid product that was used directly for next step (2.41 g, 98%). ^{1}H NMR **(**400 MHz, $CDCl_3$, δ): 4.24 (s, 2H), 2.86 (s, 4H).

The above-prepared activated ester of 2-azidoacetic acid (0.21 g, 1.11 mmol) and histamine (0.75 g, 0.65 mmol) were dissolved in a mixture of anhydrous acetonitrile (3 mL) and methanol (1 mL). K_2CO_3 (0.49 mg, 3.61 mmol) and added to reaction mixture. The solution was stirred overnight at 45 ºC. After cooling to room temperature, the reaction mixture was filtered using vacuum and the filtrate was concentrated by rotary evaporation. The residue obtained was

purified by column chromatography over silica gel using 1: 7 methanol/CH_2Cl_2 to afford a brown solid (0.09 g, 68%). ^{1}H NMR (400 MHz, $CDCl_3$, δ): 7.60 (s, 1H), 6.85 (s, 1H), 3.95 (s, 2H), 3.62 – 3.56 (q, 2H), 2.83 (t, 2H). ^{13}C NMR (100 MHz, $CDCl_3$, δ) 166.73, 134.86, 52.77, 39.19, 26.85. ESI-HRMS (*m/z*): $[M + H]^+$ calcd for $C_7H_{11}N_6O^+$, 195.0989; found 195.0990.

DLS Study

Preparation of DLS sample: 100 μL of the prepared imidazole-SCM solution was taken out and diluted to 1 mL by Millipore water. The diluted solution was used as the sample of DLS.

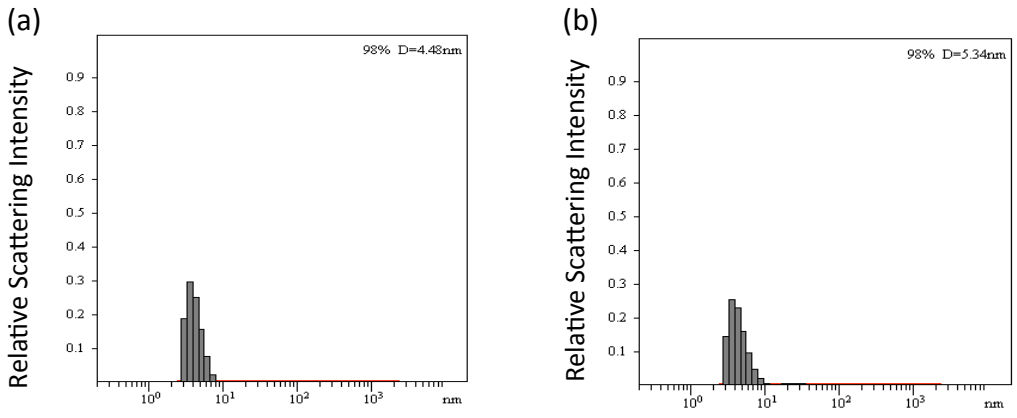

Fig. 5 Distribution of the hydrodynamic diameters of (a) imidazole-SCM and (b) imidazole*-SCM after MW normalization. MW normalization provides a concentration normalized distribution of particles, as large particles scatter much more than small particles even when they are present in very small concentration. The MW-normalized size distribution was calculated by the PRECISION DECONVOLVE program assuming the intensity of scattering is proportional to the mass of the particle squared.

^{1}H NMR Study

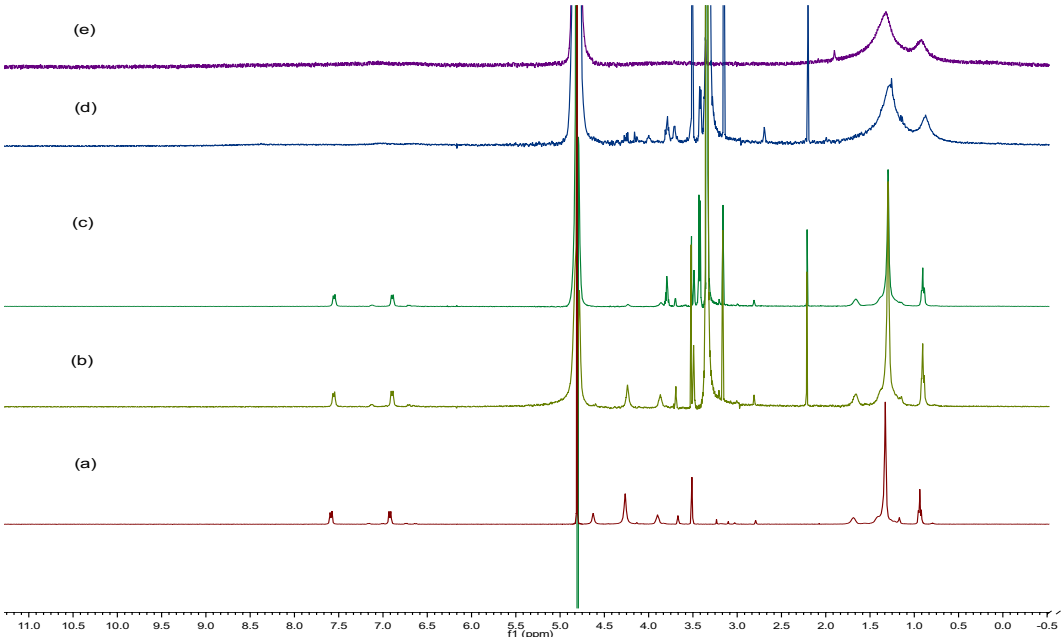

Fig. 6 Comparison of ^{1}H NMR of imidazole-SCM samples: ^{1}H NMR spectra of a 10 mM micellar solution of **1** (a) in D_2O, (b) after addition of 25% of surfactant **2**, (c) after addition of **1** equiv. of diazide cross-linker, (d) after cross-linking, and (e) after dialysis to remove water-soluble impurities.

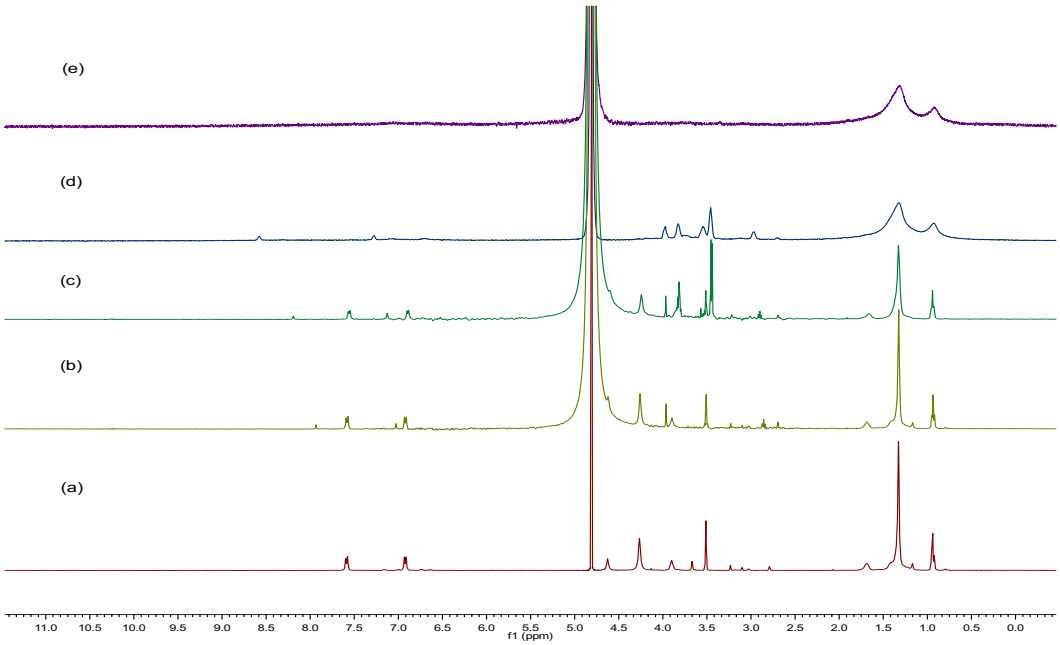

Fig. 7 Comparison of ^{1}H NMR of imidazole*-SCM samples: ^{1}H NMR spectra of a 10 mM micellar solution of **1** (a) in D_2O, (b) after addition of 25% of ligand **3**, (c) after addition of **1** equiv. of di-azide cross-linker, (d) after cross-linking, and (e) after dialysis to remove water-soluble impurities.

FT-IR Study

Preparation of FT-IR sample: The preparation of Imidazole-SCM was as follows. After dialysis (MWCO ca. 6000-8000 Da), the resultant light yellow transparent solution was evaporated by a vacuum pump at -58 °C for 2 day. The obtained white solid was subjected to the FTIR measurement (KBr pellets).

(a)

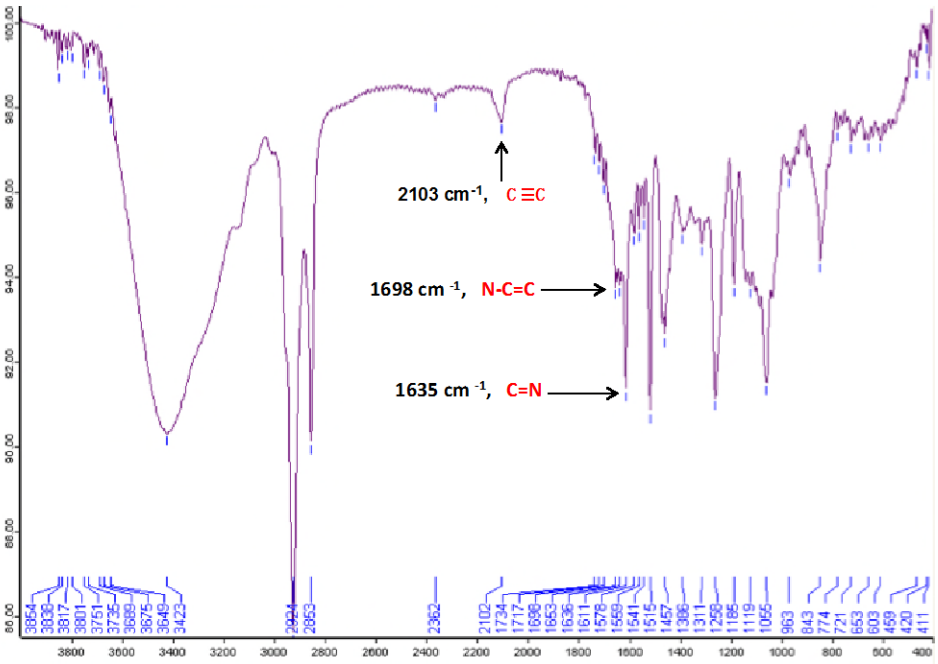

(b)

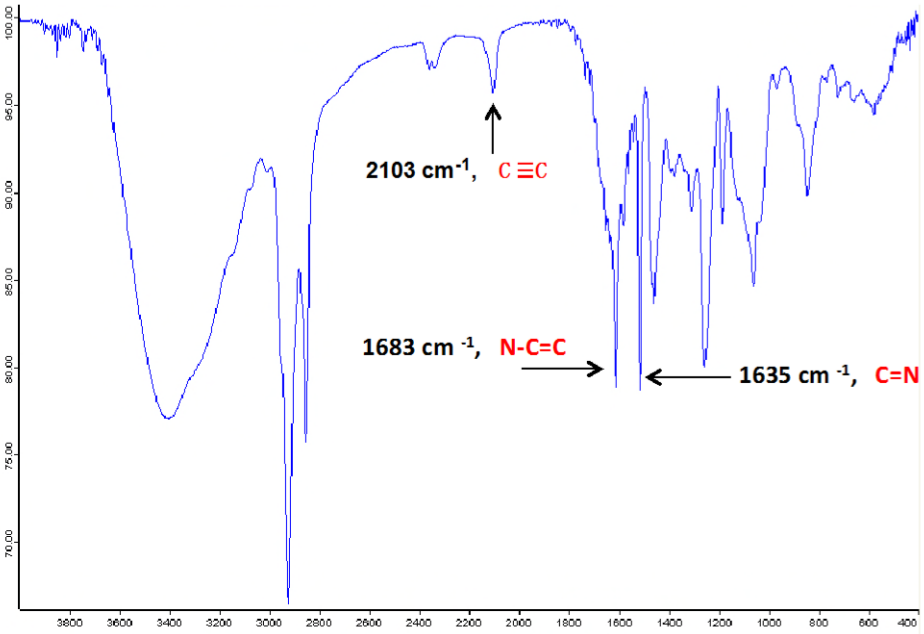

Fig. 8 Infrared spectra of (a) imidazole-SCM and (b) imidazole*-SCM.

^{1}H NMR spectrum of compound **4**

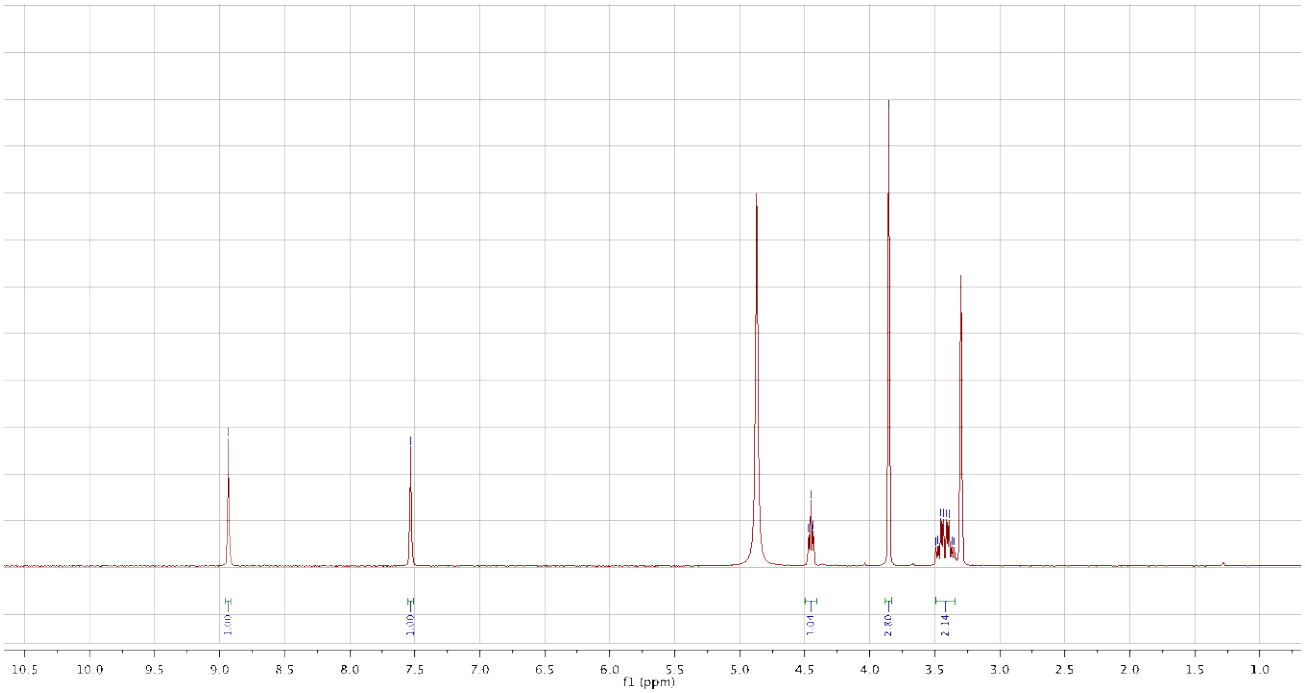

^{1}H NMR spectrum of compound **5**

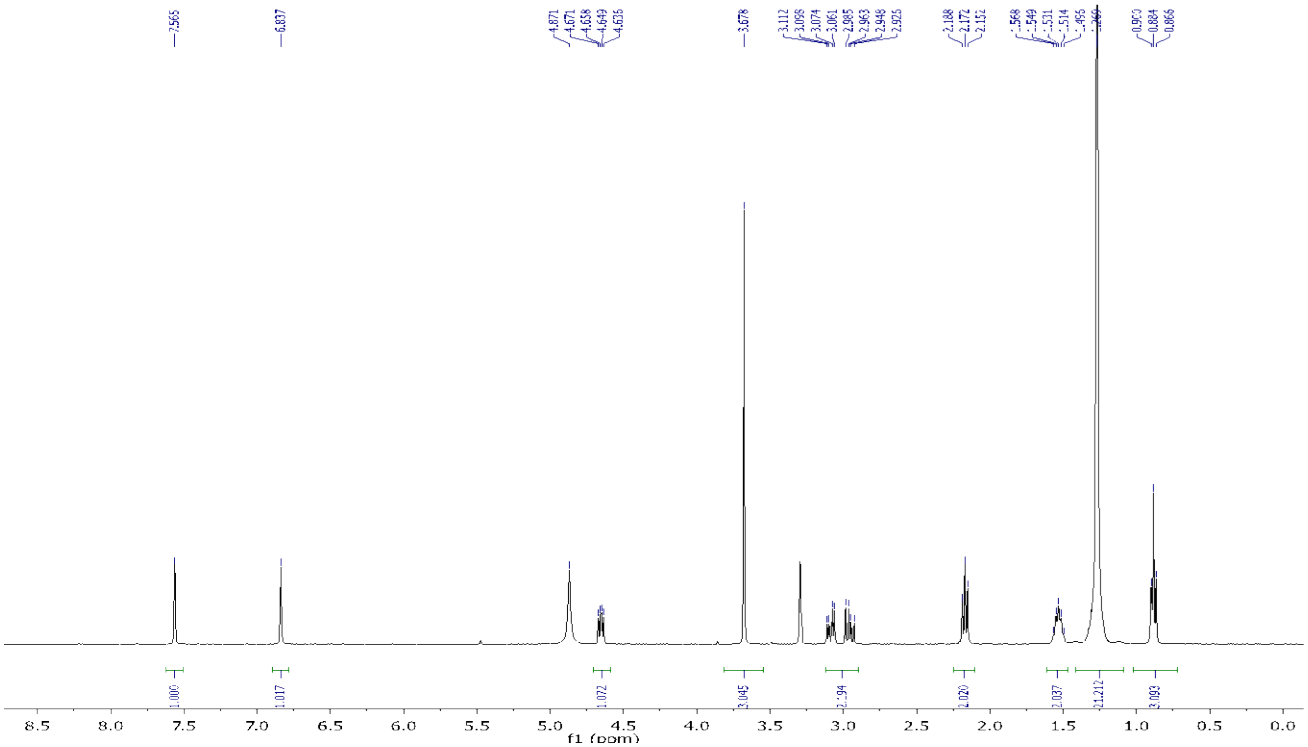

^{13}C NMR spectrum of compound **5**

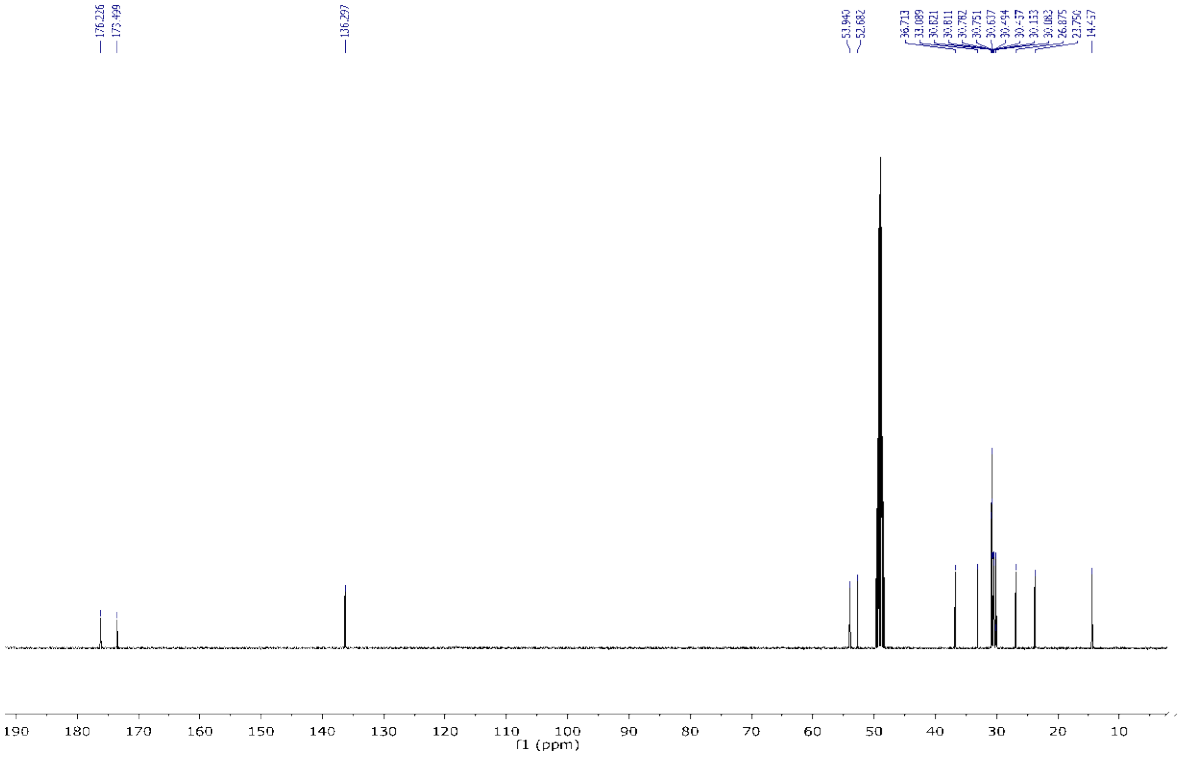

^{1}H NMR spectrum of compound **6**

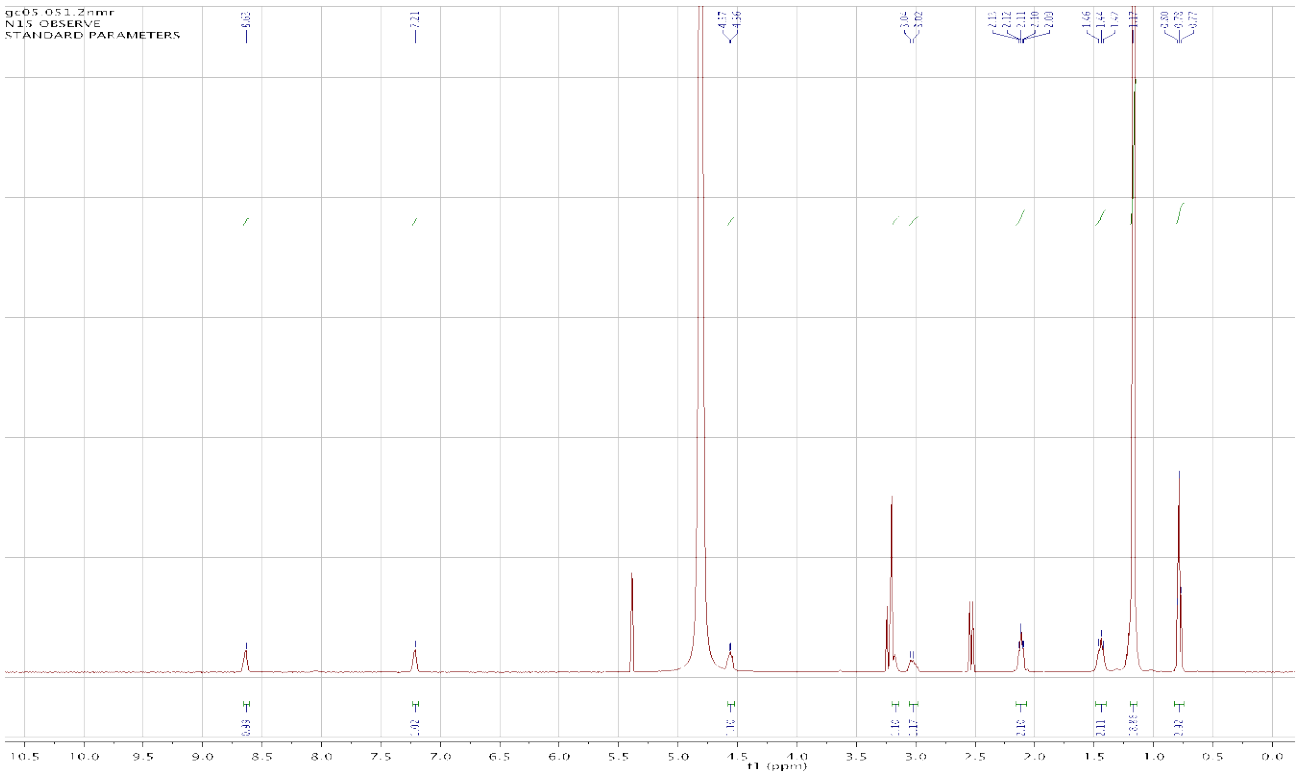

^{13}C NMR spectrum of compound **6**

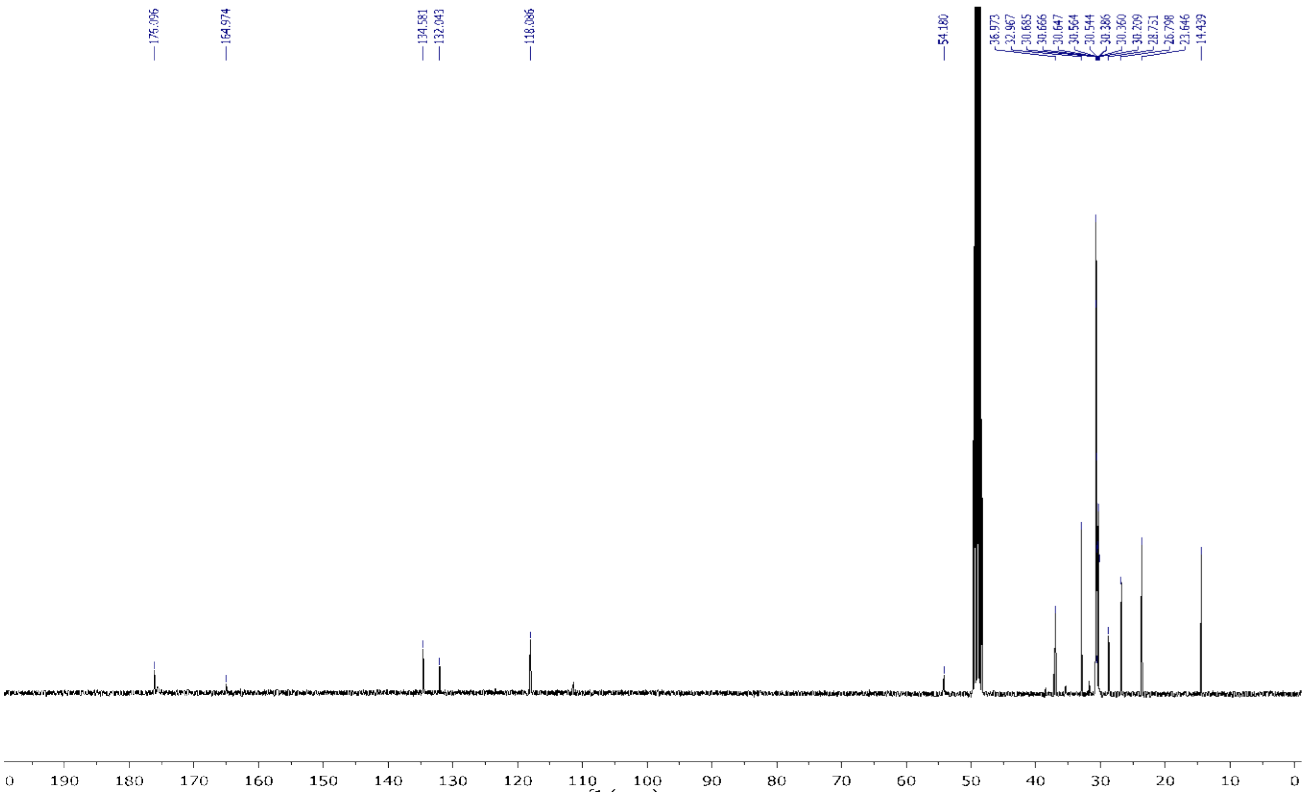

^{1}H NMR spectrum of compound **7**

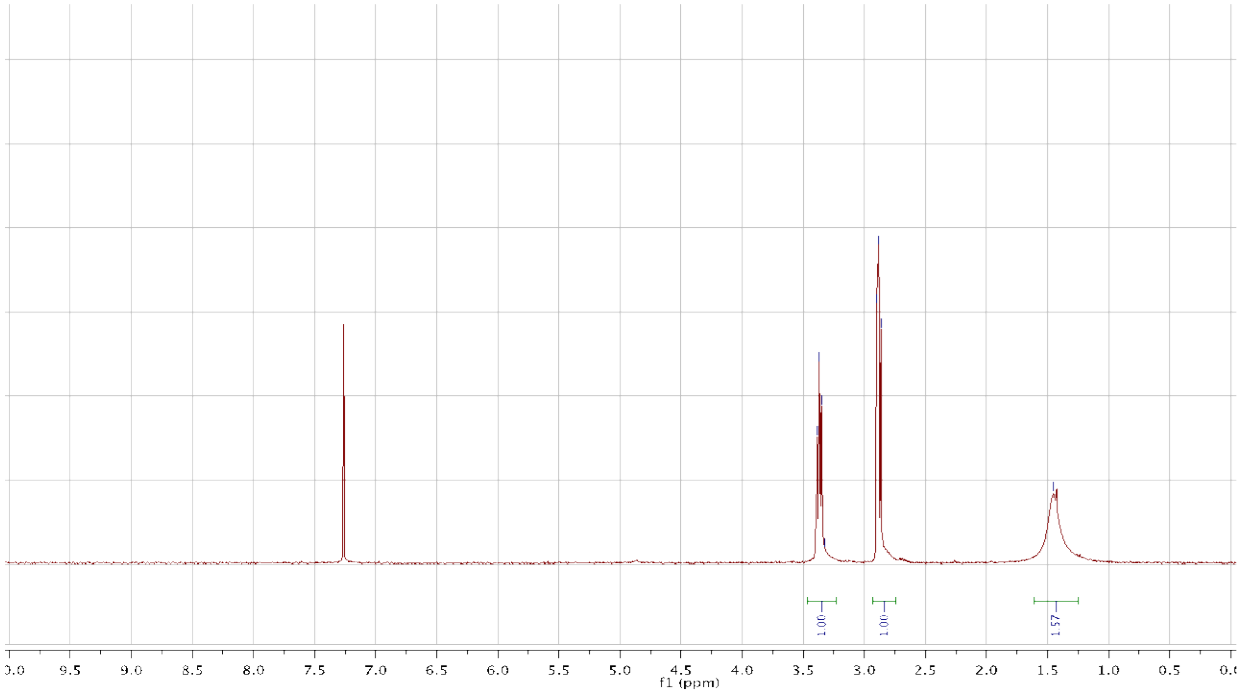

^{1}H NMR spectrum of compound **2**

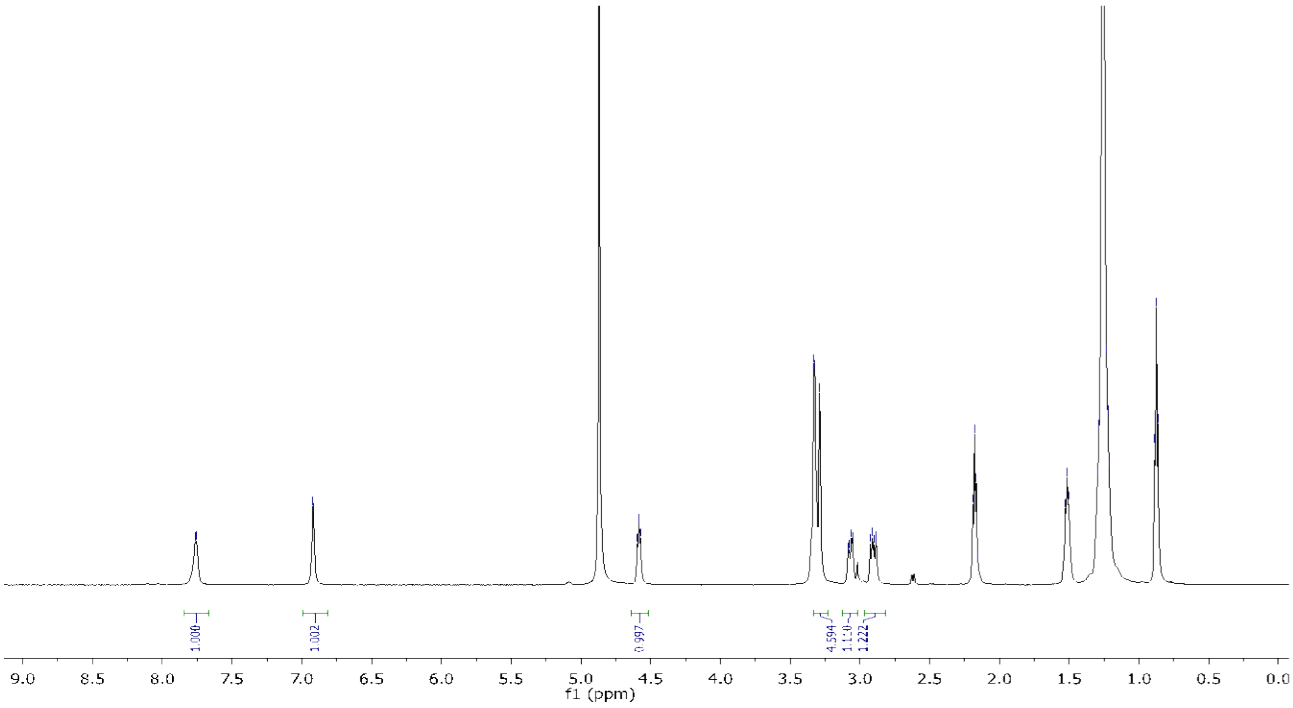

^{13}C NMR spectrum of compound **2**

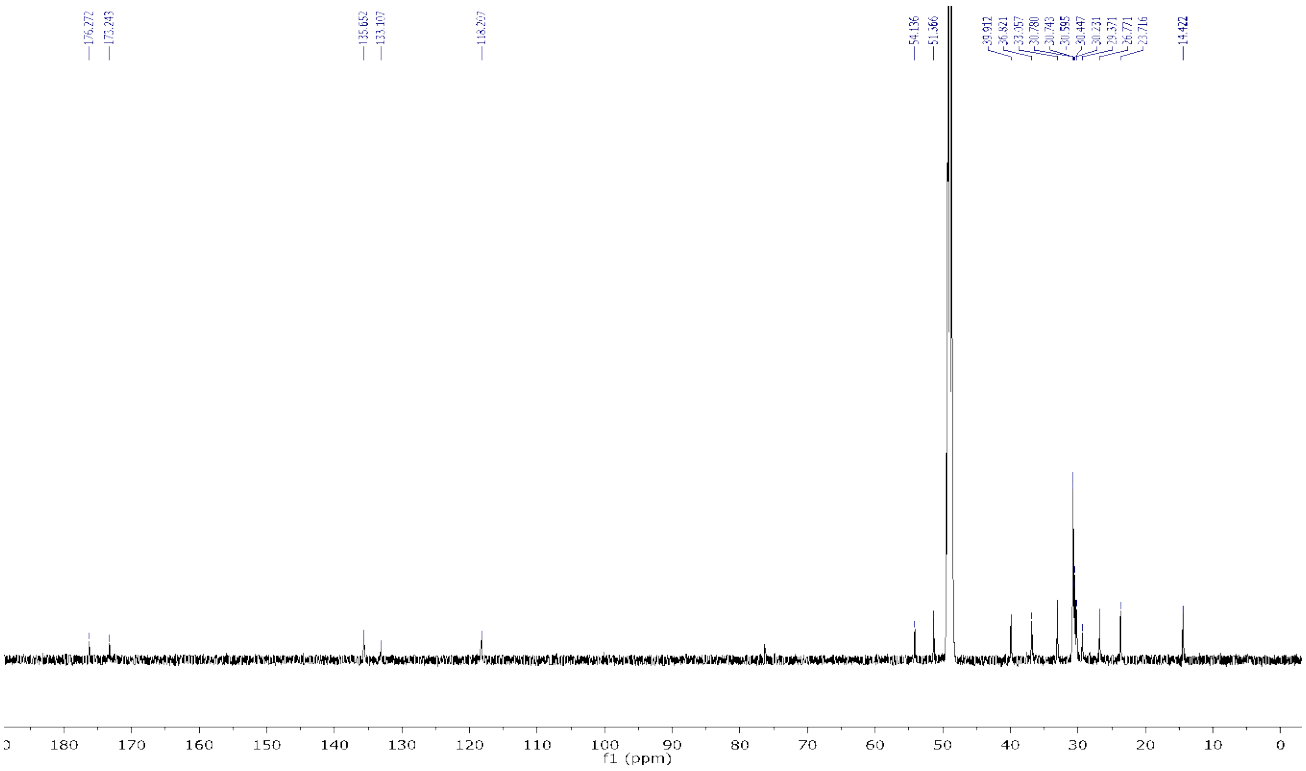

^{1}H NMR spectrum of compound **3**

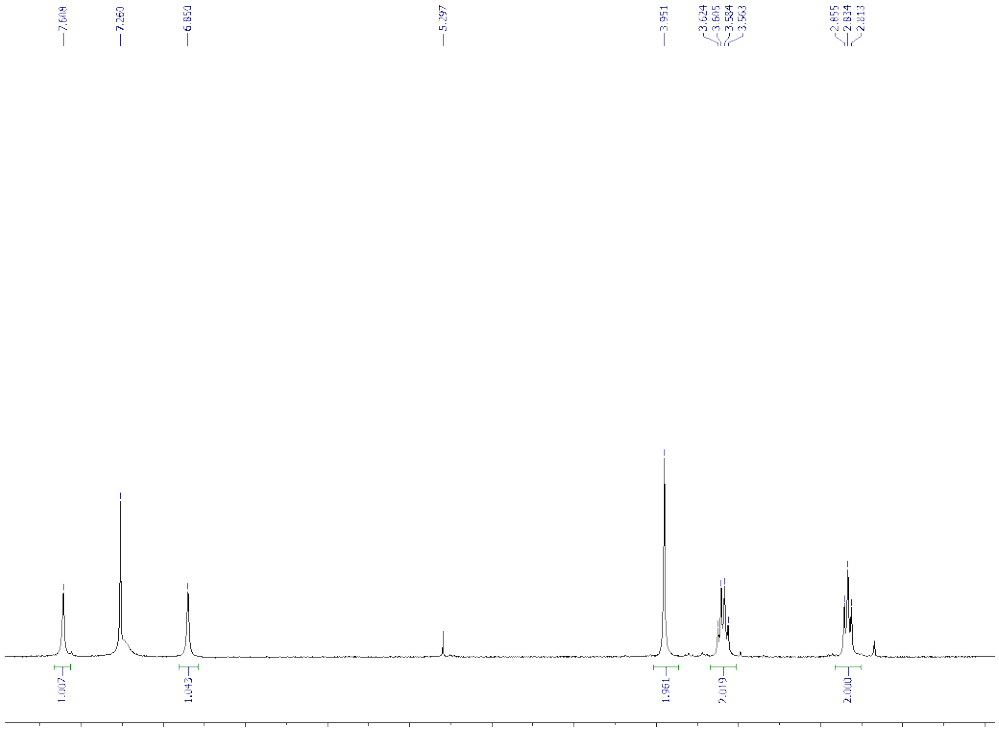

^{13}C NMR spectrum of compound **3**

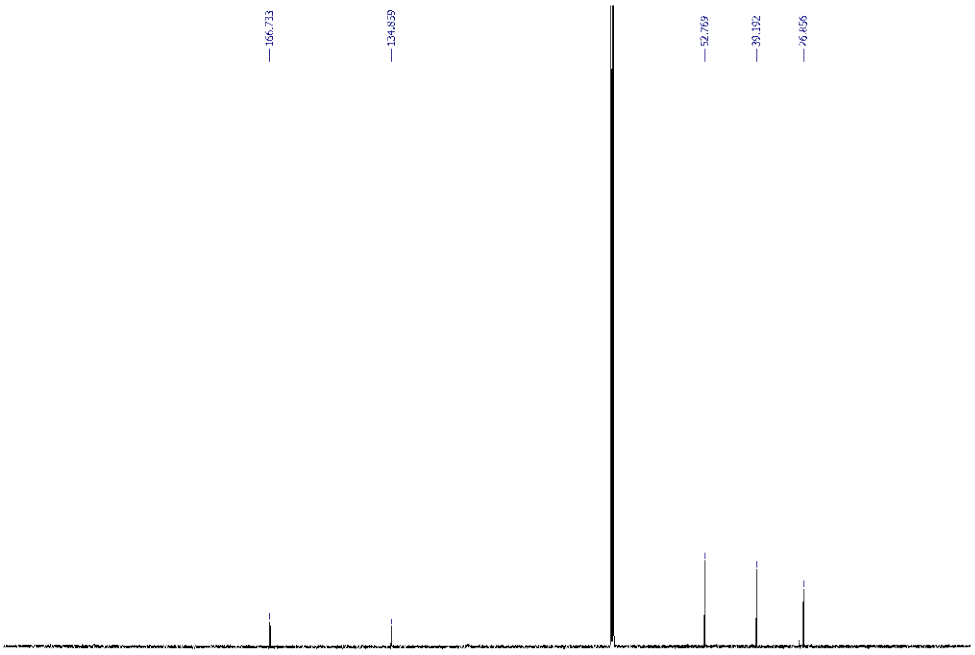

Acknowledgements

We thank the U.S. Department of Energy-Office of Basic Energy Sciences (grant no. DE-SC0002142) for supporting the research.

Notes and References

(1) F. H. Westheimer, *Tetrahedron*, 1995, **51**, 3.

(2) F. A. Johnson, S. D. Lewis and J. A. Shafer, *Biochemistry*, 1981, **20**, 44.

(3) A. J. Russell, P. G. Thomas and A. R. Fersht, *J. Mol. Biol*., 1987, **193**, 803.

(4) G. C. K. Roberts, D. H. Meadows and O. Jardetzky, *Biochemistry*, 1969, **8**, 2053.

(5) C. Marquez and W. M. Nau, *Angew. Chem., Int. Ed*., 2001, **40**, 3155.

(6) H. Bakirci, A. L. Koner, T. Schwarzlose and W. M. Nau, *Chem.–Eur. J*., 2006, **12**, 4799.

(7) (a) M. D. Pluth, R. G. Bergman and K. N. Raymond, *Science*, 2007, **316**, 85; (b) D. Fiedler, D. H. Leung, R. G. Bergman and K. N. Raymond, *Acc. Chem. Res*., 2004, **38**, 349.

(8) S. Zhang and Y. Zhao, *Macromolecules*, 2010, **43**, 4020.

(9) (a) H. C. Kolb, M. G. Finn and K. B. Sharpless, *Angew. Chem., Int. Ed*., 2001, **40**, 2004; (b) M. G. Finn, H. C. Kolb, V. V. Fokin and K. B. Sharpless, *Prog. Chem*., 2008, **20**, 1; (c) R. K. Iha, K. L. Wooley, A. M. Nystrom, D. J. Burke, M. J. Kade and C. J. Hawker, *Chem. Rev*., 2009, **109**, 5620.

(10) H.-Q. Peng, Y.-Z. Chen, Y. Zhao, Q.-Z. Yang, L.-Z. Wu, C.-H. Tung, L.-P. Zhang and Q.-X. Tong, *Angew. Chem., Int. Ed*., 2012, **51**, 2088.

(11) (a) S. Zhang and Y. Zhao, *J. Am. Chem. Soc*., 2010, **132**, 10642; (b) S. Zhang and Y. Zhao, *Chem. Commun*., 2012, **48**, 9998.

(12) X. Li and Y. Zhao, *Bioconjugate Chem*., 2012, **23**, 1721.

(13) Y.-Z. Chen, P.-Z. Chen, H.-Q. Peng, Y. Zhao, H.-Y. Ding, L.-Z. Wu, C.-H. Tung and Q.-Z. Yang, *Chem. Commun*., 2013, **49**, 5877.

(14) X. Li and Y. Zhao, *Langmuir*, 2012, **28**, 4152.

(15) G. Chadha and Y. Zhao, *J. Colloid Interface Sci*., 2013, **390**, 151.

(16) (a) R. Fornasier and U. Tonellato, J. Chem. Soc., *Faraday Trans. 1*, 1980, **76**, 1301; (b) F. M. Menger and L. G. Whitesell, *J. Am. Chem. Soc*., 1985, **107**, 707; (c) F. M. Menger, *Pure Appl. Chem*., 2005, **77**, 1873; (d) L. Pasquato, F. Rancan, P. Scrimin, F. Mancin and C. Frigeri, *Chem. Commun*., 2000, 2253; (e) P. Pengo, S. Polizzi, L. Pasquato and P. Scrimin, *J. Am. Chem. Soc*., 2005, **127**, 1616; (f) F. Mancin, P. Scrimin, P. Tecilla and U. Tonellato, Coord. *Chem. Rev*., 2009, **253**, 2150; (g) J. Zhang, X. G. Meng, X. C. Zeng

and X. Q. Yu, Coord. *Chem. Rev*., 2009, **253**, 2166.

(17) D. Matulis and V. A. Bloomfield, *Biophys. Chem*., 2001, 93, 37.

(18) J. D. Henao, Y.-W. Suh, J.-K. Lee, M. C. Kung and H. H. Kung, *J. Am. Chem. Soc*., 2008, **130**, 16142.

(19) The water-solubility of SCMs mainly derives from the large number of positive charges present on the surface.

(20) J. R. Lakowicz, Principles of Fluorescence Spectroscopy, Kluwer Academic/Plenum, New York, 2nd edn., 1999.

(21) (a) J. F. Ireland and P. A. H. Wyatt, *Adv. Phys. Org. Chem*., 1976, **12**, 131; (b) L. G. Arnaut and S. J. Formosinho, *J. Photochem. Photobiol., A*, 1993, **75**, 1.

(22) L. M. Tolbert and K. M. Solntsev, *Acc. Chem. Res*., 2002, **35**, 19.

(23) E. M. Kosower, *Acc. Chem. Res*., 1982, **15**, 259.

(24) The emission peaks of 2-naphthol in the imidazole–SCM and SCM solutions were noticeably broader than those in the CTAB solution. We suspect that, when the probe was bound by the SCMs, it was located in many slightly different binding environments that affected the electronic transitions of the probe. On the other hand, the dynamic nature of the CTAB micelle averaged out the environmental effects on the probe solubilized by the non-covalent assembly.

(25) K. M. Solntsev, Y. V. Ilichev, A. B. Demyashkevich and M. G. Kuzmin, *J. Photochem. Photobiol., A*, 1994, **78**, 39.

(26) If it were not so, the ESPT of 2-naphthol bound to the imidazole–SCMs would have displayed a large dependence on the solution pH.

(27) S. Abou-Al Einin, A. K. Zaitsev, N. K. Zaitsev and M. G. Kuzmin, *J. Photochem.*

Photobiol., A, 1988, **41**, 365.

(28) J. Slavík, Biochim. *Biophys. Acta*, 1982, **694**, 1.

(29) B. Rubalcava, D. Martinez de Munoz and C. Gitler, *Biochemistry*, 1969, **8**, 2742.

(30) (a) K. S. Broo, H. Nilsson, J. Nilsson, A. Flodberg and L. Baltzer, *J. Am. Chem. Soc*., 1998, **120**, 4063; (b) F. De Riccardis, M. Di Filoppo, D. Garrisi, I. Izzo, F. Mancin, L. Pasquato, P. Scrimin and P. Tecilla, *Chem. Commun*., 2002, 3066; (c) E. S. Orth, T. A. S. Brandao, B. S. Souza, J. R. Pliego, B. G. Vaz, M. N. Eberlin, A. J. Kirby and F. Nome, *J. Am. Chem. Soc*., 2010, **132**, 8513.

(31) Note that the hydrolysis of PNPA was performed with [CTAB] = 1.2 mM, above its CMC (0.9 mM) in water. Due to the covalent nature of the SCMs, all the hydrolysis was performed with the concentration of the cross-linked surfactant as 0.4 mM.

(32) The physical (imidazole + SCM) mixture also showed some activity at pH = 5 (Table 1, entry 10), albeit not as active as imidazole–SCMs and imidazole*–SCMs. We attributed the (weaker) pH-delaying effect to the binding and shielding of imidazole by the SCMs, similar to what happened for 2-naphthol.

(33) (a) D. M. Vriezema, M. C. Aragones, J. Elemans, J. Cornelissen, A. E. Rowan and R. J. M. Nolte, *Chem. Rev*., 2005, **105**, 1445; (b) T. S. Koblenz, J. Wassenaar and J. N. H. Reek, *Chem. Soc. Rev*., 2008, **37**, 247; (c) S. Das, G. W. Brudvig and R. H. Crabtree, *Chem. Commun*., 2008, 413; (d) M. Rakowski DuBois and D. L. DuBois, *Chem. Soc. Rev*., 2009, **38**, 62.

(34) L. Hojabri, A. Hartikka, F. M. Moghaddam, P. I. Arvidsson, *Adv. Synth. Catal*., 2007, **349**, 740.

(35) H. J. Li, X. K. Li, N. N. Liu, H. N. Zhang, J. J. Truglio, S. Mishra, C. Kisker, M. Garcia-

Diaz, P. J. Tonge, *Biochemistry-Us*., 2011, **50**, 9532.

(36) L. E. J. Smeenk, N. Dailly, H. Hiemstra, J. H. van Maarseveen, P. Timmerman, *Org. Lett*., 2012, **14**, 1194.

CHAPTER 4

ENVIRONMENTAL CONTROL OF NUCLEOPHILIC CATALYSIS IN WATER

A paper published in *Chem. Commun.*, **2014**, *50*, 2718-2720.

Geetika Chadha and Yan Zhao

Abstract

The nucleophilic catalysis by a pyridyl group in ester/phosphate ester hydrolysis was modulated by the microenvironmental hydrophobicity around the catalyst. The catalytic efficiency was enhanced thousands or tens of thousands of times and the activity was maintained well below the pK_a of the pyridyl group.

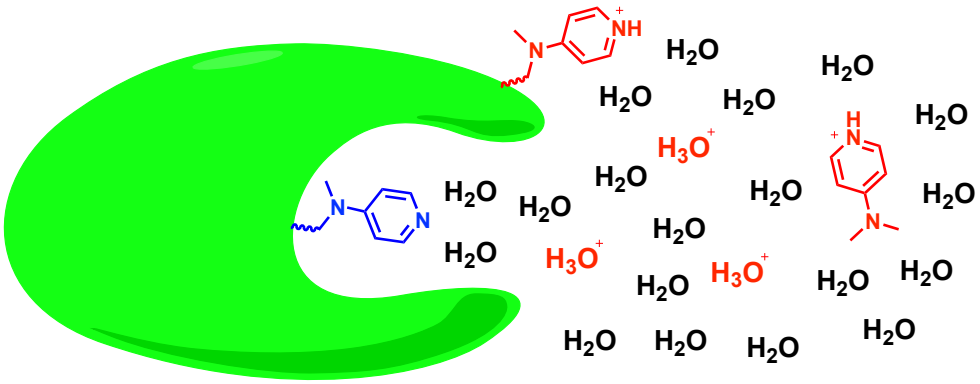

Introduction

In recent years, chemists have increasingly recognized that catalysis is a function of not just the catalytic center but also the microenvironment around it [1]. In enzymes, environmental

control is achieved through the folding of peptide strands into 3D structures and sometimes additionally the aggregation of these folded structures. The folding and aggregation create pockets and crevices in the proteins with appropriate binding and catalytic groups for the intended function. Since it remains challenging to create precisely folded synthetic tertiary and quaternary structures [2], chemists frequently resort to pre-organized scaffolds to achieve environmental control of catalysis. Dendrimers [3], star polymers [4], organic and metal–organic nanocapsules [5], multifunctional meso-porous materials [6], and metal–organic frameworks [7] have emerged as promising candidates for this purpose.

Our group recently reported a facile method to covalently capture micelles of 4-dodecyloxybenzyltripropargylammonium bromide (**1**) [8]. The resulting surface-cross-linked micelles (SCMs) are versatile water-soluble nanoparticles with interesting features such as multivalency [8], facile surface-functionalization [8,9], encapsulation of hydrophobic guests [10], tunable surface potential [11], membrane permeability [12], and controlled release under chemical stimulation [10a,13]. More recently, the SCMs were found to have enhanced surface basicity as a result of their polycationic nature [14].

4-Dimethylaminopyridine (DMAP) is a powerful nucleophilic catalyst for transacylation [15]. To maintain its nucleophilicity, the pyridyl nitrogen needs to stay deprotonated. This requirement can be met easily in an organic solvent by performing transacylation in the presence of an appropriate base. If the reaction medium is switched to a neutral aqueous solution, however, the pK_a (=9.7) [15a] of DMAP poses an immediate challenge for the catalyst to stay active.

Results and Discussion

Material Design and Synthesis

SCM in principle allows us to rationally tune the microenvironment around a covalently attached catalytic group. Because surfactant **1** has three alkynes and cross-linker **2** has two azides, a stoichiometry of [**1**]/[**2**] = 1/1.1 leaves plenty of residual alkyne groups on the surface. Subsequent surface-functionalization can be achieved easily by the addition of an azide-functionalized ligand, hydrophilic [8] or hydrophobic [9]. In this study, an azide-containing DMAP analogue **3** (0.2 equiv. to 1) was added after the surface-cross-linking was complete (Scheme 1). Our previous study showed that the click surface-functionalization was nearly quantitative under our typical reaction conditions, even for bulky polymeric [8] and hydrophobic azides [9].

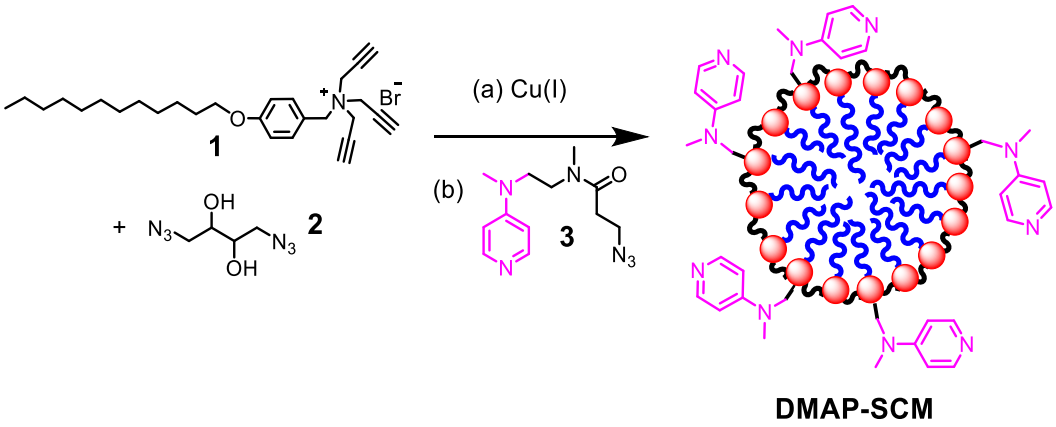

Scheme 1. Preparation of surface-functionalized DMAP-SCM.

Internal functionalization requires significant molecular engineering of the SCM. Inspired by our recently reported procedures for molecular imprinting within SCMs [16], we first solubilized polymerizable **5**, xylene, and DMPA (2,2-dimethoxy-2-phenylacetophenone, a

photoinitiator) by the mixed micelles of surfactant **4** and CTAB (Scheme 2). Surface-cross-linking with di-azide **2** catalyzed by Cu(I), surface-functionalization by azide **6**, and free-radical-core-cross-linking under UV irradiation yielded an internally functionalized SCM (Scheme 2) [16]. As reported previously, surface-functionalization by azide **6** decorated the SCMs with a layer of hydrophilic groups and was helpful for the solubility of the resulting SCMs in water.

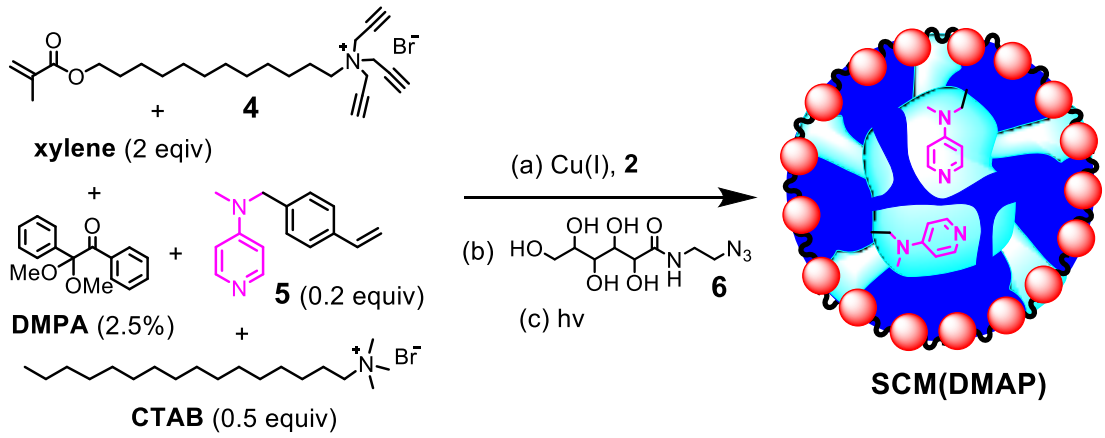

Scheme 2. Preparation of internally functionalized SCM(DMAP).

Both CTAB and xylene were temporary ‘‘space holders’’ in the above SCM and could not participate in the cross-linking. Once removed, they left behind channels and voids in the SCM that should facilitate mass transfer in the catalysis. This strategy worked well for catalytic SCMs with an encapsulated rhodium catalyst in our recent work [10b]. In our hands, the previously used 1-dodecanol and other surfactants (e.g., Brij 35) caused precipitation of the DMAP-functionalized SCMs. We varied the amounts of CTAB (25–75% to **4**) and xylene (2–6 equiv.) in the preparation and discovered that the materials made with 50% CTAB and 2 equiv. xylene had the best water solubility (Experimental Section).

Catalysis Studies

For the catalysis, we first studied the hydrolysis of *para*-nitrophenyl hexanoate (PNPH) and *para*-nitrophenyl acetate (PNPA) catalyzed by the two functionalized SCMs in HEPES aqueous buffers at different pHs. Hydrolysis leads to the formation of *para*-nitrophenol, which can be easily monitored by UV-Vis spectroscopy. The absorbance at 400 nm could be fitted into first-order kinetics to give the rate constants for the hydrolysis. The background hydrolysis rates were generally insignificant in comparison to those of the catalyzed ones [17].

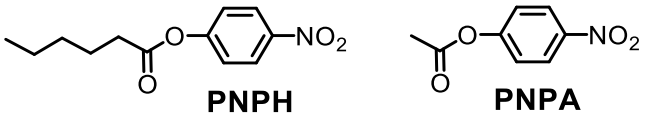

Table 1 summarizes the rate constants for the hydrolysis under different conditions. The data clearly show that DMAP attached to SCMs were far more efficient catalysts than free DMAP in aqueous solution, thousands of times faster at pH 8 and at least tens of thousands of times faster at pH 7 (entries 1–6).

We believe, in addition to the enhanced nucleophilicity at a given pH (*vide infra*), that the SCMs facilitated the hydrolysis by binding the substrate through hydrophobic interactions [17]. Evidence for the hydrophobically concentrated substrate comes from the comparison between PNPH and PNPA. The more hydrophobic substrate (PNPH) had a reactivity 1/7 of that of PNPA in aqueous solution with free DMAP as the catalyst (Table 1, entry 3). However, when catalyzed by the DMAP-functionalized SCMs, PNPH became distinctively more reactive by ~2 fold (entries 1 and 2).

Table 1. Rate constants for the hydrolysis of PNPH and PNPA in aqueous buffer catalyzed by the SCMs at 35 °C.[a]

Entry	Micelle	Solution pH	$k \times 10^5$ (min^{-1})	
			PNPH	PNPA
1	DMAP-SCM	8	11400	6410
2	SCM(DMAP)	8	25800	12740
3	DMAP	8	10	70
4	DMAP-SCM	7	3600	2180
5	SCM(DMAP)	7	23400	5930
6	DMAP	7	0[b]	0[b]
7	DMAP-SCM	6	1200	920
8	SCM(DMAP)	6	11400	2790
9	DMAP	6	0[b]	0[b]
10	DMAP-SCM	5	500	270
11	SCM(DMAP)	5	5740	1500
12	DMAP	5	0[b]	0[b]

[a] The concentration of the catalytic pyridyl group was 0.10 mM for all the SCMs. [PNPH] = [PNPA] = 0.20 mM. The reactions were performed in HEPES buffer. The relative percentage of the pyridyl to the cross-linkable surfactant was 20% for both SCMs. The rate constants were measured in duplicates and the error between the two sets of data was generally within 15%. [b] The reaction rate was too slow to be measured accurately.

A more interesting trend was found in the effect of pH on the hydrolysis. The hydrolysis slowed down for all three catalysts with decreasing pH, mostly likely as a result of a lower concentration of hydroxide in the reaction mixture. The magnitude of this effect of pH, however,

was drastically different for the three catalysts. Free DMAP immediately lost all the catalytic activity below pH 8 (Table 1, entry 6). Fig. 1 shows a plot of the relative rate constants (k_{rel}) normalized to the rate constants at pH 8 for each catalyst as a function of solution pH. Since k_{rel} compares the reactivity of the same substrate catalyzed by the same catalyst at different pHs, the hydrophobically enhanced activity cancels out.

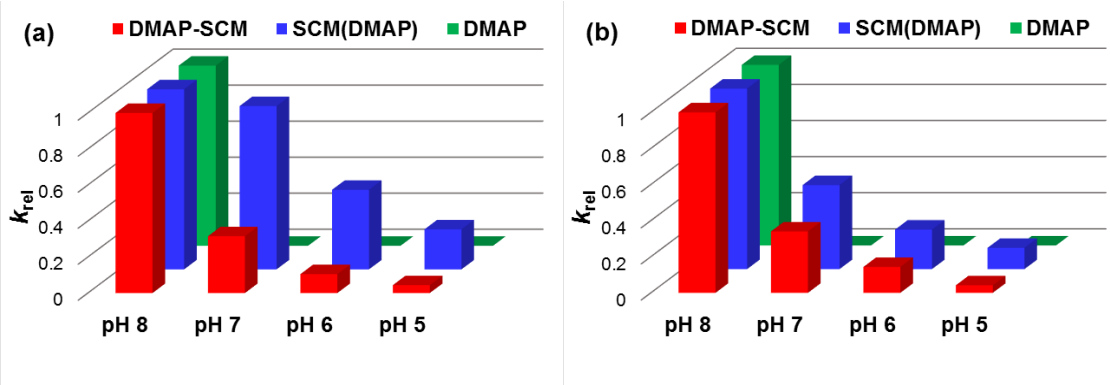

Fig. 1 Relative rate constants of hydrolysis of (a) PNPH and (b) PNPA catalyzed by the three different DMAP catalysts in HEPES buffers.

As shown in Fig. 1a, for PNPH, the free DMAP catalyst could function only at pH 8, most likely because its high pK_a (=9.7) [15a] made it protonated at lower pHs. On the other hand, the surface- functionalized DMAP-SCM was able to maintain significant activity at pH 7 (ca. 30% relative to that at pH 8) and pH 6 (ca. 10%), probably because the positive charges on the SCM and local hydrophobicity made the pyridyl group more resistant to protonation [17]. The internally functionalized SCM(DMAP) was a remarkably competent nucleophilic catalyst under acidic conditions. At pH 7, 6, and 5, its activity was 91, 44, and 22% of that at pH 8, respectively (Fig. 1a).

When the relative rates were plotted for PNPA, similar trends were observed (Fig. 1b). Although the internally functionalized SCM(DMAP) remained more resistant to protonation than the surface-functionalized ones, the pH resistance was clearly lower than that observed for PNPH (compare the blue columns in Fig. 1a and b). In contrast, the pH profiles of DMAP-SCM for PNPH and PNPA were largely the same (compare the red columns in Fig. 1a and b).

Overall, the above results suggest that, for the nucleophilic catalyst to maintain activity under acidic conditions, the catalyst should reside in a hydrophobic microenvironment. The most likely reason for the environmental hydrophobicity was that a protonated pyridinium cation could not be solvated properly in such an environment and thus was more difficult to form [18].

Why did the pH resistance depend on the hydrophobicity of the substrate? Environmental hydrophobicity around the catalyst and a hydrophobic substrate (PNPH) together clearly gave the best pH resistance (Fig. 1a, blue columns). One possibility is that the hydrophobic substrate can fill the hydrophobic space around the pyridyl group more easily inside SCM(DMAP) than the less hydrophobic PNPA. Such binding of the hydrophobic substrate makes it even more difficult for the pyridyl nitrogen to be protonated under the reaction conditions, resulting in the observed stronger pH resistance. It is also possible that, for an internally functionalized SCM(DMAP), multiple pyridyl groups exist in the structure, with some located in more hydrophobic environments than others. Those in the more hydrophobic environments should have a stronger resistance toward protonation and were the ones chiefly responsible for the residual catalytic activity observed at lower pHs.

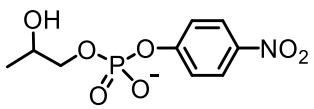

HPNPP

To further confirm the importance of environmental hydrophobicity to the protonation resistance, we studied the catalytic hydrolysis of 2-hydroxylpropyl-4-nitrophenyl phosphate (HPNPP), an activated phosphate ester. The substrate is a model compound for RNA hydrolysis and is much more hydrophilic compared to PNPH and PNPA.

Table 2. Rate constants for the hydrolysis of HPNPP in aqueous buffer catalyzed by the SCMs at 35 °C.[a]

Entry	Micelle	Solution pH	$k \times 10^5$ (min^{-1})
1	DMAP-SCM	8	50
2	SCM(DMAP)	8	110
3	DMAP	8	2.4
4	DMAP-SCM	7	20
5	SCM(DMAP)	7	40
6	DMAP	7	0[b]
7	DMAP-SCM	6	3.3
8	SCM(DMAP)	6	7.5
9	DMAP	6	0[b]
10	DMAP-SCM	5	0[b]
11	SCM(DMAP)	5	0[b]
12	DMAP	5	0[b]

[a] The concentration of the catalytic pyridyl group was 0.10 mM for all the SCMs. [HPNPP] = 0.20 mM. The reactions were performed in HEPES buffer. The rate constants were measured in duplicates and the error between the two sets of data was generally within 15%. [b] The reaction rate was too slow to be measured accurately.

As shown by the data in Table 2, the phosphate ester was somewhat less reactive than PNPH or PNPA when catalyzed by free DMAP in aqueous solution—this should reflect the different intrinsic reactivity and generic ability of DMAP to catalyze the reactions. Significantly, both SCMs, whether with the DMAP on the surface or in the interior, displayed much lower catalytic efficiencies in the phosphate ester hydrolysis than in the ester hydrolysis. The reaction rates only increased by 20–50-fold in the former (Table 2, entries 1–3) instead of thousands or tens of thousands of times as observed in the ester hydrolysis (Table 1, entries 1–6). Clearly, with the less hydrophilic substrate, the enhancement in catalytic activity was much lower for the same catalytic group. As seen in Fig. 2, both DMAP-functionalized SCMs lost their catalytic activity nearly completely at pH 6.

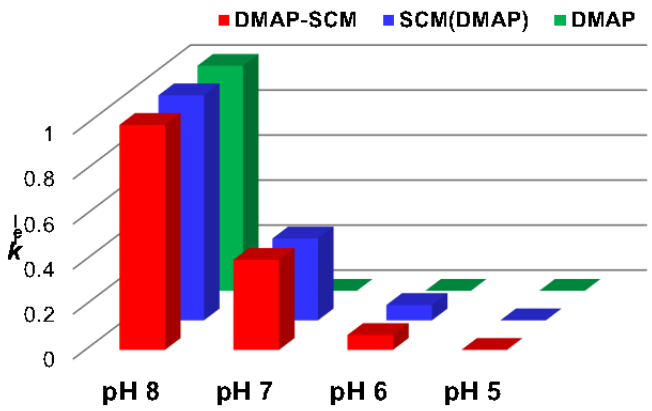

Fig. 2 Relative rate constants of hydrolysis of HPNPP catalyzed by the three different DMAP catalysts.

Conclusion

In summary, this work has shown that unconventional catalysis—i.e., nucleophilic catalysis under acidic conditions that typically protonate/deactivate the catalyst—can be rationally engineered through controlling the microenvironment around the catalyst. Not only so, the nature of the substrate itself is important for the observed environmentally enhanced catalysis. The interdependency of the environmentally enhanced catalysis and the substrate highlights the importance of the environment to a particular catalytic reaction. Chemists have just begun to use rational environmental control to modulate the activity and selectivity of catalysts [1]. It is not difficult to imagine that, with more sophisticated control of the microenvironment around the catalyst; extraordinary activity and selectivity can be obtained, as demonstrated elegantly by enzymatic catalysts with just 20 amino acids and readily available metal ions.

Acknowledgement

We thank the U.S. Department of Energy – Office of Basic Energy Sciences (grant DE-SC0002142) for supporting the research.

Experimental Section

General Experimental Methods

All reagents and solvents were of ACS-certified grade or higher and used as received from commercial suppliers. Millipore water was used to prepare buffers and nanoparticles. ^{1}H and ^{13}C NMR spectra were recorded on a VARIAN MR-400 or on a VARIAN VXR-400 spectrometer. Dynamic light scattering (DLS) was performed on a PD2000DLSPLUS dynamic light scattering

detector. Mass spectrometry was performed on AGILENT 6540 QTOF mass spectrometer. UV-Vis spectra were recorded on a Cary 100 Bio UV-Visible spectrophotometer.

Syntheses

Syntheses of compounds **1** [19], **2** [19], **4** [20], and **6** [20] were previously reported.

Scheme 3. Synthesis of compound **3**

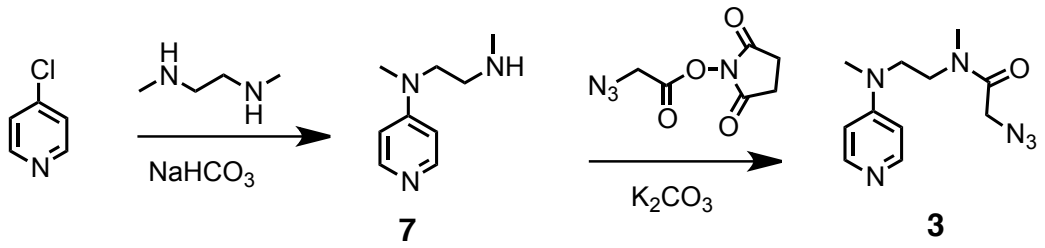

Scheme 4. Synthesis of compound **5**

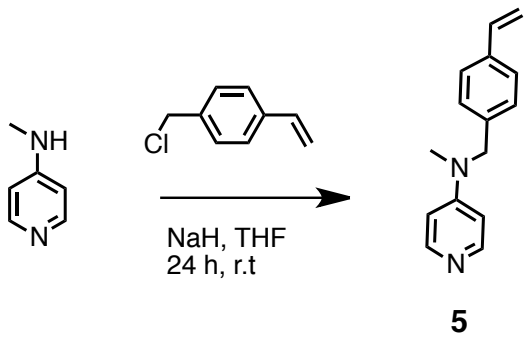

Compound 7 [19]. A mixture of 4-chloropyridine hydrochloride (0.25 g, 1.70 mmol), N, N-dimethyl-1,2-ethanediamine (0.46 mL, 4.25 mmol), and sodium bicarbonate (0.43 mg, 5.10 mmol) in isoamyl alcohol (50 mL) was heated to reflux for 48 h. The mixture was concentrated by rotary evaporation and the residue was purified by column chromatography over silica gel using CH_2Cl_2/CH_3OH (5: 1) and CH_3OH/TEA (4: 0.5) as the eluents to give a yellowish oil (0.20 g, 71%). ^1H NMR (400 MHz, $CDCl_3$, δ) 8.18 (dd, 2H), 6.51 (dd, 2H), 3.44 (t, 2H), 2.98 (s, 3H), 2.77 (t, 2H), 2.44 (s, 3H).

Compound 3. A solution of compound **7** (0.08 g, 0.48 mmol), azidoacetic acid N-hydroxysccinimide ester [21] (0.192 g, 0.96 mmol), and K_2CO_3 (0.40 g, 2.88 mmol) in acetonitrile (5 mL) was stirred for 2 d under nitrogen. The solid was removed by filtration. The filtrate was concentrated in vacuo to give a yellow oil, which was purified by preparative TLC using 3:1 CH_2Cl_2/CH_3OH as the developing solvent to afford a white powder (90 mg, 75%). ^1H NMR (400 MHz, $CDCl_3$, δ) 8.31 (d, 2H), 6.79 (d, 2H), 3.86 (s, 2H), 3.70 (t, 2H), 3.60 (t, 2H), 3.17 (s, 3H), 2.99 (s, 3H). ^{13}C NMR (100 MHz, $CDCl_3$, δ): 167.8, 153.4, 149.9, 106.4, 50.5, 48.1, 46.1, 37.4, 35.9. [M + H]+ calcd for $C_{11}H_{16}N_6O$, 249.1458 found, 249.1460.

Compound 5 [22]. NaH (0.05 g, 60 % in mineral oil, 1.38 mmol) was added to a solution of 4-(methylamino)pyridine (0.10 g, 0.92 mmol) in dry THF (5 mL) at 0 ^oC under nitrogen. The mixture was stirred at room temperature for 2 h and cooled to 0 ^oC again, followed by slow addition of 4-vinyl benzyl chloride (0.09 mL, 0.64 mmol) in dry THF (2 mL). The reaction mixture was allowed to warm to room temperature and was stirred for 24 h. The insoluble solid was removed by filtration and the filtrate was concentrated in vacuo. The residue was dissolved in CH_2Cl_2 (50 mL). The organic solution was washed with water (2 × 30 mL), dried with anhydrous Na_2SO_4, filtered, and concentrated in vacuo. The residue was purified by column chromatography over silica gel with CH_2Cl_2/MeOH = 10/1 to 5/1 as the eluents to give a light brown powder. (0.18 g, 89%) 1H NMR (400 MHz, CDCl3, δ): 8.20 (d, 2H), 7.36 (d, 2H), 7.11 (d, 2H), 6.71 (dd, 1H), 6.54 (dd, 2H), 5.73 (d, 1H), 5.23 (d, 1H), 4.50 (s, 2H), 3.07 (s, 3H). ^{13}C NMR (100 MHz, CDCl3, δ): 154.0, 149.4, 136.8, 136.5, 136.2, 126.6, 126.6, 113.9, 106.7, 54.8, 37.8.

Preparation of DMAP-SCM. Compound **3** (1.7 mg, 0.0068 mmol), 1,4-diazidobutane-2,3-diol (compound **2**, 4.6 mg, 0.026 mmol), $CuCl_2$ (10 μL of a 9 mg/mL aqueous solution, 0.5 μmol), and sodium ascorbate (100 μL of a 13 mg/mL aqueous solution, 5 μmol) were added to a micellar solution of compound **1** (10 mg, 0.02 mmol) in Millipore water (2.5 mL). The reaction mixture was stirred slowly at room temperature for 24 h after which the mixture was dialyzed for 3 d against deionized water using 500 Da molecular weight cut-off tubing. The detailed preparation, cross-linking chemistry, and characterization of the SCMs were reported previously [19,20,24,25].

Preparation of SCM(DMAP). To a micellar solution of compound **4** (20 mg, 0.047 mmol) in D_2O (2.0 mL), cetyltrimethylammonium bromide (CTAB, 8.6 mg, 0.024 mmol), xylene (12 μL, 0.094 mmol), compound **5** in DMF (35 μL of a solution of 60 mg/mL, 0.0096 mmol), and 2,2-dimethoxy-2-phenylacetophenone (DMPA, 6 μL of a 55 mg/mL solution in DMSO, 0.0012 mmol) were added. The mixture was subjected to ultrasonication for 10 min before compound **2** (8.89 mg, 0.052 mmol), $CuCl_2$ (10 μL of a 16 mg/mL solution in D_2O, 0.0012 mmol), and sodium ascorbate (100 μL of a 23 mg/mL solution in D_2O, 0.012 mmol) were added. After the reaction mixture was stirred slowly at room temperature for 12 h, compound **6** (26 mg, 0.094 mmol), $CuCl_2$ (10 μL of a 16 mg/mL solution in D_2O, 0.0012 mmol), and sodium ascorbate (100 μL of a 23 mg/mL solution in D_2O, 0.012 mmol) were added. After being stirred for another 6 h at room temperature, the reaction mixture was transferred to a glass vial, purged with nitrogen for 15 min, sealed with a rubber stopper, and irradiated in a Rayonet reactor for 12 h. The reaction mixture was poured into acetone (8 mL). The precipitate was collected by centrifugation

and washed with a mixture of acetone/water (5 mL/1 mL) five times. The off-white powder was re-dissolved in 2.4 mL of Millipore water to give a 20 mM stock solution of SCM(DMAP).

Kinetic measurement

p-Nitrophenyl acetate (PNPA, 50 mg) was dissolved in 10 mL of methanol. The methanol stock solution (10 mM) was stored in a refrigerator and used within a week. *p*-Nitrophenyl hexanoate stock solution (PNPH, 12 mg/5mL in acetonitrile, 10 mM) was prepared freshly each day. HPNPP was prepared according to a literature procedure [26]. A stock solution (10 mM) of HPNPP in Millipore water was prepared. For the kinetic experiments, a typical procedure is as follows: Aliquots of the SCM(DMAP) solution were added to a series of cuvettes containing 800 μL of HEPES buffer (25 mM, pH = 4, 5, 6, 7, 8). The concentration of the catalytic pyridyl group was 0.10 mM in all cases. The cuvettes were placed in the UV-Vis spectrometer and equilibrated to 35.0 °C. After 5 min, aliquots (40 μL) of the PNPA aqueous solution, prepared freshly each day by mixing 3.7 mL of the methanol PNPA stock solution with 6.3 mL of deionized water, were added to the cuvettes. The hydrolysis was monitored by the absorbance of *p*-nitrophenol at 400 nm over a period of 6 min for PNPA, 1–4 min for PNPH, and 3 h for HPNPP. The experiments were generally performed in duplicates.

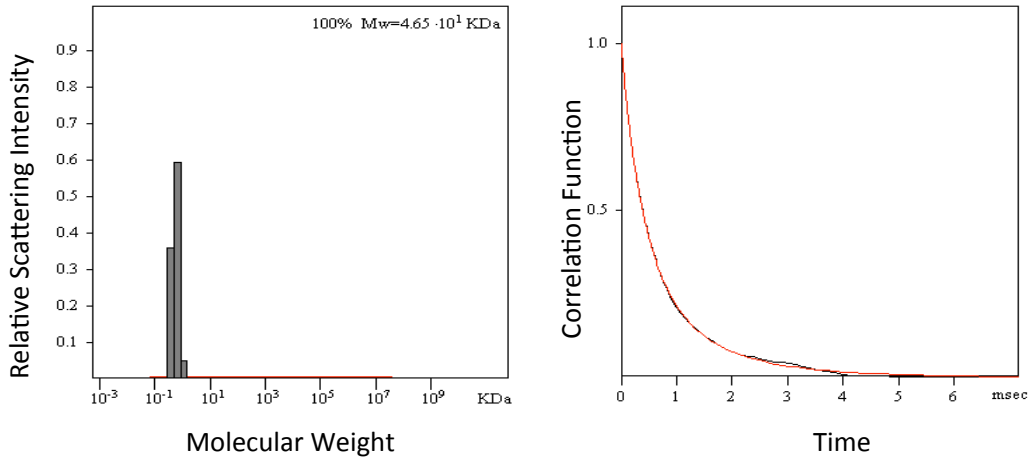

Fig. 3 Distribution of the molecular weights of the SCM(DMAP) and the correlation curve for DLS. The molecular weight distribution was calculated by the PRECISION DECONVOLVE program assuming the intensity of scattering is proportional to the mass of the particle squared.

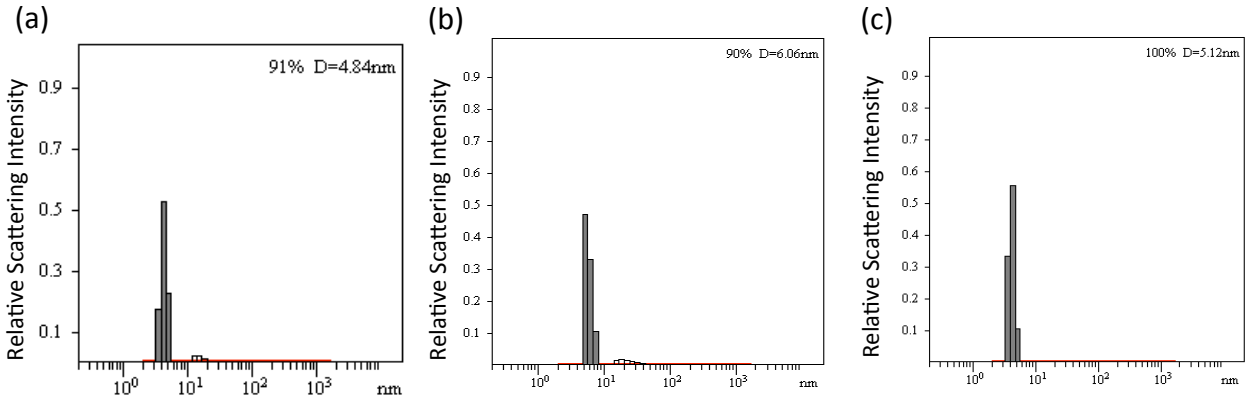

Fig. 4 Distribution of the hydrodynamic diameters of the nanoparticles in water as determined by DLS for (a) alkynyl-SCM (b) surface-functionalized SCM, and (c) SCM(DMAP) after purification.

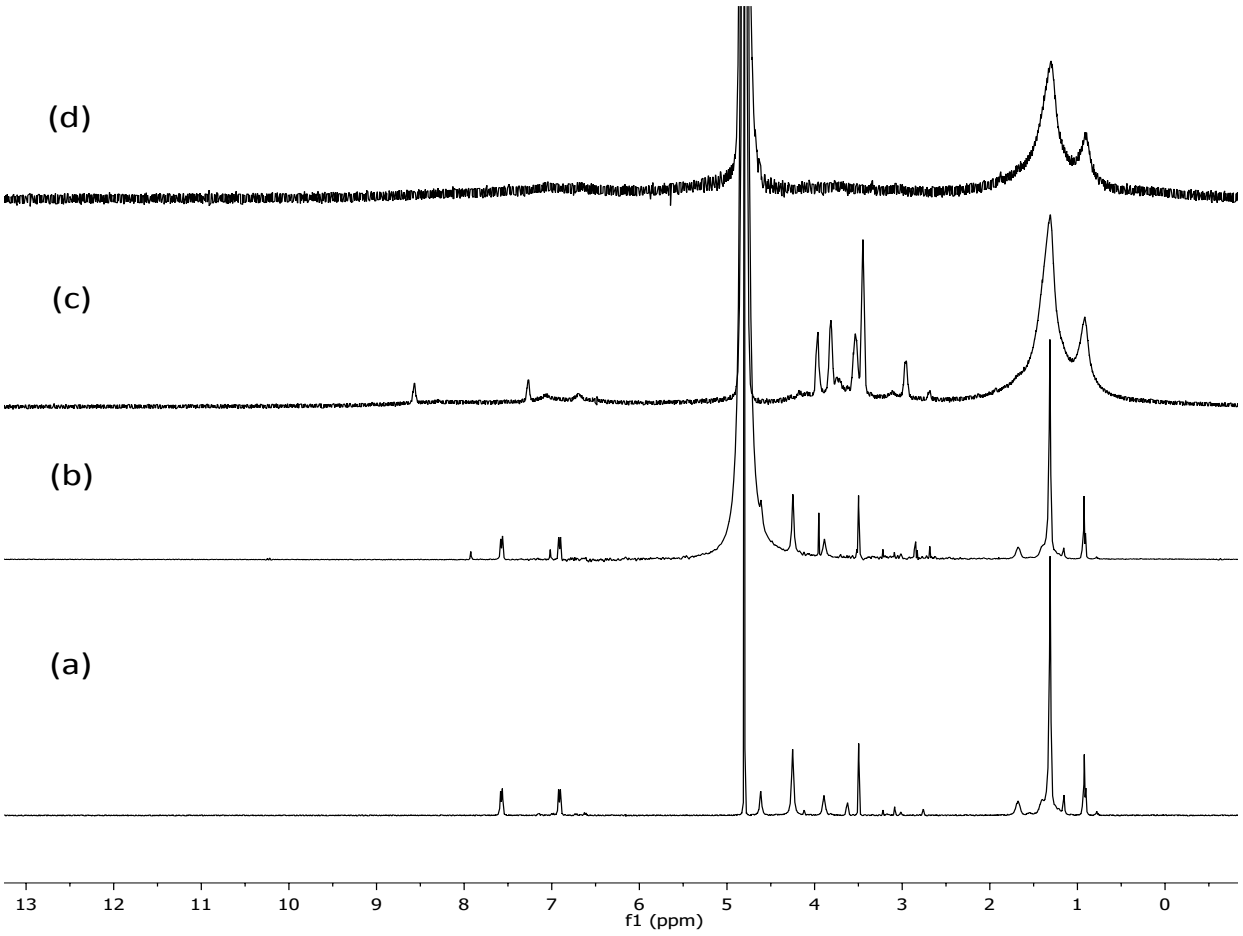

Fig. 5 ^{1}H NMR spectra of (a) 10 mM micellar solution of **1** in D_2O, (b) after the addition of 0.2 equiv. of compound **3**, (c) after surface-crosslinking, and (d) purified DMAP-SCM in D_2O.

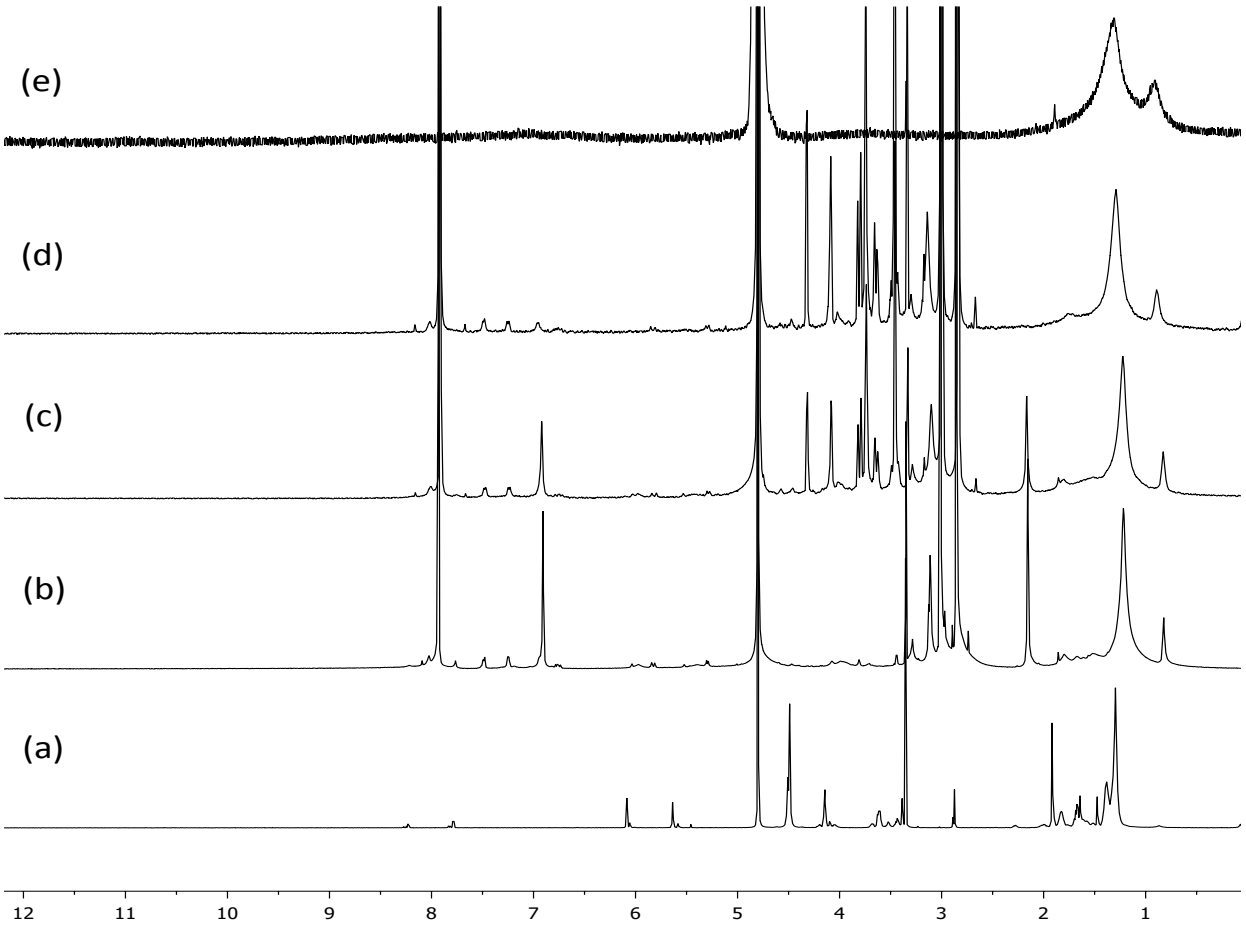

Fig. 6 ^{1}H NMR spectra of (a) 10 mM micellar solution of **4** in D_2O, (b) after surface-crosslinking (12 h after the addition of compound **5**, compound **2**, xylene, CTAB, DMPA, and Cu(I) catalysts), (c) after surface-functionalization with compound **6**, (d) after core-cross-linking (after 12 h under UV irradiation), and (e) purified SCM(DMAP) in D_2O.

^{1}H and ^{13}C NMR spectra of key compounds

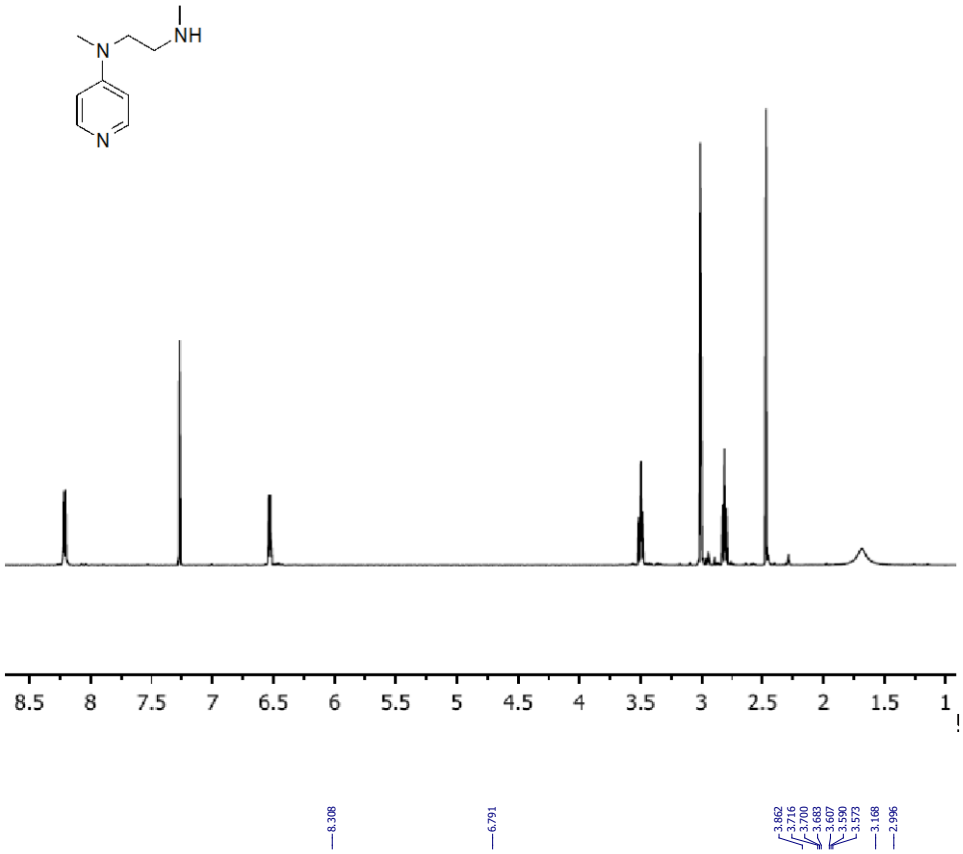

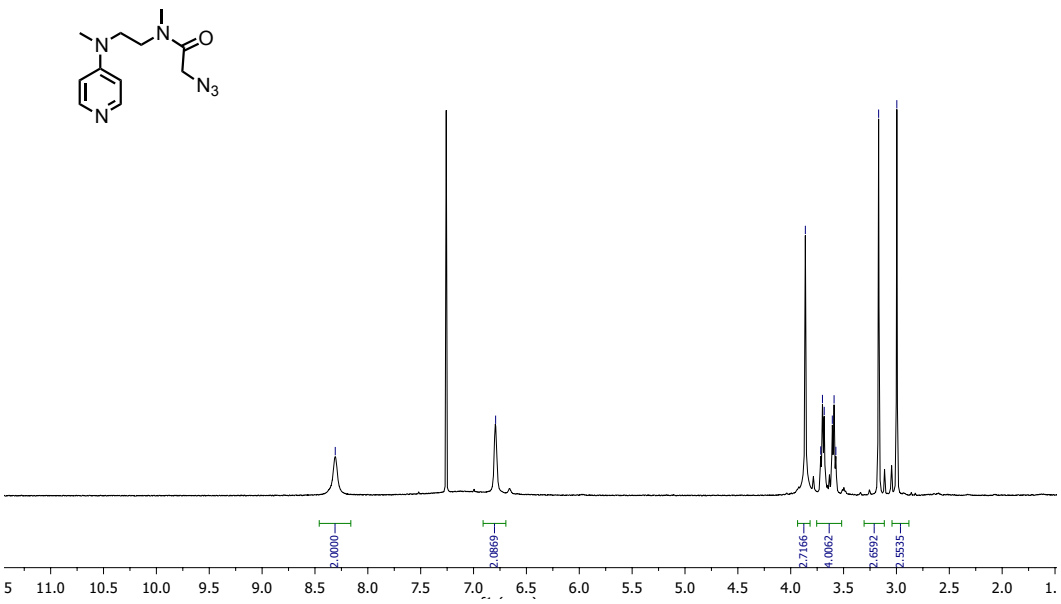

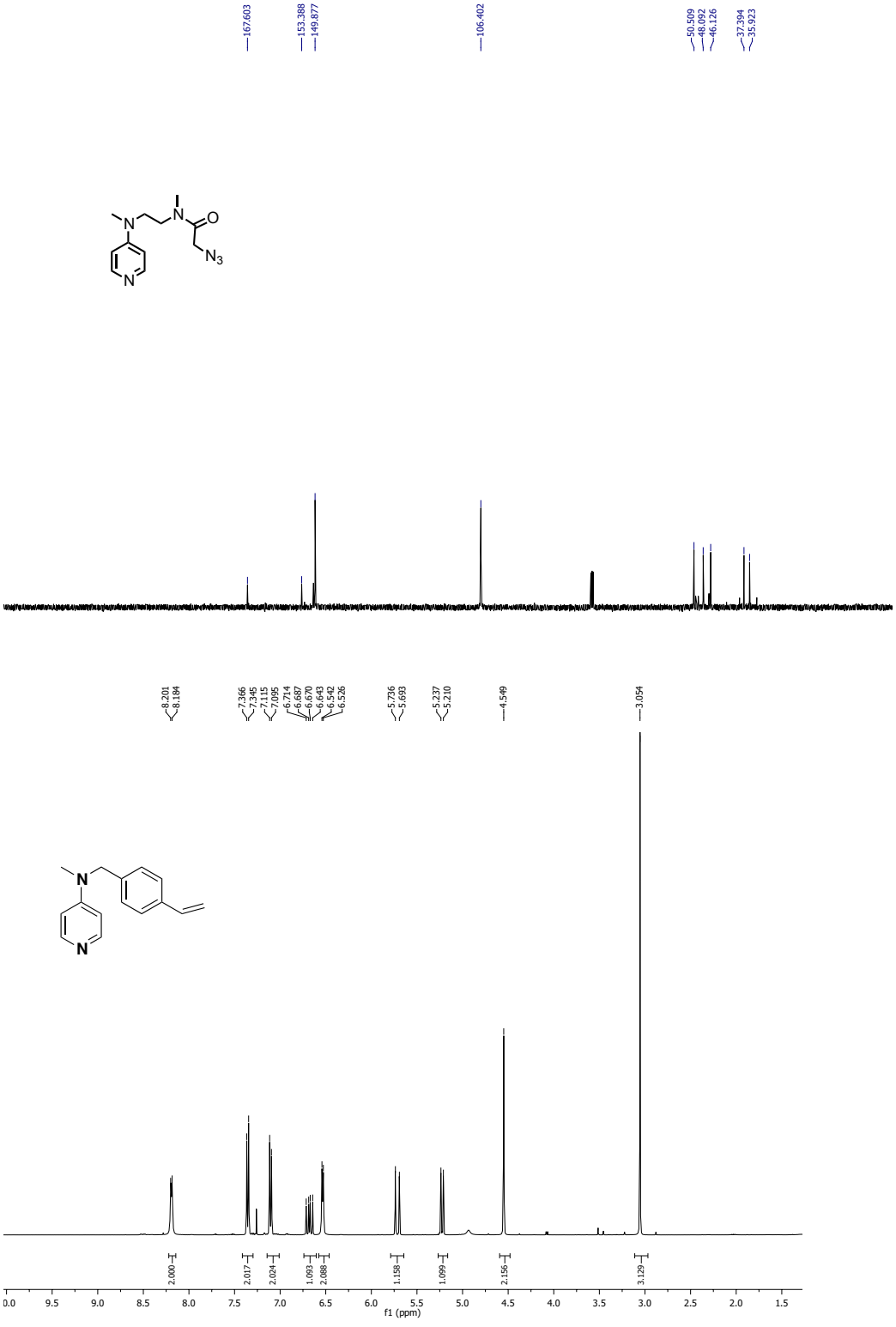

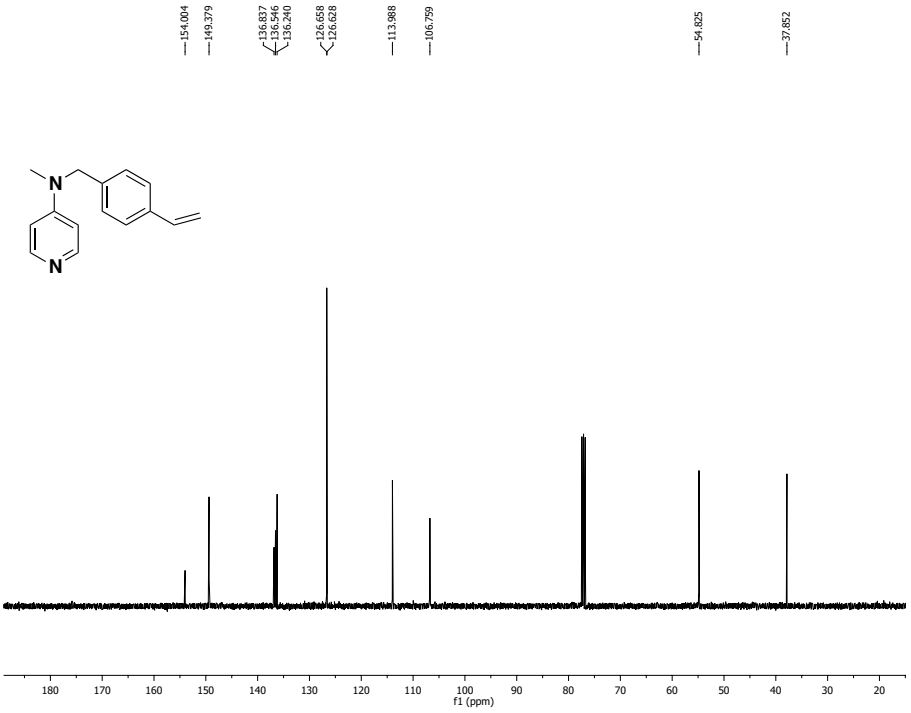

Notes and References

(1) S. Das, G. W. Brudvig and R. H. Crabtree, *Chem. Commun*., 2008, 413.

(2) (a) S. H. Gellman, *Acc. Chem. Res*., 1998, **31**, 173; (b) D. J. Hill, M. J. Mio, R. B. Prince, T. S. Hughes and J. S. Moore, *Chem. Rev*., 2001, **101**, 3893; (c) Foldamers: Structure, Properties, and Applications, ed. S. Hecht and I. Huc, Wiley-VCH, Weinheim, 2007.

(3) (a) R. M. Crooks, M. Q. Zhao, L. Sun, V. Chechik and L. K. Yeung, *Acc. Chem. Res*., 2001, **34**, 181; (b) M. Zhao and R. M. Crooks, *Angew. Chem., Int. Ed*., 1999, **38**, 364; (c) G. A. Somorjai and Y. M. Li, *Top. Catal*., 2010, **53**, 832.

(4) (a) Y. G. Chi, S. T. Scroggins and J. M. J. Frechet, *J. Am. Chem. Soc*., 2008, **130**, 6322; (b) V. Rodionov, H. Gao, S. Scroggins, D. A. Unruh, A.-J. Avestro and J. M. J. Fr´echet, *J. Am. Chem. Soc*., 2010, **132**, 2570.

(5) (a) D. Fiedler, D. H. Leung, R. G. Bergman and K. N. Raymond, *Acc. Chem. Res*., 2004, **38**, 349; (b) D. M. Vriezema, M. C. Aragones, J. Elemans, J. Cornelissen, A. E. Rowan and R. J. M. Nolte, *Chem. Rev*., 2005, **105**, 1445; (c) J. Rebek, *Angew. Chem., Int. Ed*., 2005, **44**, 2068; (d) M. Yoshizawa, J. K. Klosterman and M. Fujita, *Angew. Chem., Int. Ed*., 2009, **48**, 3418.

(6) (a) A. Corma, *Chem. Rev*., 1997, **97**, 2373; (b) S. Huh, H.-T. Chen, J. W. Wiench, M. Pruski and V. S. Y. Lin, *Angew. Chem., Int. Ed*., 2005, **44**, 1826; (c) S. Hudson, J. Cooney and E. Magner, *Angew. Chem., Int. Ed*., 2008, **47**, 8582; (d) J. M. Thomas and R. Raja, *Acc. Chem. Res*., 2008, **41**, 708.

(7) (a) L. Ma, C. Abney and W. Lin, *Chem. Soc. Rev*., 2009, **38**, 1248; (b) A. Corma, H. Garc´ıa and F. X. Llabr´es i Xamena, *Chem. Rev*., 2010, **110**, 4606; (c) J. Lee, O. K. Farha, J. Roberts, K. A. Scheidt, S. T. Nguyen and J. T. Hupp, *Chem. Soc. Rev*., 2009, **38**, 1450; (d) D. Farrusseng, S. Aguado and C. Pinel, *Angew. Chem., Int. Ed*., 2009, **48**, 7502.

(8) S. Zhang and Y. Zhao, *Macromolecules*, 2010, **43**, 4020.

(9) H.-Q. Peng, Y.-Z. Chen, Y. Zhao, Q.-Z. Yang, L.-Z. Wu, C.-H. Tung, L.-P. Zhang and Q.-X. Tong, *Angew. Chem., Int. Ed*., 2012, 51, 2088.

(10) (a) S. Zhang and Y. Zhao, *J. Am. Chem. Soc*., 2010, **132**, 10642; (b) S. Zhang and Y. Zhao, *Chem. Commun*., 2012, **48**, 9998.

(11) X. Li and Y. Zhao, *Bioconjugate Chem*., 2012, **23**, 1721.

(12) Y.-Z. Chen, P.-Z. Chen, H.-Q. Peng, Y. Zhao, H.-Y. Ding, L.-Z. Wu, C.-H. Tung and Q.-Z. Yang, *Chem. Commun*., 2013, **49**, 5877.

(13) X. Li and Y. Zhao, *Langmuir*, 2012, **28**, 4152.

(14) G. Chadha and Y. Zhao, *J. Colloid Interface Sci*., 2013, **390**, 151.

(15) (a) G. Ho¨fle, W. Steglich and H. Vorbru¨ggen, *Angew. Chem., Int. Ed. Engl*., 1978, **17**, 569; (b) R. Murugan and E. F. V. Scriven, *Aldrichimica Acta*, 2003, **36**, 21; (c) M. R. Heinrich, H. S. Klisa, H. Mayr, W. Steglich and H. Zipse, *Angew. Chem., Int. Ed*., 2003, **42**, 4826.

(16) J. K. Awino and Y. Zhao, *J. Am. Chem. Soc*., 2013, **135**, 12552.

(17) G. Chadha and Y. Zhao, *Org. Biomol. Chem*., 2013, **11**, 6849.

(18) D. Matulis and V. A. Bloomfield, *Biophys. Chem*., 2001, **93**, 37.

(19) S. Y. Zhang, Y. Zhao, *Macromolecules*, 2010, **43**, 4020.

(20) J. K. Awino, Y. Zhao, *J. Am. Chem. Soc*., 2013, **135**, 12552.

(21) H. K. Cho, Z. Q. Zhong, Y. Zhao, *Tetrahedron,* 2009, **65**, 7311.

(22) P. S. Ghosh, A. D. Hamilton, *Chem. Eur. J*., 2012, **18**, 2361.

(23) C. K. W. Kwong, R. Huang, M. Zhang, M. Shi, P. H. Toy, P. H. *Chem. Eur. J.,* 2007, **13**, 2369.

(24) Peng, H.-Q.; Chen, Y.-Z.; Zhao, Y.; Yang, Q.-Z.; Wu, L.-Z.; Tung, C.-H.; Zhang, L.-P.; Tong, Q.-X. *Angew. Chem. Int. Ed.*, 2012, **51**, 2088.

(25) Chen, Y.-Z.; Chen, P.-Z.; Peng, H.-Q.; Zhao, Y.; Ding, H.-Y.; Wu, L.-Z.; Tung, C.-H.; Yang, Q.-Z. *Chem. Commun.*, 2013, **49**, 5877.

(26) J. S. W. Tsang, A. A. Neverov, R. S. Brown, *J. Am. Chem. Soc.,* 2003, **125**, 1559.

CHAPTER 5

SELF-ASSEMBLED LIGHT HARVESTING NANOPATICULATE MATERIALS FOR LONG-RANGE ENERGY TRANSFER IN AQUEOUS SOLUTION

A manuscript to be submitted

Geetika Chadha and Yan Zhao

Abstract

A robust light harvesting system was constructed using a dansyl labeled surfactant and by introducing eosin Y through electrostatic interaction. Magnified 'Antenna Effect' observed due to both intra-micellar and inter-micellar energy-transfer processes, was facilitated by extremely high binding constants between the acceptor and the donor units, as well as the close distance between the donor chromophores. The light energy absorbed by the dansyl groups within the cross-linked micelles was transferred, with high quantum efficiency to Eosin Y/ calcein/ SR101 that served a dual function of an energy sink and a non-covalent cross-linker.

Introduction

Conversion of light energy to chemical or electrical potential is the fundamental process behind important processes including photosynthesis [1], photocatalysis [2], and photovoltaics [3,4]. Nature has optimized the materials needed for both light harvesting and conversion. Some natural light-harvesting complexes, for example, consist of >200 antenna chromophores to absorb light energy, with efficient energy-migration from one chromophore to another before the

energy is funneled to a reaction center [5]. The efficiency of these light-harvesting complexes approaches that of a nearly perfect "Einstein photochemical machine," [5b] making them outstanding models for chemists and materials scientists to mimic. Unfortunately, the highly complex protein framework used to organize the light-absorbing dyes in the natural systems is not only too difficult to synthesize but also too expensive and fragile for most technological applications.

Previously, we reported a strategy to create light-harvesting nanoparticles from our multivalent surface-cross-linked micelles (SCMs) [6]. The SCMs are synthesized by cross-linking the micelles of 4-dodecyloxybenzyltripropargylammonium bromide (**1**) [7] and are versatile multifunctional water-soluble nanoparticles useful in molecular recognition [8], encapsulation, controlled release [9], catalysis [10], and imaging [11]. Since SCMs typically have multiple alkyne groups on the surface; their multifunctionalization is straightforward [7]. In our previous light-harvesting SCMs, antenna chromophores, i.e., 9,10-bis(4-methylphenyl)anthracene (DPA), were installed by a click reaction between an azido derivative of DPA and alkyne-functionalized SCMs in a THF/water mixture [6]. Because the DPA groups in the resulting light-harvesting SCM were close enough for efficient energy migration and yet far enough to avoid excimer formation or self-quenching, facile light-harvesting effect was observed in the DPA-functionalized SCM, in the organic medium (i.e. THF). One acceptor molecule (Eosin Y or EY), for example, was found to quench the emission of ca. 50 molecules of the DPA donor on the SCM, when the negatively charged EY bound to the positively charged SCM through electrostatic interactions. The energy-transfer distance between the donor and the acceptor in such a scenario far exceeded the Förster distance (R_0) of DPA and EY, and could only be possible via a combined DPA–DPA energy migration and DPA–EY energy transfer [6].

In this work, we sought to further increase the antenna effect and hoped to further increase the number of donor chromophores that could be quenched by an acceptor. Our key strategy was to utilize a fluorescent cross-linkable surfactant **2**, which has the same tripropargylammonium headgroup as **1** and a dansyl-like fluorophore in the structure. Its synthesis is discussed in detail in the Experimental Section.

Results and Discussion

Material Design and Synthesis

Surfactant **1** has a critical micelle concentration (CMC) of 0.14 mM [9a]. According to the fluorescence studies (see Experimental Section for details), the CMC of **2** is ca. 0.3 mM in water. In our SCM preparation, we kept the total concentrations of the surfactants at 10 mM while varying the ratio between **1** and **2** from 80:20 all the way to 0:100. The idea was to vary the density of the fluorophore in the SCM so that we could minimize self-quenching or at least keep it under a manageable level. In the presence of the di-azide crosslinker **3** [7], Cu(I) catalyzed 1,3-dipolar cycloaddition was performed to capture the micelle, leading to the formation of water soluble nanoparticles with different densities of fluorophore units on the surfaces; known as dansyl-SCMs (Scheme 1).

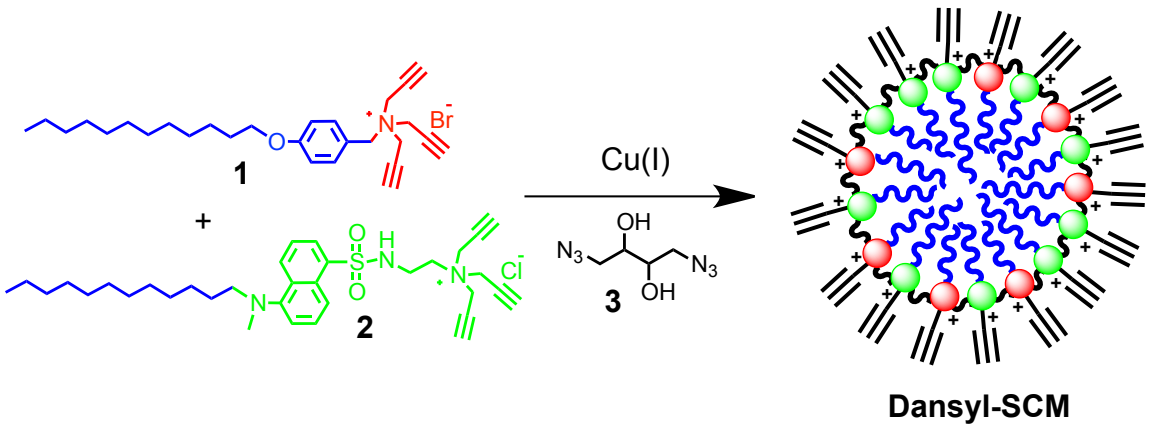

Scheme 1. Preparation of dansyl-SCM.

According to Fig. 1, the emission spectra of surfactant **2** showed a significant blue shift at CMC. This suggests that micellization brings the fluorophore units in close proximity of each other [12,13]. The common observation encountered in bringing fluorophores together is self-quenching and/or excimer formation, which in turn reduced overall energy transfer efficiency [14,15]. For our system, small amount of decrease in the quantum efficiency was observed upon comparing the quantum yield of the free surfactant **2** with different sets of dansyl-SCMs (Table 1, entry 6 with entry 1–5). We believe that crosslinking the micelles will lead to hydrophobicity-enhanced emission, which is responsible for increase in the quantum yield but at the same time crowding the chromophores in a rigid space will also reduce the quantum yield due to self-quenching. For SCMs, both these reasons are contributing to the overall observed quantum yield. The average size of the dansyl-SCMs (Set 1–5) ranged from ca. 4 – 7 nm.

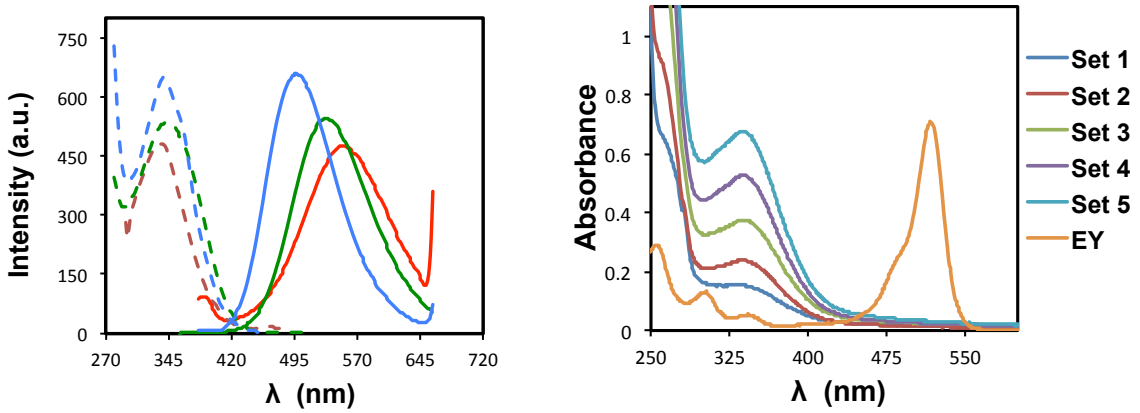

Fig. 1 (a) Emission spectra (solid lines on right) at λ_{ex} = 343 nm and excitation spectra (broken lines on left) at λ_{em} = 490 nm (with λ_{max} = 330 nm) for; dansyl-SCM–Set 5 (blue, 0.007 mM), surfactant **2** (red, 0.007 mM) and surfactant **2** (green, 0.30 mM); (b) absorbance spectra of dansyl-SCM [0.3 mM] (λ_{max} = 340 nm) and EY [0.010mM] (λ_{max} = 520 nm); in Milli-pore water.

Table 1. Characterization of dansyl-SCM prepared from **1** and **2**.[a]

Entry	[**1**]/[**2**]	DLS Diameter (nm)	QY (%)[b]
1	80:20	3.7	17
2	60:40	4.3	10
3	40:60	6.7	8.3
4	20:80	6.2	7.2
5	0:100	5.3	5.3
6	0:100[a]	---	19[a]

[a] Quantum yield of the free surfactant **2** (2% in water, 10% in 1:1 v/v water/MeOH and 19% in MeOH). [b] Quantum yields were determined using quinine sulfate in 0.05 M H_2SO_4 as a standard, by the excitation at 343 nm. The quantum yields were calculated according to equation $\Phi = \Phi_S \times I/I_S \times OD_S/OD \times \eta^2/\eta_S^2$, in which Φ is the quantum yield, Φ_S = 0.577 for quinine sulfate, I is the integrated intensity, η is the refractive index ($\eta^2 = \eta_S^2$ as water was used for both system), OD is the optical density. The subscript S refers to the standard.

After evaluating the efficient overlap between the emission spectra of donor (dansyl-SCM) and excitation spectra of acceptor (see Experimental Section for details), our first choice was to test Eosin Y (EY) disodium salt as the energy acceptor for studying energy transfer. We titrated a solution of dansyl-SCM (Set 5) in Millipore water with EY.

With the addition of EY to aqueous solution of dansyl–SCMs, the donor emission at 490 nm was observed to decrease upon selective donor excitation at 343 nm (Fig. 2a). Importantly, irradiation of EY at 343 nm in the absence of dansyl-SCM gave negligible emission. This data indicated that a small amount of EY [4.34 μM] had the ability to

completely quench the emission intensity of our donor system, which is evidence for effective Förster energy transfer from dansyl-SCM to EY. Based on our previous findings [6], this result was expected as the electrostatic interaction between the negatively charged EY and positively charged dansyl-SCM causes spontaneous assembly of the acceptor molecule (EY) onto the surface of the nanoparticle. The resulting quenching data hence obtained was fitted into the 1:1 binding isotherm to generate association constant K_a = (0.50 ± 0.02) × 10^8 M^{-1} and the $(dansyl)_n$ concentration C_0 = (1.4 ± 0.2) × 10^{-8} M, by using a nonlinear least-squares curve fitting (Fig. 2b). Table 2 displays the association constant values for all the sets having different fluorophore ratios for dansyl-SCM (entry 1–5).

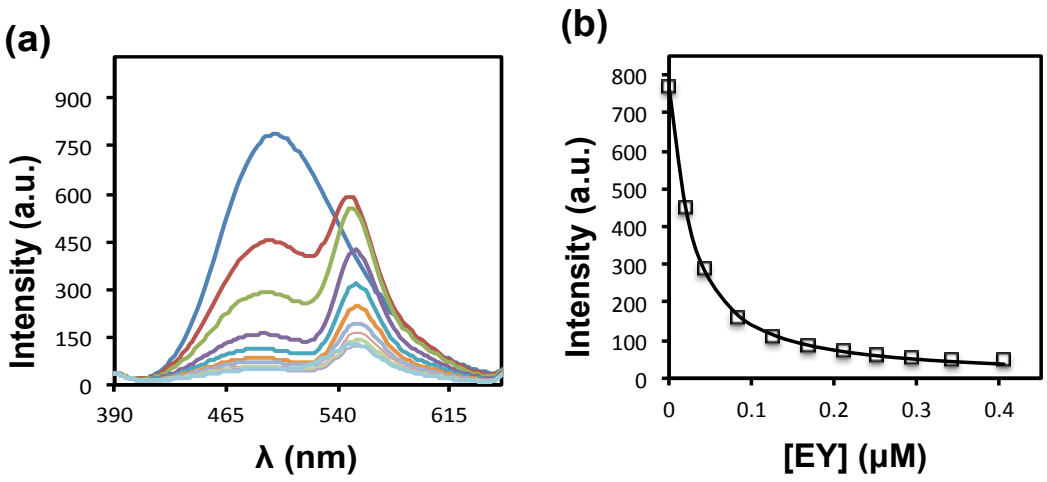

Fig. 2 (a) Fluorescence spectra of dansyl-SCM (Set 5 = 7 μM in Millipore water) in the presence of different concentrations of EY. The concentrations of EY was 0.00, 0.88, 1.59, 2.40, 3.47, 4.34, 5.73, 7.19, 8.52, 9.97 μM from top to bottom. (b) The nonlinear least-squares analysis of I_F for Set 5 versus the concentration of EY.

Table 2. Quenching of dansyl-SCM by EY.[a]

Entry	[**1**]/[**2**]	K_a ($\times 10^8$ M^{-1})	C_0 ($\times 10^{-8}$ M)	n	x
1	80:20	1.2 ± 0.1	4.4 ± 0.4	9	1
2	60:40	1.2 ± 0.1	4.7 ± 0.3	34	1
3	40:60	0.89 ± 0.04	1.3 ± 0.2	80	2
4	20:80	0.91 ± 0.03	2.4 ± 0.1	130	3
5	0:100	0.50 ± 0.02	1.4 ± 0.2	510	9
6	0:100[b]	1.3 ± 0.1	--[e]	--[e]	--[e]
7	0:100[c]	1.4 ± 0.2	--[e]	--[e]	--[e]
8	0:100[d]	2.5 ± 0.2	--[e]	--[e]	--[e]
9	0:100[f]	9.1 ± 0.1	6.8 ± 0.2	730	12

[a] Nonlinear least-squares fittings of I_F versus the EY concentration were performed using equation $I_F=I_0+((I_{lim}-I_0)/(2*C_0))*(C_0+C_{EY}+(1/K_a)-((C_0+C_{EY}+(1/K_a))\text{^}2-4*C_{EY}*C_0)\text{^}(1/2))$, in which I_F was the observed emission intensity of dansyl-SCM, I_0 the emission intensity of dansyl-SCMs in the absence of EY, I_{lim} the emission intensity of the fully complexed dansyl-SCM (assumed to be zero in the curve fitting), C_0 the concentration of (dansyl)n, and C_{EY} the concentration of EY. K_a = association constant, n = number of the dansyl fluorophores (= surfactant **2)** per light harvesting unit, x = number of dansyl-SCM units quenched per EY (Set 1 = 23/(0.2×60), Set 2 = 43/(0.4×60), Set 3 = 238/(0.6×60), Set 4 = 166/(0.8×60), Set 5 = 364/(1×60)). [b] The titration was performed with 0.4 μM of sodium phosphate in the solution. [c] The titration was performed with 0.4 μM of 1,3,5-benzenetricarboxylate in the solution. [d] The titration was performed with ~ 0.4 μM of polyacrylic acid, sodium salt in the solution. [e] The error on C_0 in the curve-fitting was too large to be reliable. [f] The titration was performed with calcein.

We used the absorption spectra to calculate the concentration of the fluorophore (dansyl units) in the solution [16] based on which the number of dansyl fluorophore involved in the light-harvesting unit was calculated: n = 510 for Set 5 [6, Table 2]. To our surprise this number was 10 times higher than our previous finding—DPA functionalized light-harvesting SCMs [6]. The n value, which is indicative of the number of fluorophores effectively quenched by one EY molecule, presently far exceeded the aggregation number of the surfactant in SCM i.e. ~ 50–60 [see Table 3]. These results suggested that, in current scenario, the energy migration pathway involved association of multiple fluorophores from different units and not just one light harvesting dansyl-SCM unit. This number was observed to be the highest for Set 5, which is expected as it has the largest population of dansyl chromophore per unit. The n value was similarly calculated for other sets (entry 1–4), thereby displaying efficient participation of 9, 34, 80 and 130 fluorophores in the energy migration process for Set 1, Set 2, Set 3 and Set 4, respectively. Another evidence for the aggregation among the donor systems comes from DLS studies. Table 3 displays increase in size of Set 5 from ca. 4 nm to ca. 30 nm upon titration with EY. We also monitored the change in the molecular weight for donor system (also studied for Set 1 to 4) upon EY addition, which displayed a consistent increase in their respective sizes. This helped us to calculate the aggregation number of our donor system that amounts to ca. 60.

Table 3: Displaying the distribution of molecular weight and hydrodynamic diameter of dansyl-SCM (Set 5)

Set 5	EY [μM]	Diameter	Molecular weight [KDa]	*x*'
1	0	4 nm	5.8×10^1	---
2	0.02	31 nm	3.7×10^3	63
3	0.04	25 nm	2.8×10^3	48
4	0.08	27 nm	3.4×10^3	59
5	0.12	34 nm	4.2×10^3	72
6	0.17	28 nm	2.3×10^3	39

***x*'** = Aggregation number of dansyl-SCM units on EY titration

We used these *n* values to calculate *x*–the number of light harvesting units of dansyl-SCM involved in energy transfer. Based on the number of fluorophoes in each of these different sets [11], we calculated $x = 1, 1, 2, 3, 9$ for Set 1 to 5, respectively. To our surprise, we found that 9 units of dansyl-SCM (for Set 5) participated in energy-migration-assisted energy transfer pathway. This result suggested that the electrostatic attraction through EY was strong enough to overcome the energy barrier of bringing multiple poly-cationic nanoparticles in close proximity of each other, thereby facilitating the association of multiple units together and resulting in a magnified antenna effect. To our benefit, EY was serving a dual purpose–acting as an energy-sink and also a binder due to its anionic nature [17,18]. This means that no matter which dansyl-SCM unit absorbs light, energy migration occurs readily from donor to donor; via both inter–(that is, within the same micelle) and intra–unit (among other micelles) migration and finally to the acceptor, as shown in Scheme 2 [19]. For control experiment, we tested the fluorescence

resonance energy transfer (FRET) efficiency in presence of SCM, i.e. the non-chromophoric counterpart of cross-linked micelle. Our data (see Experimental Section for details) reflects that the presence of dansyl chromophore is crucial for the energy migration. All fluorescence studies were repeated at least three times. No significant difference was observed and the errors in the data were generally <5%.

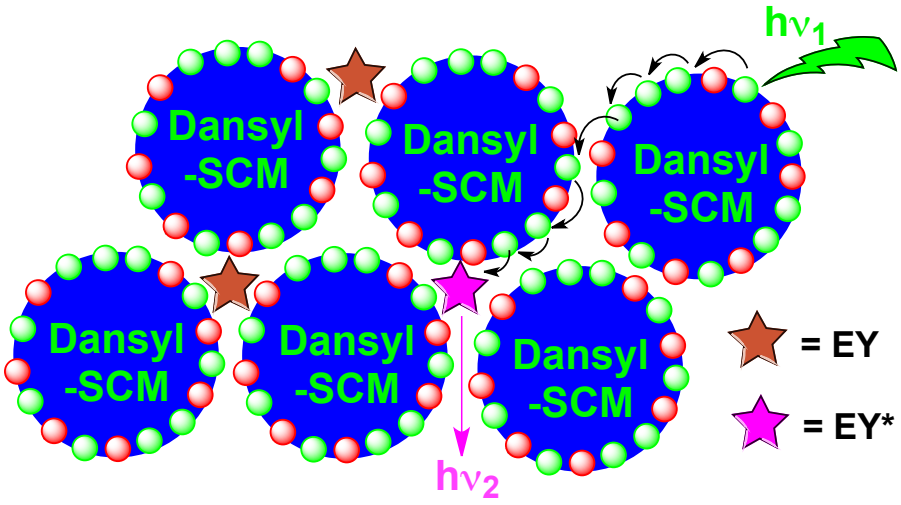

Scheme 2. Pathway involved in light harvesting system for dansyl-SCM in presence of EY behaving as a binder and as an energy acceptor.

We were interested in looking into whether or not the bulky, di-anionic energy acceptor EY was capable of using its own charge to its advantage. For this study, we decide to use external additives. The idea was to add to a solution of dansyl-SCM an anionic molecule in an amount that would start the initial aggregation. In the presence of these anionic additives, the fluorophores are brought to the close proximity of one another to further facilitate energy migration [20]. We then titrated this solution with EY and monitored the decrease of emission

peak at 490 nm. For our study we used sodium phosphate (Fig. 3a), 1,3,5-benzenetricarboxylate (Fig. 3b), and polyacrylic acid sodium salt (Fig. 3c) as anionic additives.

A consistent trend for all three cases was observed where for any given amount of EY, the quenching of emission intensity for the donor system was significantly more in the presence of external additive than where the additive was absent. We used nonlinear least-squares curve fitting to calculate association constant (K_a) for these three sets (Table 2, entry 6–8). Our data suggested that the addition of these external anionic cross-linkers, significantly increased the association constant by ~ 3 (for sodium phosphate), ~ 3 (for 1,3,5-benzenetricarboxylate), and ~ 5 (for polyacrylic acid sodium salt) times, which in-turn lead to an enhancement in their antenna effect (compare entries 6, 7 and 10, respectively, with entry 5). These results further support our reasoning that anionic charge (energy acceptor EY) initiates aggregation.

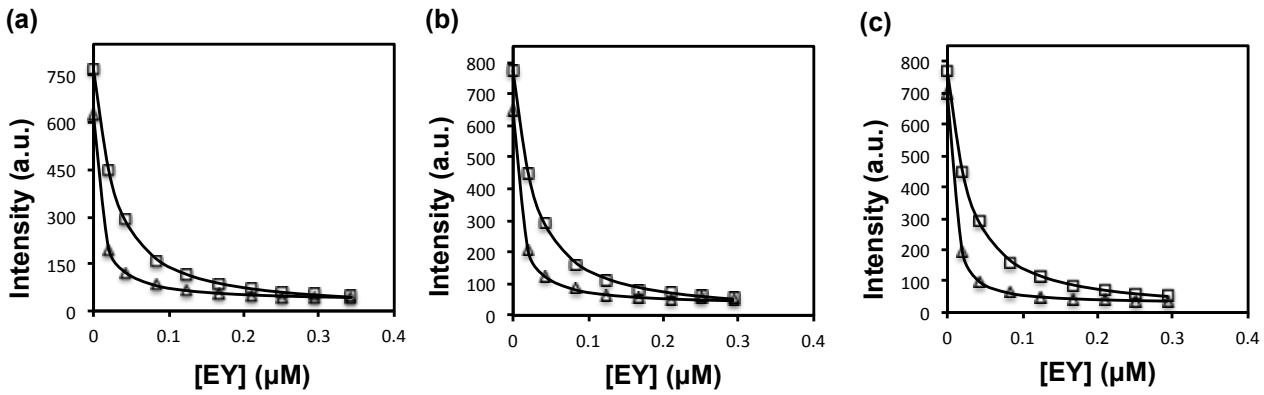

Fig. 3 Relative nonlinear least-squares analysis of dansyl-SCM with EY, (□) without additive and (Δ) with additive, in Millipore water.

Another evidence supporting the formation of dansyl-SCM aggregates comes from DLS study where it was observed that the hydrodynamic diameter of Set 5 is sharply increased from

ca. 5 nm to 294 nm on polyacrylic acid, sodium salt [0.4 μM] addition (see Experimental Section for details). The overall size stayed consistent upon successive addition of energy acceptor-EY. Similar increase in size was observed in case of 1,3,5-benzenetricarboxylate and sodium phosphate.

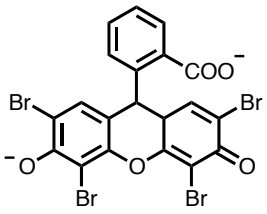

Eosine Y (EY)

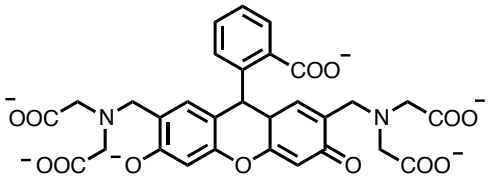

Calcein

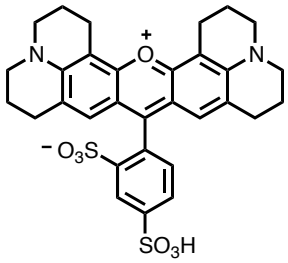

SR101

In order to study the effect of increased magnitude of electrostatic attraction, we decided to titrate dansyl-SCM with another energy acceptor–calcien (see Experimental Section for details). Compared to EY, calcein has 4 more units of anionic charge. We hypothesized that an increase in the anionic character with calcein should facilitate higher degree of association among the fluorophores and hence, encourage higher energy migration. Table 2, entry 9 suggests that our hypothesis holds true—displaying 18 times higher binding ability (i.e., $K_{Calcein}/K_{EY}$) in presence of calcein as an energy acceptor and binder. The data suggests that calcein was able to effectively channel energy among 730 fluorophores (*n* value) by bringing 12 dansyl-SCM units (*x* value) in close proximity. This impressively large numbers highlight enhanced antenna effect in our nanoparticulate material. The proof of aggregation was also monitored by DLS for all the sets.

Although calcein excellently served our purpose of a poly-anionic energy acceptor, due to its strong overlap with donor's emission (i.e., dansyl-SCMs), we encountered difficulty in its peak separation. To address this problem, we decided to use a red-shifted dye—Sulforhodamine

101 (or SR101) which would also act as a secondary energy acceptor. SR101 was carefully chosen because of its effective spectral overlapping (see Experimental Section for details). This triple-dye-system was designed such that dansyl served as a common donor for EY and SR101, while EY acted both as an energy acceptor for dansyl group and as a donor for SR101. The idea was to investigate the pathway of from energy being captured by the multiple dansyl chromophoric units on the SCM surfaces, transferred to EY and then eventually funneled to SR101.

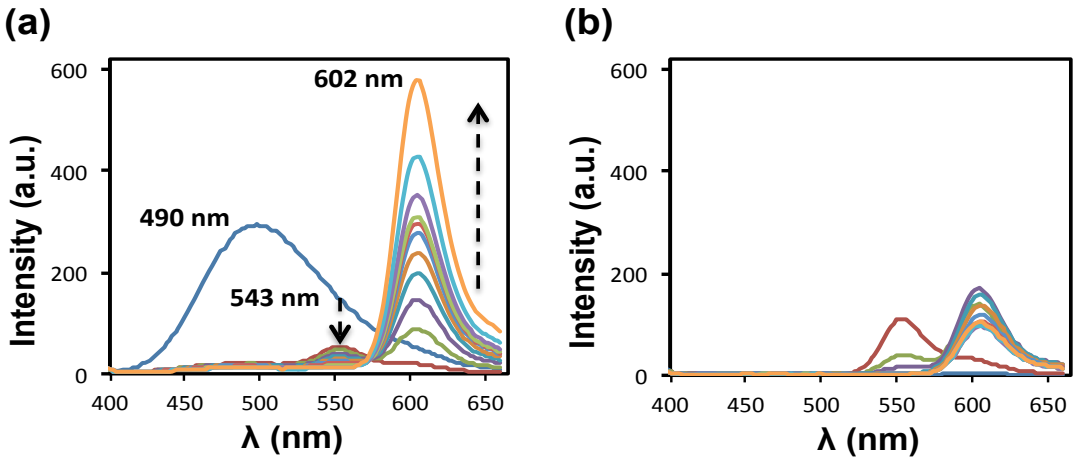

Fig. 4 Fluorescence spectra of (a) dansyl-SCM (Set 5 = 7 μM) and (b) control-SCM [7 μM], both in the presence of EY [0.2 μM] titrated with different concentrations of SR101 (0.00, 0.020, 0.043, 0.083, 0.125, 0.168, 0.210, 0.250, 0.293, 0.343, 0.406 μM from bottom to top), upon selective excitation of donor at 343 nm.

To test whether energy transfer could take place within these multiple fluorophores, we prepared three different solutions with same concentration of donor dansyl-SCM but with varying amount of EY added. Set I with EY = 0.08 μM–concentration required to initiate donor emission quenching, Set II with EY = 0.2 μM–concentration required to completely quench

donor emission [Fig. 4a] and Set III with EY = 0.4 μM–excess concentration after complete quenching donor emission. Addition of EY lead to quenching of the donor emission at 490 nm with formation of acceptor-EY emission at 543 nm. These sets were then titrated with SR101 and all of them consistently displayed efficient FRET—starting from donor dansyl to acceptor EY followed by EY to acceptor SR101 with now a decrease in the peak at 543 nm followed by a corresponding increase in the distinctive peak for SR101 at 602 nm [21].

To test FRET efficiency in absence of the dansyl-donor system, we repeated our studies in presence of the control–SCM; the non-chromophoric cross-linked micelle system. Fig. 4b displays an absence of FRET for the case where SCM + EY were titrated with SR101; thereby highlighting the importance of the donor antennas on the periphery of the nanoparticle to efficiently capture the incidental light and foster energy migration among the dyes.

Conclusion

In conclusion, we have demonstrated a facile preparation of fluorophore-labeled surface cross-linked-water-soluble nanoparticles using an easily performed one-pot click reaction. The significance of this design lies in its ability to amplify the magnitude of "antenna effect". The micelle system facilitates an easy modification of the number of donors, where several of these chromophoric molecular species are capable to absorb the incident light and efficiently channel the excitation energy to a common energy acceptor. It is also noteworthy that the antenna effect can be further extended to three chromophores and the FRET nanoparticle ability can be applied to energy transfer triad dye series. This strategy could open new applications of chromophoric micelles in signal amplification and biological sensing. In addition, future work in this field is envisioned towards advancement in complex mimics of natural photosynthetic systems to

employ light energy in chemical reactions.

Acknowledgement

We thank NSF (CHE-1303764) for partial support of the research.

Experimental Section

General Experimental Methods.

All reagents and solvents were of ACS-certified grade or higher and used as received from commercial suppliers. Millipore water was used to prepare buffers and nanoparticles. ^{1}H and ^{13}C NMR spectra were recorded on a VARIAN MR-400 spectrometer. Dynamic light scattering (DLS) was performed on a PD2000DLSPLUS dynamic light scattering detector. Mass spectrometry was performed on AGILENT 6540 QTOF mass spectrometer. UV-Vis spectra were recorded on a Cary 100 Bio UV-Visible spectrophotometer and fluorescence spectra were recorded on a Varian Cary Eclipse Fluorescence spectrophotometer.

Preparation of dansyl-SCMs

1,4-Diazidobutane-2,3-diol (compound **3**, 3.8 mg, 0.022 mmol), $CuCl_2$ (13.5 μL of a 5 mg/mL aqueous solution, 0.5 μmol), and sodium ascorbate (49.5 μL of a 20 mg/mL aqueous solution, 5 μmol) were added to a micellar solution of compound **2** (12 mg, 0.02 mmol) in Millipore water (2.0 mL). The reaction mixture was stirred slowly at room temperature for 24 h after which the mixture was dialyzed for 3 days against deionized water using 500 Da molecular weight cut-off tubing.

Determination of Critical Micelle Concentration (CMC) of compound 2

To 12 separate vials, 100, 90, 80, 70, 60, 50, 40, 30, 20, 10, 5, and 3 μL of the stock solution of surfactant **1** (26 mg, 0.043 mmol) in 2.5 mL Millipore water was added. Millipore water was added to each vial to make the total volume 2.0 mL. Fluorescence spectra were recorded at the excitation wavelength of 343 nm. The final results were based on duplicate experiments with separately prepared solutions.

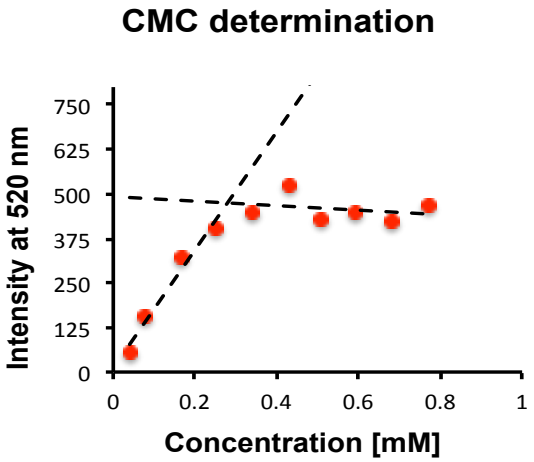

Fig. 5 Surfactant **2** I_{520} as a function of [**2**].

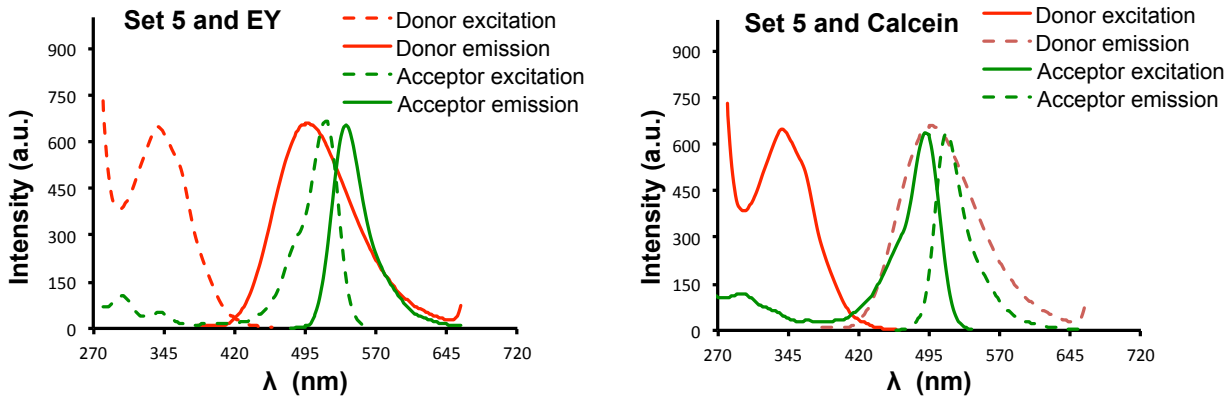

Fig. 6 Emission spectra (solid lines) and excitation spectra (broken lines) of energy donor dansyl-SCM–Set 5 (in red) and energy acceptor dye - eosin Y and calcein (in green), in Millipore water.

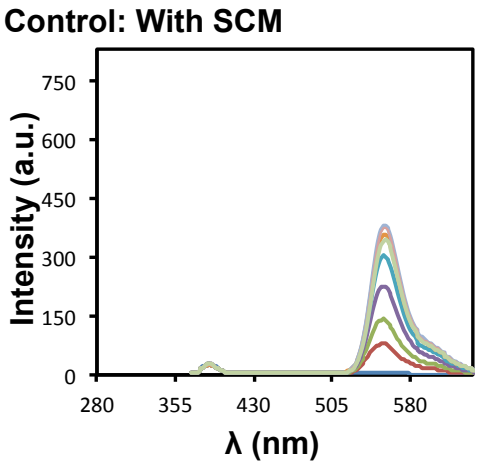

Fig. 7 Emission spectra at λ_{ex} = 343 nm of aqueous solution of control-SCM [7 μM] titrated with [EY] was 0.00, 0.020, 0.043, 0.083, 0.125, 0.168, 0.210, 0.250, 0.293, 0.343, 0.406 μM.

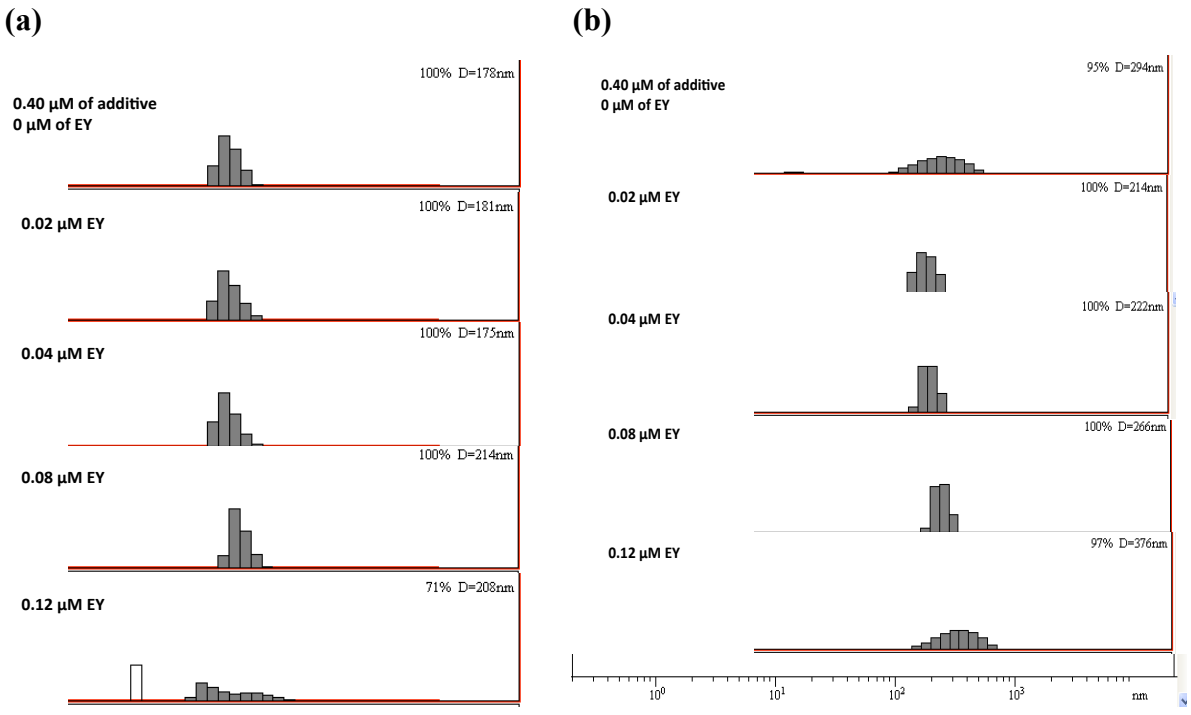

Fig. 8 Distribution of hydrodynamic diameter of dansyl-SCM–Set 5 [7 μM] with addition of polyacrylic acid, sodium salt [0.4 μM] during titration study with EY, (a) with mass normalization and (b) without mass normalization.

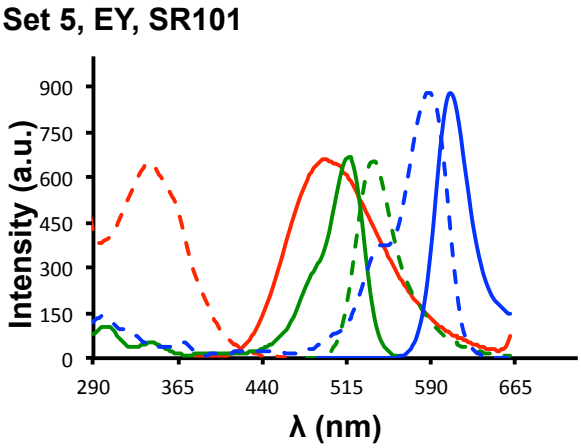

Fig. 9 Comparison of emission (solid lines) and excitation spectra (broken lines) of donor system—dansyl-SCMs–Set 5 (red), energy acceptor—eosin Y (green) and secondary energy acceptor Sulforhodamine 101 (blue); in Milli-pore water.

Syntheses

Scheme 3. Synthesis of compound **2**

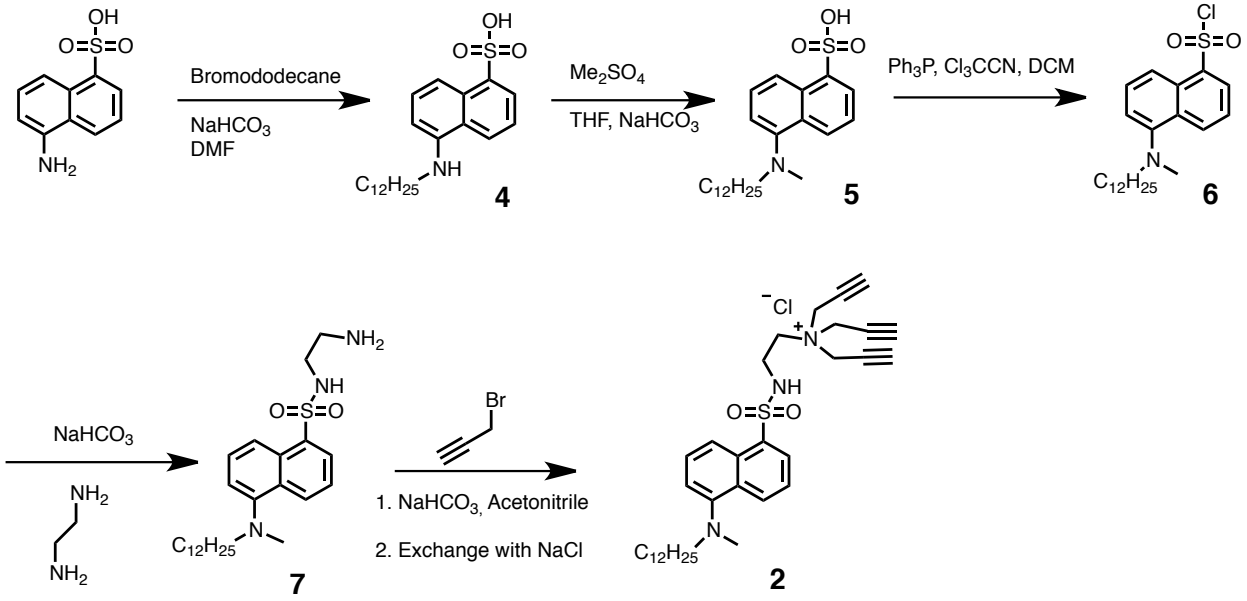

Compound 4. A mixture of 5-amino-1-naphthalene sulfonic acid (6.00 g, 26.8 mmol), sodium bicarbonate (6.80 g, 80.6 mmol) and 1-bromododecane (9.60 mL, 40.2 mmol) in dimethyl formamide (50 mL) was stirred and heated at 125 ºC for 3 h. The mixture was poured into water (500 mL) containing sodium chloride (156 g), and pH was lowered from 8.9 to 3.0 with concentrated hydrochloric acid (~ 3 mL). The solid formed, was isolated by filtration, washed with water (3 × 50 mL) and dried under vacuum to give a brown powder. This solid was re-dissolved in water (100 mL) by adding sodium hydrogen carbonate (3.50 g). Concentrated HCl (~ 1 mL) was added drop-wise to lower down the pH from 7.9 to 3. Precipitate was separated by filtration, dried under high vacuum and then recrystallized using 2:1 isopropanol/water to yield a dark brown solid (5.97 g, 57%). ^{1}H NMR (400 MHz, 1:1 $CDCl_3/CD_3OD$, δ): 8.53 (d, J = 8.5 Hz, 1H), 7.71 (d, J = 7.3 Hz, 1H), 7.44 (d, J = 8.6 Hz, 1H), 7.19 (dd, J = 8.7, 7.4 Hz, 1H), 7.11 (d, J = 7.8 Hz, 1H), 6.91 (t, J = 7.9 Hz, 1H), 3.24 – 3.15 (m, 2H), 1.69 (p, J = 7.7 Hz, 2H), 1.35 – 1.06 (m, 18H), 0.77 (t, J = 6.8, 3H). ^{13}C NMR (101 MHz, $(CD_3)_2S$=O, δ): 144.7, 130.1, 125.5, 125.2, 125.0, 124.8, 122.6, 31.3, 29.1, 29.0, 28.9, 28.8, 28.8, 28.7, 28.7, 28.5, 26.2, 22.1, 14.0. ESI-HRMS (*m/z*): $[M - H]^-$, calcd for $C_{22}H_{32}NO_3S^-$, 390.2108; found 390.2103.

Compound 5. Compound **4** (1.00 g, 2.55 mmol) was dissolved in water (40 mL) containing sodium bicarbonate (0.70 g, 7.68 mmol). The resulting solution was stirred at 15 ºC for 5 min and dimethyl sulfate (0.25 mL, 2.55 mmol) was added. After 6 h, another batch of dimethyl sulfate (0.25 mL, 2.55 mmol) was added to the reaction mixture. The solution was stirred at room temperature, overnight and then heated to 80 ºC for 0.5 h. After cooling to room temperature, the pH was adjusted to 3 using HCl (1 M). The solid, which formed overnight, was filtered, washed with water and dried under high vacuum to give a dark brown solid (0.97 g,

94%). ^{1}H NMR (400 MHz, CD_3OD, δ): 8.64 (d, J = 8.5 Hz, 1H), 8.32 – 8.23 (m, 2H), 7.64 – 7.50 (m, 2H), 7.24 (d, J = 7.6 Hz, 1H), 3.05 (dd, J = 8.5, 6.5 Hz, 2H), 2.84 (s, 3H), 1.62 (p, J = 7.2 Hz, 2H), 1.27 (m, 18H), 0.88 (t, J = 6.7 Hz, 3H). ^{13}C NMR (101 MHz, $(CD_3)_2S$=O, δ): 144.7, 130.2, 130.1, 125.3, 124.8, 109.6, 62.8, 52.8, 31.3, 31.3, 29.0, 28.9, 28.9, 28.8, 28.7, 28.6, 28.4, 25.7, 22.1, 14.0. ESI-HRMS (*m/z*): $[M - H]^-$, calcd for $C_{23}H_{34}NO_3S^-$, 404.2265; found 404.2268.

Compound 6 [22]**.** A solution of triphenyl phosphine (0.15 g, 0.59 mmol) in anhydrous dichloromethane (3 mL) was added to a mixture of compound **5** (0.08 g, 0.19 mmol) and trichloroacetonitrile (0.06 mL, 0.59 mmol) dissolved in anhydrous dichloromethane (2 mL). The reaction mixture was heated to reflux for approximately 3.5 h, under inert atmosphere. After cooling to room temperature, the solvent was removed using rotary evaporator and the residue was purified by column chromatography over silica gel using 40:1 hexane/ethyl acetate as eluent to afford a bright yellow oily product (0.70 g, 87%). ^{1}H NMR ((400 MHz, $CDCl_3$, δ): 8.63 (d, J = 8.5 Hz, 1H), 8.36 (d, J = 8.5 Hz, 1H), 8.27 (d, J = 7.5 Hz, 1H), 7.60 (t, J = 7.3 Hz, 1H), 7.47 (t, J = 7.1 Hz, 1H), 7.20 (d, J = 7.6 Hz, 1H), 3.04 – 2.92 (m, 2H), 2.77 (s, 3H), 1.58 – 1.48 (m, 2H), 1.16 (m, 18H), 0.79 (t, J = 6.9Hz, 3H).^{13}C NMR (101 MHz, $cdcl_3$, δ) 152.2, 139.8, 133.5, 131.2, 129.7, 129.6, 129.1, 123.0, 118.7, 117.8, 57.6, 43.0, 32.1, 29.8, 29.8, 29.8, 29.8, 29.8, 29.7, 29.6, 27.6, 27.4, 22.9, 14.3. ESI-HRMS (*m/z*): $[M]^+$, calcd for $C_{23}H_{34}$ $ClNO_2S$, 424.2072; found 424.2073.

Compound 7. Ethylenediamine (0.36 mL, 5.41 mmol) was added dropwise to a solution of compound **6** (0.23 g, 0.54 mmol) in anhydrous dichloromethane (10 mL). After the reaction mixture was stirred for 15-20 min, at room temperature under inert atmosphere, the organic layer was washed with brine (7 × 10 mL), dried over anhydrous Na_2SO_4 and evaporated under vacuum

to yield a yellow oily product (0.23 g, 96%). ^{1}H NMR 400 MHz, CD_3OD, δ): 8.48 (d, *J* = 8.5 Hz, 1H), 8.21 (dd, *J* = 25.9, 7.9 Hz, 2H), 7.46 (dt, *J* = 22.1, 7.9 Hz, 2H), 7.22 – 7.10 (m, 2H), 2.97 (t, *J* = 7.5 Hz, 2H), 2.87 (t, *J* = 5.6 Hz, 2H), 2.76 (s, 3H), 2.68 (t, *J* = 5.6 Hz, 2H), 1.59 – 1.51 (m, 2H), 1.29 – 1.12 (m, 22H), 0.81 (t, *J* = 6.8 Hz, 4H). ^{13}C NMR (100 MHz, $CDCl_3$, δ): 151.9, 134.9, 130.9, 130.4, 129.8, 129.6, 128.4, 123.3, 119.1, 116.9, 57.6, 45.6, 42.8, 41.1, 32.1, 29.9, 29.8, 29.8, 29.8, 29.7, 29.6, 29.5, 27.7, 27.4, 22.8, 14.3. ESI-HRMS (*m/z*): $[M + H]^+$, calcd for $C_{25}H_{42}N_3O_2S^+$, 448.2992; found 448.2993.

Compound 2 [22]**.** A mixture of compound **7** (0.13 g, 0.29 mmol) and sodium bicarbonate (38 mg, 0.45 mmol) in dry acetonitrile (5 mL) was treated dropwise with a solution of propargyl bromide (0.04 mL, 0.45 mmol). After 6 h, another batch of propargyl bromide (0.04 mL, 0.45 mmol) was added to the reaction mixture while being heated to reflux for total 18 h. The resulting solution was cooled to room temperature, filtered to remove sodium bicarbonate, concentrated under vacuum, re-dissolved in dichloromethane (30 mL) and washed several times with brine, dried using $MgSO_4$, concentrated and then purified by column chromatography over silica gel using 1:8 methanol/CH_2Cl_2 as eluent to afford a viscous brown oily product (0.12 g, 72%). ^{1}H NMR (400 MHz, $CDCl_3$, δ): 8.57 – 8.44 (m, 2H), 8.32 (d, *J* = 8.6 Hz, 1H), 8.09 (d, *J* = 7.2 Hz, 1H), 7.58 (t, *J* = 8.1 Hz, 1H), 7.41 (t, *J* = 7.9 Hz, 1H), 7.21 (s, 1H), 7.15 (d, *J* = 7.6 Hz, 1H), 4.80 (s, 7H), 3.87 – 3.80 (m, 2H), 3.50 (q, *J* = 5.3, 4.7 Hz, 2H), 3.09 – 2.88 (m, 10H), 2.74 (s, 3H), 1.52 (q, *J* = 6.9 Hz, 2H), 1.33 (t, *J* = 7.4 Hz, 7H), 1.19 (d, *J* = 11.6 Hz, 23H), 0.85 – 0.76 (m, 4H). ^{13}C NMR (101 MHz, $cdcl_3$) δ 151.4, 134.0, 130.9, 130.4, 129.4, 128.9, 128.7, 122.8, 119.6, 117.3, 77.3, 77.2, 77.0, 76.7, 70.0, 60.5, 57.4, 53.6, 51.0, 45.8, 42.8, 37.7, 31.9, 29.7, 29.6,

29.6, 29.5, 29.3, 27.5, 27.2, 22.6, 18.6, 17.4, 14.1. ESI-HRMS (*m/z*): $[M - Cl]^+$, calcd for $C_{34}H_{48}N_3O_2S^+$, 562.3462; found 562.3456.

Spectra of key compounds:

^{1}H NMR spectrum of compound **4**

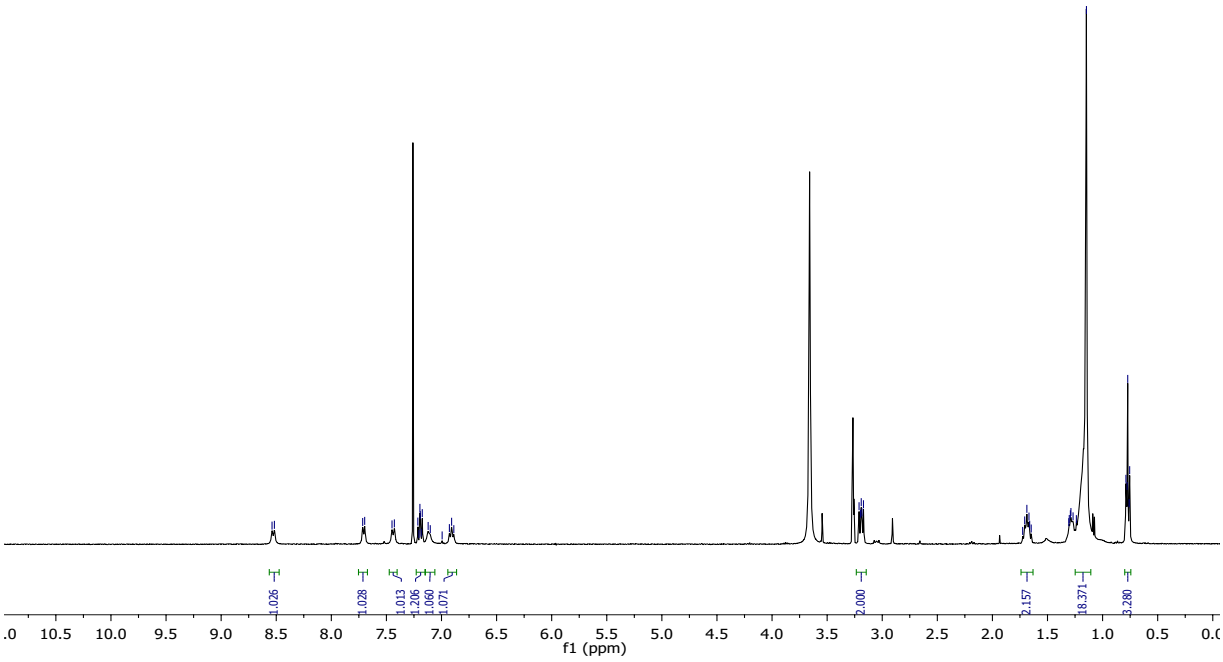

^{13}C NMR spectrum of compound **4**

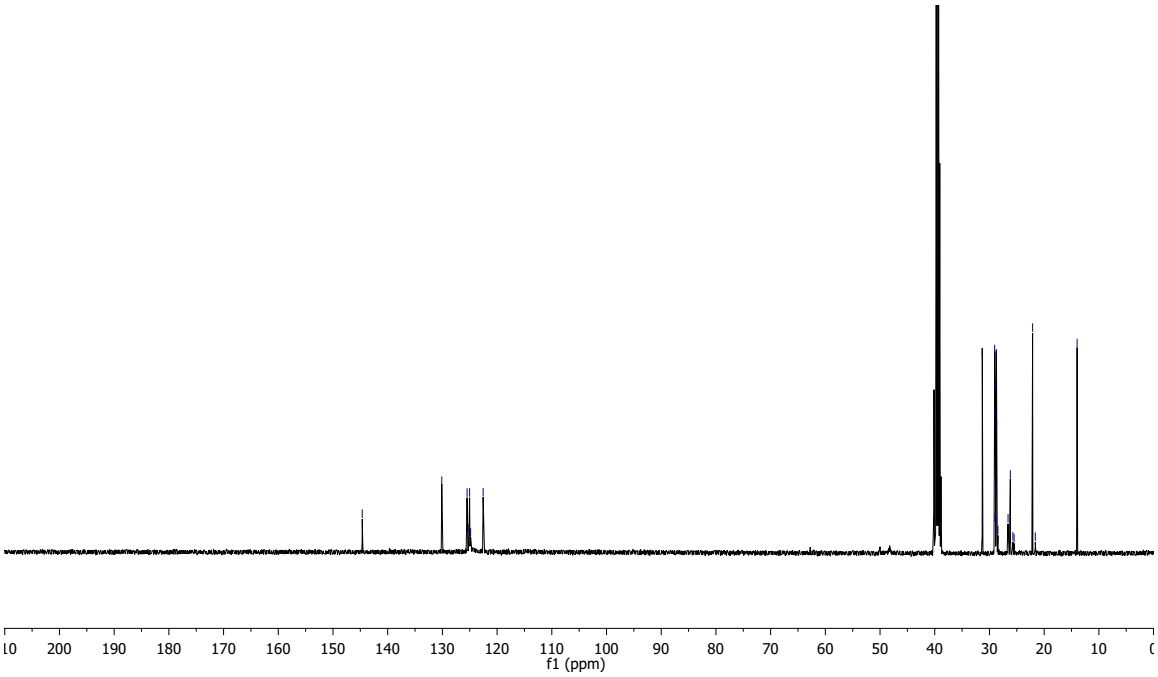

^{1}H NMR spectrum of compound **5**

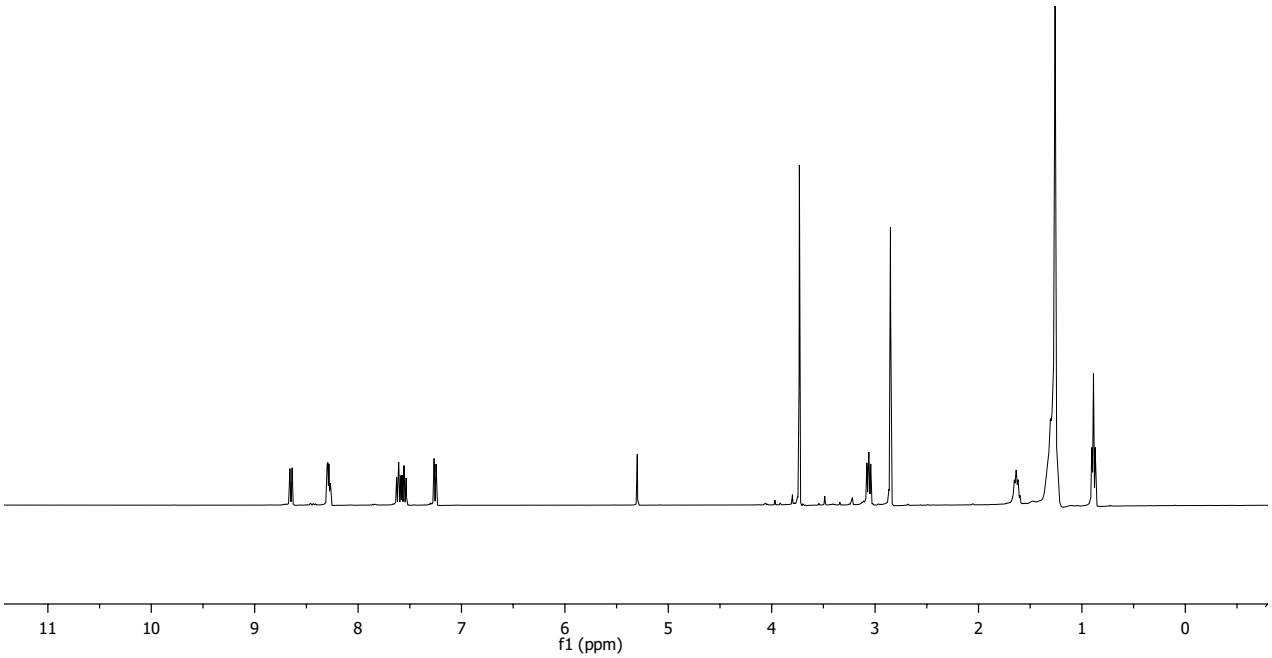

^{13}C NMR spectrum of compound **5**

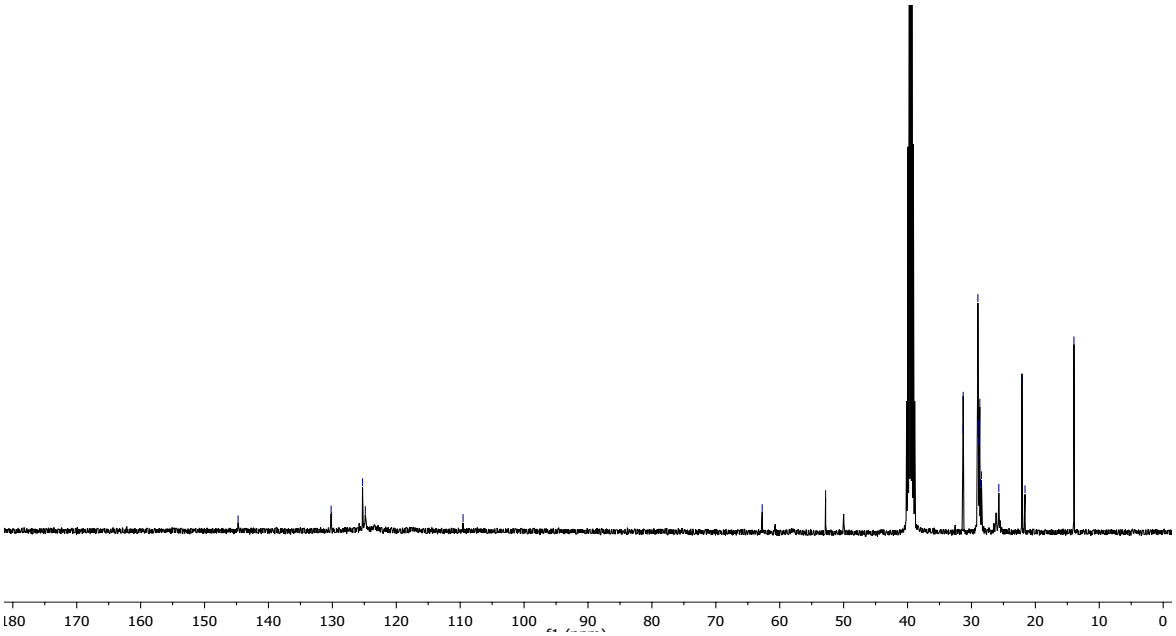

^{1}H NMR spectrum of compound **6**

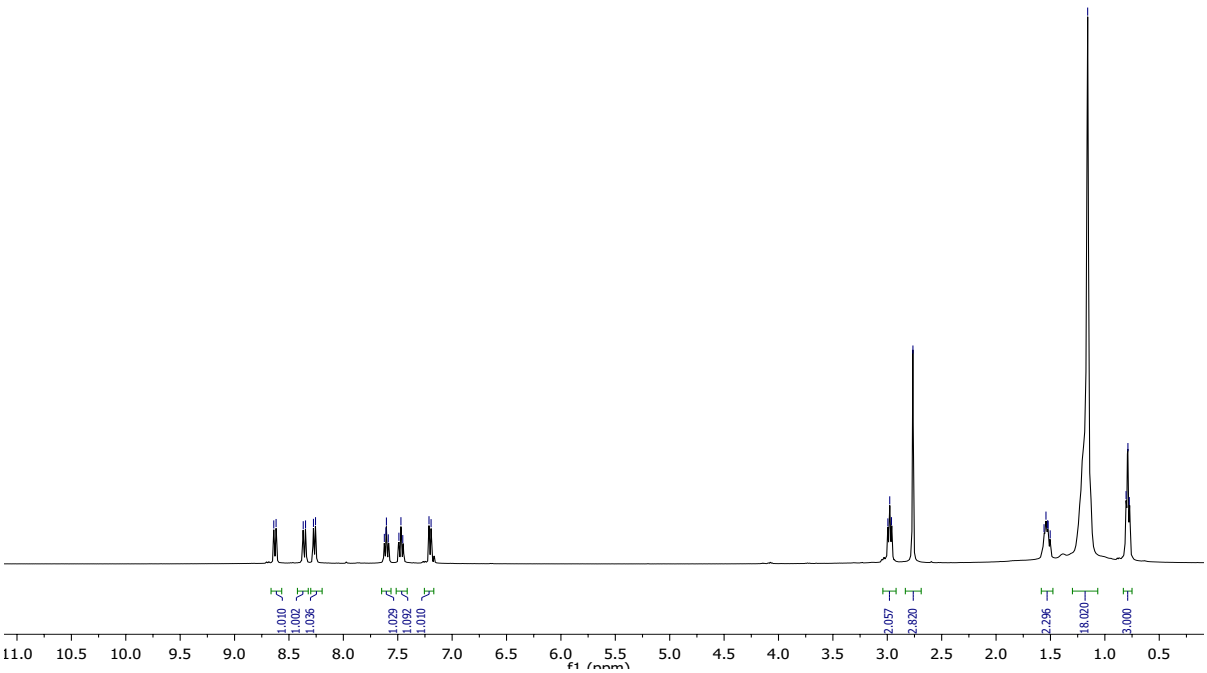

^{13}C NMR spectrum of compound **6**

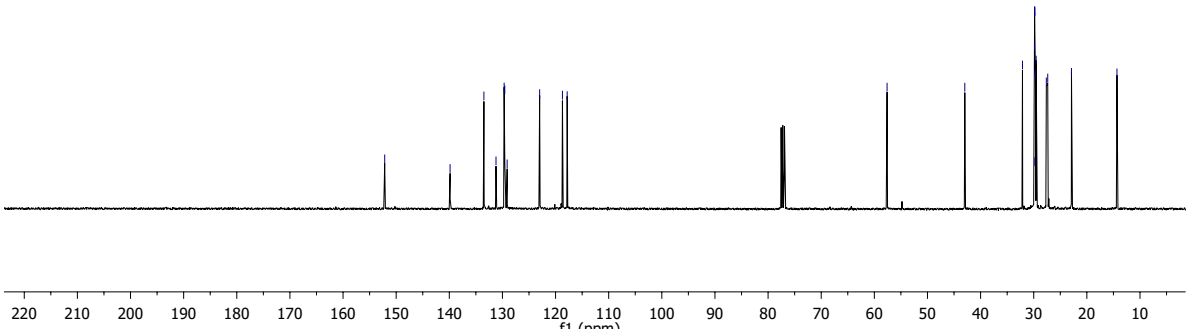

^{1}H NMR spectrum of compound **7**

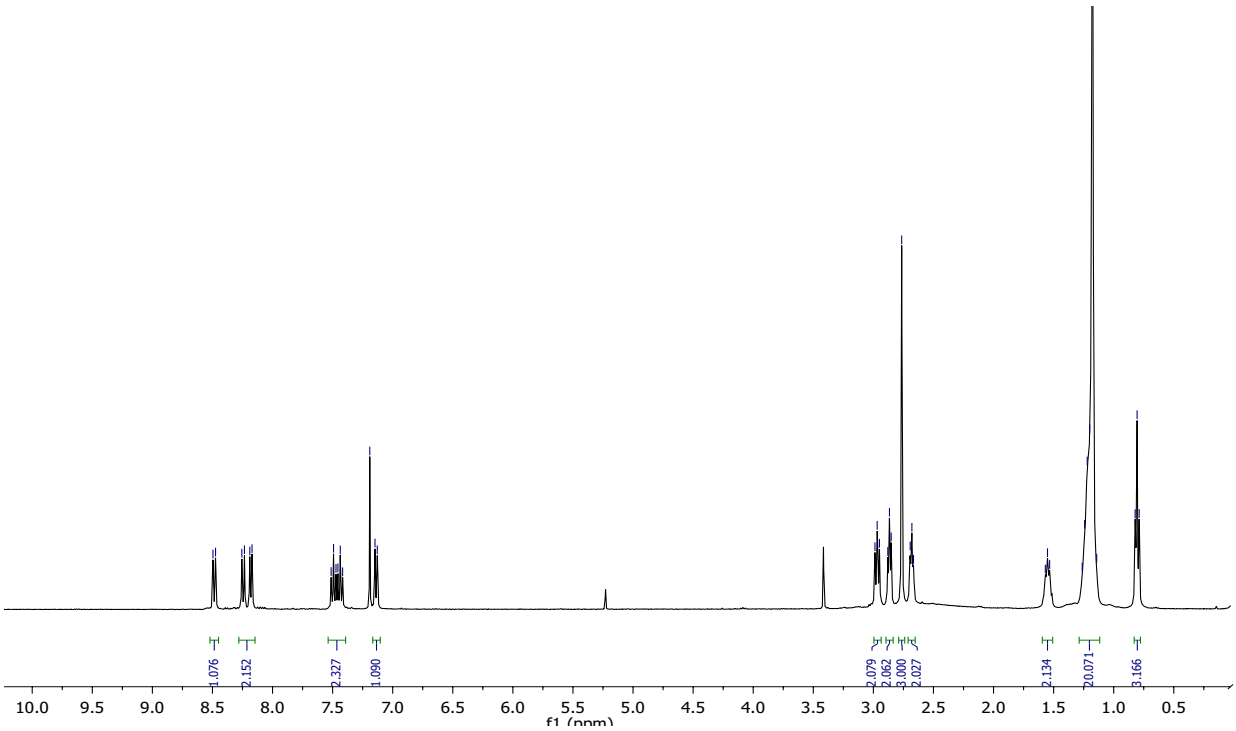

^{13}C NMR spectrum of compound **7**

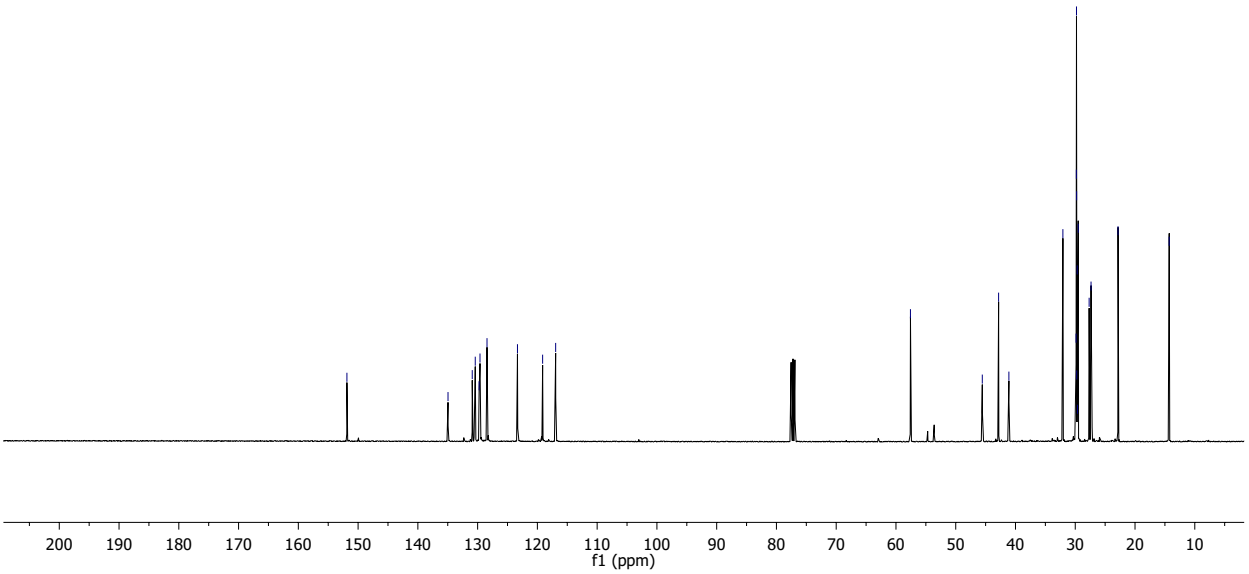

^{1}H NMR spectrum of compound **1**

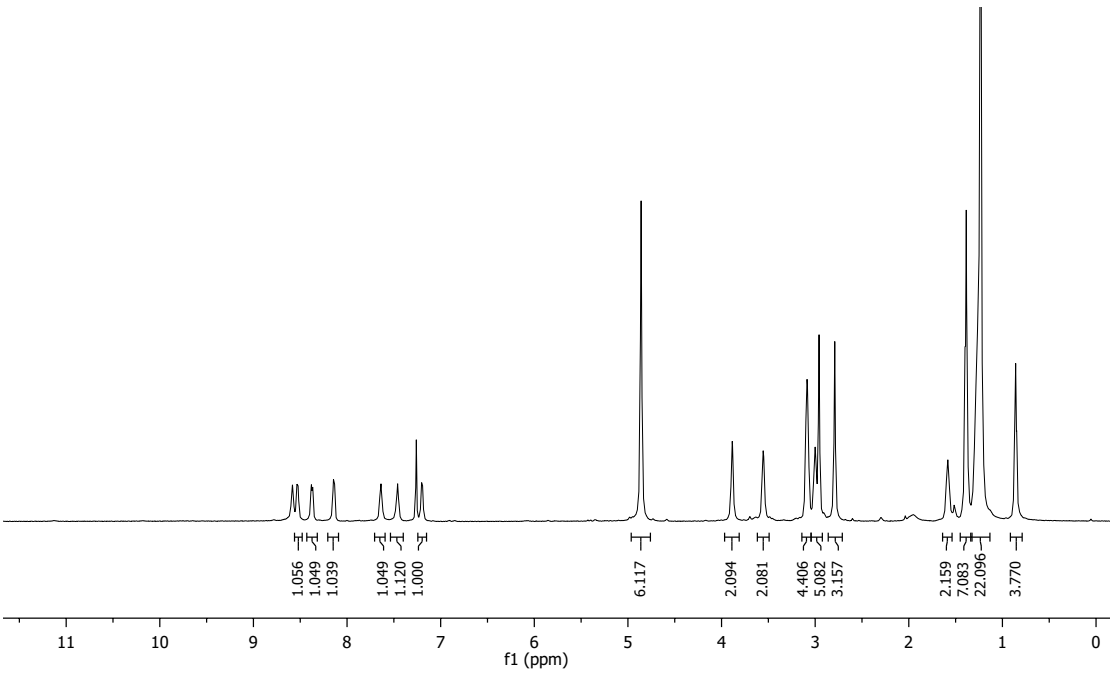

^{13}C NMR spectrum of compound **1**

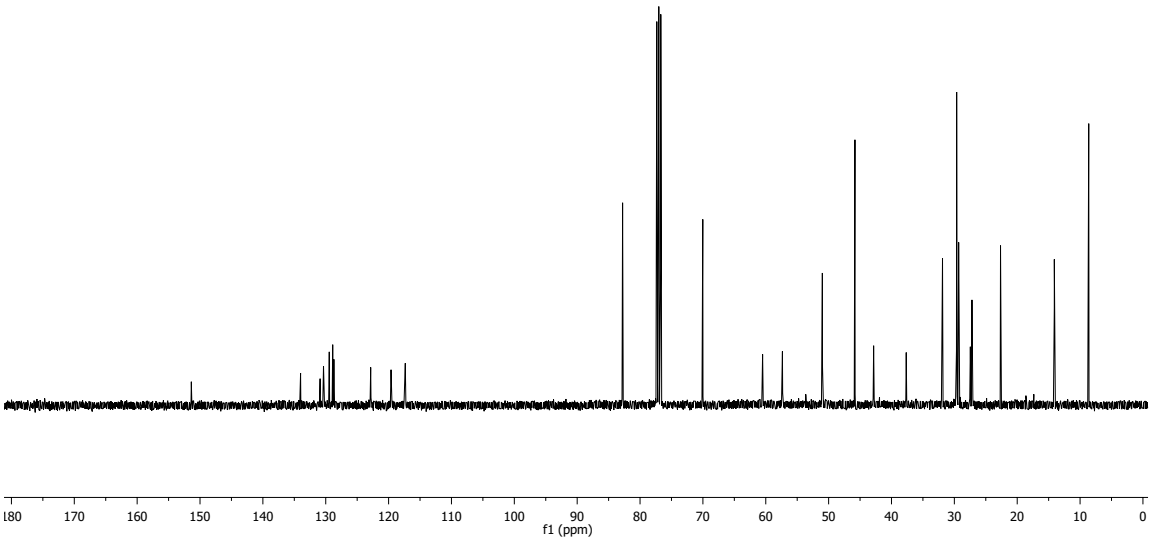

Notes and References

(1) Y. C. Cheng, G. R. Fleming, *Annu. Rev. Phys. Chem*., 2009, **60**, 241.

(2) H. Takeda, M. Ohashi, T. Tani, O. Ishitani and S. Inagaki, *Inorg. Chem*., 2010, **49**, 4554.

(3) Y.-G. Kim, J. Walker, L.A. Samuelson, J. Kumar, *NanoLett*., 2003, **3**, 523.

(4) A. Hagfeldt, G. Boschloo, L. Sun, L. Kloo, H. Pettersson, *Chem. Rev*., 2010, **110**, 6595.

(5) G. H. Krause and E. Weis, *Annual Review of Plant Physiology and Plant Molecular Biology*, 1991, **42**, 313; (b) N. Nelson and A. Ben-Shem, *Nat Rev Mol Cell Bio*, 2004, **5**, 971; (c) G. D. Scholes, G. R. Fleming, A. Olaya-Castro and R. van Grondelle, *Nat. Chem*., 2011, **3**, 763.

(6) H.-Q. Peng, Y.-Z. Chen, Y. Zhao, Q.-Z. Yang, L.-Z. Wu, C.-H. Tung, L.-P. Zhang and Q.-X. Tong, *Angew. Chem. Int. Ed*., 2012, **51**, 2088.

(7) S. Zhang and Y. Zhao, *Macromolecules*, 2010, **43**, 4020.

(8) J. K. Awino and Y. Zhao, *J. Am. Chem. Soc*., 2013, **135**, 12552.

(9) (a) S. Zhang and Y. Zhao, *J. Am. Chem. Soc*., 2010, **132**, 10642; (b) X. Li and Y. Zhao, Langmuir, 2012, **28**, 4152; (c) X. Li and Y. Zhao, *Bioconjugate Chem*., 2012, **23**, 1721.

(10) (a) S. Zhang and Y. Zhao, *Chem. Commun*., 2012, **48**, 9998; (b) G. Chadha and Y. Zhao, *Org. Biomol. Chem*., 2013, **11**, 6849; (c) G. Chadha and Y. Zhao, *Chem. Commun*., 2014, **50**, 2718.

(11) Y.-Z. Chen, P.-Z. Chen, H.-Q. Peng, Y. Zhao, H.-Y. Ding, L.-Z. Wu, C.-H. Tung and Q.-Z. Yang, *Chem. Commun*., 2013, **49**, 5877.

(12) G. Brotas, J. Farinhas, Q. Ferreira, J. Morgado and A. Charas, *Synth Metal*., 2012, **162**, 2052.

(13) N. S. Lee, G. Sun, L. Y. Lin, W. L. Neumann, J. N. Freskos, A. Karwa, J. J. Shieh, R. B. Dorshow, K. L. Wooley, *J. Mater. Chem*., 2011, **21**, 14193.

(14) S. J. Farley, D. L. Rochester, A. L. Thompson, J. A. K. Howard, J. A. G. Williams, *Inorg. Chem.*, 2005, **44**, 9690.

(15) B. K. An, S. H. Gihm, J. W. Chung, C. R. Park, S. K. Kwon and S. Y. Park, *J. Am. Chem. Soc*., 2009, **131**, 3950.

(16) Concentration calculated using optical data (Set 1 = 0.4 μM, Set 2 = 1.6 μM, Set 3 = 1.4 μM, Set 4 = 3.2 μM, Set 5 = 7.0 μM).

(17) T. G. Wensel, C. H. Chang C. F. Meares, *Biochemistry*, 1985, **24**, 3060.

(18) (a) T. Wen, N. B. Li, H. Q. Luo, *Anal Chem*., 2013, **85**, 10863. (b) E. N. Frolov, V. I. Goldanskii, A. Birk, F. Parak, *Eur. Biophys. J*., 1996, **24**, 433.

(19) D. Beljonne, G. Pourtois, C. Silva, E. Hennebicq, L. M. Herz, R. H. Friend, G. D. Scholes, S. Setayesh, K.Mullen, and J. L. Bredas. *Proc. Natl Acad. Sci*., 2002, **99**, 10982.

(20) R. Grünberg, Nat. Methods, 2013, 10, 1021.

(21) L. Wang and W. Tan, *Nano Lett*., 2006, **6**, 84.

(22) O. Chantarasriwong, D. O. Jang, W. Chavasiri, *Tetrahedron Lett*., 2006, **47**, 7489.

CHAPTER 6

GENERAL CONCLUSIONS

This dissertation illustrates the preparation and study of different types of cross-linked micellar systems. Covalently crosslinking the surfactants not only restricts their intermicellar exchange, but also created systems with profound differences from their noncovalent assemblies. Surface cross-linked micelles (SCMs) represent a versatile platform for multivalency allowing simple synthetic preparation and facile post-modification. In this work, these robust water-soluble nanoparticles demonstrated several interesting properties, including sensitivity to aqueous pH catalysis, ability to modify p*K*a value, easy surface and core functionalization, scaffold for a light harvesting system, and enhanced surface basicity. This dissertation summarized my research progress on the development of SCM based light harvesting models and environmentally controlled catalysis.

We first explored of the physical properties of SCM. Specifically, the nanoparticle was shown to possess two binding sites, favoring polar and nonpolar excited states of the fluorescent probe. Compared to dynamic CTAB, cross-linking the micelles in SCM lead to better shielding of the guest molecules and prevented exposure to the bulk solvent. This initiated a slowing down of ESPT for polyanionic photoacid–pyranine, caused by enhancement in the "hydrophobic shielding" effect. Additionally, stronger surface basicity and the ability to stabilize anionic transition states make the polycationic SCMs suitable candidates to hydrolyze activated phosphate esters, at neutral pH.

In an effort to label the SCM with a catalytic group, we also synthesized an imidazole surfactant. The polycationic nature and local hydrophobicity of the prepared imidazole-functionalized surface cross-linked micelles enables modification of the acid/base property of the functional group. The unusual ability of imidazole-SCM to catalyze ester hydrolysis (PNPA) under acidic conditions is an elegant way to demonstrate unique control of the microenvironment for catalysis selectivity and/or activity. Investigation into the hydrophobic effect was done by comparing imidazole*-SCM (with C16 chain) with imidazole-SCM. The result was an increased catalysis with imidazole*-SCM which validated our hypothesis, suggesting a beneficial role of C16 as a hydrophobic anchor. It works by not only positioning the imizadole groups in a relatively hydrophobic local environment, but also possibly bringing the catalytic groups closer to the polycationic micellar surface and making them more resistant towards protonation. Evidence for the enhanced surface basicity and local hydrophobicity of functionalized-SCM also comes from fluorescence studies of 2-naphtol and ANS, at different pHs.

Continuing this work, we aimed to rationalize the influence of environment in aqueous nucleophilic catalysis. Extending the functionalization ability, we were able to anchor the catalytic group-DMAP in the core of the SCM. This work also highlights the significance of engineering smart materials with ability to create channels and pores to facilitate mass transfer during catalysis. Efficient hydrolysis for different substrates (PNPA, PNPH and HPNPP) showed the ability of SCM(DMAP) to perform nucleophilic catalysis under acidic conditions. The effect was larger for SCM(DMAP), as the internal functionalized DMAP remained more pH resistant/active than the surface-functionalized DMAP-SCM. This work is a step towards highlighting synergic effects between a substrate's

inherent nature and local environment of a catalytic group to achieve unconventional catalysis, as demonstrated by enzymes.

Finally, we also worked towards synthesis and application of a chromophore labeled cross-linked micellar system as a light-harvesting model. Upon self-assembly and covalent capture of dansyl surfactants, we prepared an energy donor system with the ability to vary antenna chromophore density. Efficient transfer of energy from multiple chromophores (both intermicellar and intramicellar transfer) to a single acceptor (EY/calcein) was displayed. Energy migration involving triad dye system was also evaluated. Evidence for the acceptor molecule to function both as an energy sink and as an aggregation-causing agent comes from fluorescence and DLS studies. Unlike dansyl-SCM, no FRET was observed for non-chromophore counterpart–SCM, indicating how critical is the presence of multiple chromophores at the micellar interface for the observed antenna effect. Our findings may encourage efforts towards application of multifunctional cross-linked micellar systems as sensors, photocatalytic units, dye-sensitized solar cells, and artificial electronic and photonic devices.